ER-5214

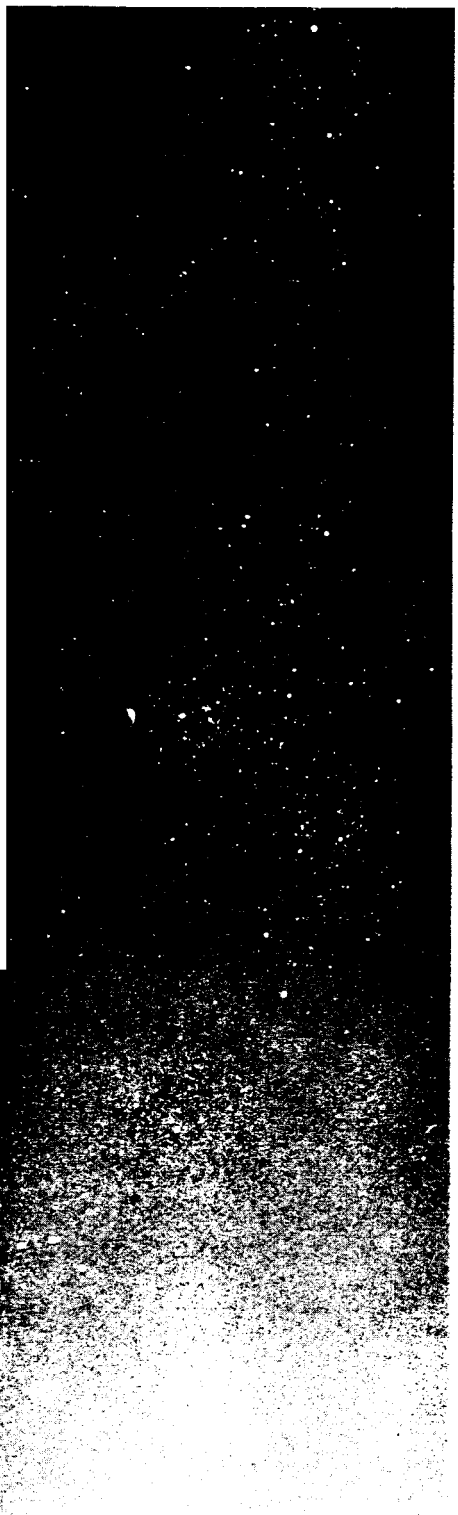

MERCURY WETTING AND NON-WETTING CONDENSING RESEARCH

LEWIS RESEARCH CENTER

Contract NAS 3-2159

Progress Report No. 3

JULY - DECEMBER, 1962

TAPCO a division of
Thompson Ramo Wooldridge Inc.

PROJECT

512-009377-08

ER-5214
PROGRESS REPORT NO. 3

MERCURY WETTING AND NON-WETTING CONDENSING RESEARCH

CONTRACT NAS 3-2159

PREPARED BY:	CHECKED BY:	APPROVED BY:
R. G. Gido Research Engineer	A. Koestel Senior Engineering Specialist	
A. Koestel Senior Engineering Specialist		

This research was sponsored by the National Aeronautics and Space Administration, Lewis Research Center. Significant contributions to the program made by Dr. Peter Griffith, Dr. Simon Ostrach, Mr. C. T. Jaenke, and Mr. Glenn White are gratefully acknowledged.

DATE	DEPARTMENT
January, 1963	Rankine Power Systems

Thompson Ramo Wooldridge Inc.

CLEVELAND, OHIO, U. S. A.

NOTICE

This report was prepared as an account of Government sponsored work. Neither the United States, nor the National Aeronautics and Space Administration (NASA), nor any person acting on behalf of NASA:

A.) Makes any warranty or representation, expressed or implied, with respect to the accuracy, completeness, or usefulness of the information contained in this report, or that the use of any information, apparatus, method, or process disclosed in this report may not infringe privately owned rights; or

B.) Assumes any liabilities with respect to the use of, or for damages resulting from the use of any information, apparatus, method or process disclosed in this report.

As used above, "person acting on behalf of NASA" includes any employee or contractor of NASA, or employee of such contractor, to the extent that such employee or contractor of NASA, or employee of such contractor prepares, disseminates, or provides access to, any information pursuant to his employment or contract with NASA, or his employment with such contractor.

Requests for copies of this report should be referred to:

National Aeronautics and Space Administration
Office of Scientific and Technical Information
Washington 25, D.C.
Attention: AFSS-A

TABLE OF CONTENTS

TABLE OF CONTENTS (Continued)

LIST OF ILLUSTRATIONS

LIST OF ILLUSTRATIONS (Continued)

LIST OF ILLUSTRATIONS (Continued)

LIST OF TABLES

1.0 SUMMARY

AUTH-ABST

This report covers the work performed between July 1 and November 30, 1962 on Contract NAS 3-2159, Wetting and Non-Wetting Mercury Condensing Research. The investigation consists of both an analytical and an experimental phase. The experimentation consists of local pressure drop measurements for condensing mercury in horizontal straight and tapered steel tubes. Both wetting and non-wetting conditions are explored. The analysis consists of the formulation of a dropwise condensing fluid mechanic model for correlating the data obtained from the non-wetting forced convection condensation tests. Also included is a hydrodynamic stability analysis of liquid films for application to wetting condensing and its multitude of possible flow patterns. This analysis is required to match the proper flow regime with its pressure drop correlation.

The test data are compared with the Lockhart-Martinelli correlation to indicate agreement and note shortcomings. The state of the art of two-phase fluid mechanics is reviewed to give the reader a proper perspective of the work being done and the work that has been done.

Non-wetting pressure drop data are tabulated herein with only preliminary attempts of correlation indicated. The final report will include the wetting data currently being obtained as well as the comprehensive results of correlation currently being compiled.

2.0 INTRODUCTION

The purpose of the wetting and non-wetting condensing research program, sponsored by NASA under contract NAS3-2159, was to refine procedures for designing low heat flux* mercury condensers for space power systems. This study placed particular emphasis on the differences between wetting and non-wetting condenser performance and the different design considerations required.

Mercury is considered to be "non-wetting" (i.e., the contact angle is greater than 90 degrees) with most fabrication materials presently planned for use in Rankine cycle space power plants. These systems will operate up to temperatures of approximately 1200°F or less (Ref 1 and 2), and presenrly are constructed from either the stainless steels or Haynes-25 type (high cobalt content) materials. It has been observed, however, that mercury will wet these materials with sufficient time and temperature.

The change from non-wetting to wetting significantly affects the condensing flow regime, and therefore wetting and non-wetting must be understood by designers of mercury condensers. During non-wetting a dropwise flow regime has been obtained in glass tubes in tests run at TRW. Some over-all condensing and adiabatic data (e.g., total pressure drop) have also been obtained at TRW. References 3, 4, and 5 present an analysis of dropwise condensation of mercury. Further development of this drop analysis was required to account for the change in drop size with length. In addition, local pressure measurements along the tube in more extensive temperature and flow ranges were required.

When mercury wets the wall a thin film of liquid mercury forms on the tube wall. This film is more unstable than drops; consequently, more flow regimes exist and the fluid dynamics are more complex. When mercury forms a continous liquid film which can readily transmit wave phenomena, sensitivity to small body force disturbances may increase. The waves may cause spray (drop formation) as well as serious slugging with attendant pressure and inventory fluctuations. A significant amount of experimentation and some analysis has already been done on adiabatic wetting two-phase flow and usefulness to the case at hand was investigated. However, data with heat transfer, more analysis, and local pressure measurements were still required for the case of wetting mercury condensation.

The program described in this report was instigated to obtain local pressure drop data for the wetting and non-wetting condensing of mercury. The state of the art of wetting and non-wetting condensing theory and analysis is established and refinements are made.

* In direct radiator-condenser systems, condensing heat flux is limited by the heat rejection area to approximately 15,000 Btu/hr-ft^2.

3.0 PROGRAM OBJECTIVES

The basic program objectives were to provide both experimental data and mathematical tools for the design of a low-heat flux zero gravity mercury condenser in which either wetting or nonwetting condensing may occur. The data should be useful to check on theory as well as to provide raw data for the designer of condenser components. Both the data and analysis should be applicable to condenser materials, configurations, flow ranges, and saturation levels of interest for present-day mercury Rankine cycle space power systems.

Stainless steel was originally selected as the condensing tube material, but Haynes-25 type material was subsequently substituted. The geometries selected for test are listed below:

Configuration	Conditions		Test Series
	Non-Wetting	Wetting	
0.319 inch ID constant diameter by 8 feet long	Yes	Yes	A,F
0.397 inch ID constant diameter by 8 feet long	Yes	No	E
0.4 to 0.2 inch ID linear diameter taper by 7 feet long	Yes	Yes	D

These geometries were chosen because they cover the range of tube sizes presently under consideration in advanced mercury direct radiator-condensers.

The ranges of flow rate, pressure level, and condensing lengths over which data are of interest for direct application to advanced mercury condenser design are summarized below:

Tube Configuration	Flow Rate lb/min	Inlet Pressure Psia	Condensing Length, ft
Constant Diameter	1 1/4 to 3	11 to 30	4 to 8
Tapered	1 1/4 to 3	11 to 30	7.5

A greater variation of flow rate, pressure level, condensing length and configuration is also of interest, as extreme variations of Reynold's and Froude numbers would be useful for extrapolation of the data. From system considerations, however, pressure levels higher than 30 psia have been found impractical as cycle efficiency is unnecessarily decreased. Also, for the tube sizes and saturation levels chosen, flow rate must be limited because unreasonably high vapor inlet velocities may result. Also, flows less than about 1 1/4 pounds per minute for the tube sizes investigated are too sensitive to gravity to provide any useful zero-gravity data. To provide greater insight into the phenomena occurring,

pressure readings were taken at intervals of 18 inches along the condensing section. Pressure readings at smaller intervals might affect the internal phenomena while larger intervals would be less "local".

To establish and refine the present state of the art of condensing theory and analysis (1) existing adiabatic two-phase flow theory was applied to the case of wetting condensation; (2) film buildup and film stability during wetting condensation were considered; and (3) the existing theory for non-wetting pressure drop was refined to include the effect of drop size variation along the condensing tube.

4.0 TWO-PHASE FLOW THEORY AND ANALYSIS

Design of a forced convection condenser for operation in a variable gravity environment requires consideration of the following factors:

1. flow regime,
2. pressure drop,
3. density, or liquid and vapor contents
4. amplitude and frequency of pressure fluctuation.

Knowledge of the flow regime is required so that the proper pressure drop and density equations may be applied. Pressure drop must be calculated to insure that system requirements are met. Inventory allocation must also be known and therefore mean density or liquid and vapor contents must be known. Finally, pressure fluctuations must be investigated to insure that excessive oscillations are not present. Tolerance limits for pressure fluctuations must first be defined by system (principally pump and turbine) requirements.

The present state of the art of condenser design allows only estimation of the relationships between the above parameters on the basis of correlations of adiabatic test results, and the estimation is primarily true for wetting fluids only. The sections below review modified adiabatic approaches and present unique analytical treatments for the prediction of wetting film stability and non-wetting mercury condensing pressure drop.

The design procedure for a zero-gravity condenser should be similiar to that for the horizontal 1 g case, if the annular flow regime is predominant during wetting condensing (which it is, as indicated in Appendix B) and if the drop agglomeration is small during the non-wetting. Horizontal 1 g condensing data in constant diameter tubes with high vapor inlet velocities and in tapered tubes with high velocities throughout are expected to be very similiar to zero-gravity data. The high axial velocity component creates an initial inertia force that predominates over the gravity force, thereby minimizing the gravity effect. Based on the comparison of some data with theory in Section 7.0, inlet vapor velocities of roughly 150 feet per second or higher appear adequate.

In a constant diameter tube, the major frictional and droplet or wave drag effects on pressure drop occur in the high vapor velocity or high quality region and therefore should not be significantly affected by gravity. In the low quality (velocity) region, however, liquid distribution is significantly affected by gravity. As a result, the pressure pulsations and local pressure drop may be significantly affected. The over-all pressure drop for the tube is not significantly affected, however, since the low vapor velocity should result in low pressure gradients.

In tapered tubes the velocity is almost entirely constant. If the velocity is sufficiently high, identical flow regimes will result in the horizontal 1 g and zero gravity cases. The exact effects of gravity on the condensing process are only a matter of speculation at this time and analysis must await the completion of zero-gravity experimentation.

It has been observed that mercury systems can operate with either wetting or non-wetting condensation. The surface chemistry aspects relating the wetting and non-wetting states are complex and the transition is not well understood. Consequently, the wetting and non-wetting analytical considerations that are required are presented independently below.

4.1 CONDENSATION OF WETTING FLUIDS

Two approaches to the prediction of the flow regime, pressure drop, density, and pressure fluctuations are possible for the wetting condensation of fluids such as mercury:

1. The annular flow pattern can be assumed. Local film thickness along the tube can be computed and energy dissipation and stability can be analyzed. A key missing link in this approach is the analytical tools required to perform the stability calculations. Section 4.1.1 reviews the situation.

2. Existing two-phase adiabatic and diabatic data and correlations may be employed. Section 4.1.2, "Horizontal Two-Phase Flow," reviews this approach.

The film stability approach described in Section 4.1.1 is more theoretically correct, but also is less understood and thus cannot be used for actual design of a wetting condenser at this time. Practically speaking, the "modified adiabatic" approach to the fluid dynamic design of a wetting mercury condenser suggested in Section 4.1.2 is the only means presently available. The effects of heat transfer, zero gravity, and equilibrium length requirements in this approach are still unknown.

The following sections contain much discussion of adiabatic two-phase phenomena, because observing diabatic phenomena as precisely as required is difficult. Wherever possible, however, the considerations required to relate adiabatic and diabatic results are presented.

4.1.1 Film Stability Analysis

The information required to approach the design of a wetting condenser by analyzing film buildup and stability is far from complete. This is basically due to lack of (1) consistency and experimental verification of the theories for the stability of thin films and (2) means for predicting the effect of surface irregularities (waves, etc.) on pressure drop. In the section below, reason (1) is discussed extensively as the calculation of film stability is important in determining the flow regime, pressure drop, density, and amplitude and frequency of fluctuation.

Pressure drop calculations for the case of an annular film could be made on the basis of the film wave friction factors for the wave heights and lengths that may exist. Very little information of this sort is known to be available. In case liquid droplets are entrained in the vapor as a result of film breakup, a consideration of the drag effect of these drops in transit is required. The analysis of Section 4.2 would then be applicable.

Computation of the local film thickness at each point along the tube requires determination

of three factors:

1. Interfacial shear stress caused by condensing momentum transfer and frictional shear,

2. body force vector,

3. liquid flow rate.

The local vapor and liquid flow rates at each point are established by heat transfer considerations alone. Several rigorous analyses for computing film thickness have been published (Ref 6, 7, 8 and 9). Test data have substantiated these equations.

Accurate computation of the film thickness and interfacial energy dissipation depends on the designer's knowledge of interfacial shear and its dependency on the structure of the liquid-vapor interface which has as yet not been either experimentally or theoretically established.

After the annular film thickness has been established, the stability analysis can be initiated. This analysis will determine whether the annular flow pattern indeed exists and if the proposed design will meet the objectives of pressure drop.

No suitable general stability equation valid for all situations is available. The designer can either use flow regime maps - such as the map illustrated in Figure 15 - Page 33 - on which the local condensing flow conditions can be superimposed or he can locally apply adiabatic stability criteria involving the Weber, Reynold's, Froude numbers and the property ratios along the condensing film. A procedure such as this requires that the growth rate of the instability be large compared to the velocity of the liquid film. The effect on stability of the vapor velocity normal to the liquid interface caused by condensation is, of course, ignored in this approach.

When instabilities manifest themselves, the designer should answer the following logical questions:

1. Is the instability objectionable?

2. Are objectionable low frequency, high amplitude liquid slugs formed, or is spray formed which may be tolerable?

3. How is the heat transfer and pressure drop affected by the altered flow regime?

This requires some knowledge of what is objectionable and what is tolerable. In addition, the designer must postulate the size of the detached and entrained liquid. This estimate could be scaled to wavelength. Unstable waves which are small compared to the tube diameter will form spray and those which are large compared to the tube diameter or vapor space will form slugs. The size of the liquid slug or drop and velocity of flow determine the frequency

and amplitude of the pressure pulses.

In any event, the stability of wetting films must be predictable. The present state of the art is reviewed below and criteria for film stability are presented.

4.1.1.1 Review of Wetting Film Stability

Most of the existing research concerning the breakup of liquid films was motivated by the practical problem of liquid film cooling for rocket nozzles. It is basically experimental, although some simplified analyses were also made. Much of this work was done for plane flows. This will not be extensively discussed herein because the basic configuration of interest for condensers is annular flow. Emphasis will, therefore, be given to the studies dealing with that type of flow.

The striking aspect resulting from a survey of the literature on annular flow is that many different criteria are suggested for the film breakup and some work indicates that parameters found by others to be significant are not important. Relatively few attempts are made to explain the differences; the nature of most of the papers is the description of the particular studies made. For example, one of the most extensive experimental investigations was performed by Dunkler (Ref 10 and 11) who found that over the range of conditions which he studied in the downward annular flow in a vertical tube, there were essentially two significant changes in the nature of the flow. The first of these he associated with a basic change in the wave structure which occurs when the energy transmitted across the interface reaches some critical value and the second he thought to be associated with a liquid film velocity effect which decreases the wave amplitude. Dunkler further concluded from his results that the liquid Reynold's number was not a significant parameter which determines wave motion and wave height.

The experiments described by Kinney et al in Reference 12 were performed in horizontal ducts. They found that the liquid film surface became wavy when a critical liquid flow rate was exceeded. Furthermore, for more viscous liquid films this critical flow rate was higher. One can thus infer that in contradistinction to the work by Dunkler on a single-phase liquid film on the outside of a vertical cylinder, the liquid Reynold's number is indeed a significant parameter. Brauer (Ref 13) was also led to believe from his experiments that the occurrence of surface waves is associated with the transition of the liquid film from laminar to turbulent flow, i.e., is related to a critical liquid Reynold's number. The experiments of Reference 12 covered a wider range of liquid viscosities than did Dunkler's experiments; this is perhaps an explanation of this discrepancy. It is also important to note that because the authors of Reference 12 seemed to be unaware of the basic governing parameters and physical mechanisms, their tests and correlations were unduly extensive, i.e., they varied the liquid velocity by itself, then the viscosity by itself, etc.

More seemingly contradictory results were obtained by Knuth (Ref 14) who found surface waves for all liquid flow rates in horizontal ducts. For liquid flow rates larger than some critical value he found a second type of surface wave (ones with long wavelengths). Thus, there now appear to be two distinct and different interfacial instabilities. The disagreement

between the results of References 12 and 14 was attributed to the differences in the methods of liquid injection in the experiments. Knuth, however, agreed with Kinney et al that the instability depended on the liquid Reynold's number. Recall this disagrees with Dunkler's conclusion. Further, References 12 and 14 are in agreement that the gas Reynold's number has a negligible effect on the interfacial stability whereas Laird (Ref 15) shows that over isolated ranges of operation the gas Reynold's number does influence the interface. Other work could also be cited to show the types of contradictions prevalent in this regard.

Although the existing work seemingly contains contradictions and disagreements, it does indicate that objectionable phenomena can occur in two-phase flows when the gas-liquid interface becomes wavy. It is, therefore, essential to discuss the possible causes of such interfacial waviness from a fundamental viewpoint. A body of fundamental knowledge exists which does not appear to have been generally known heretofore to the people investigating interfacial stability in two-phase flows.

There are essentially four different types of instabilities which singly or in combination can cause an interface to become wavy and can thereby lead to film breakup or slugging in the flow: (1) hydrodynamic instability, (2) Kelvin-Helmholtz instability, (3) Rayleigh-Taylor instability, and (4) Bénard instability.

Hydrodynamic instability is the case in which a fluid is undergoing transition from laminar to turbulent flow as a result of amplification by viscosity of infinitesimal disturbances in the fluid. These disturbances originate either inside or outside the film. (Actually, all instabilities to be discussed here are hydrodynamic, but special meaning is given to this phase herein for convenience.) Hydrodynamic stability of boundary layers in a homogeneous fluid has been extensively studied (see Reference 16 for a summary), and it has been conclusively established that such waviness occurs under certain conditions.

The above hydrodynamic stability analyses were recently extended in Reference 17 for nonhomogeneous fluid flow. In particular, consideration is given therein to the specific case of two contiguous, viscous, incompressible fluids in plane motion; one fluid is bounded by a solid wall below and the other fluid above. The second fluid is unbounded above. The fluid motion is steady and unidirectional, parallel to the interface, and the shear rate in each fluid is uniform. As in the case of the stability of homogeneous fluids, the mathematical analysis is based on small disturbance theory and leads to an eigenvalue problem in a system of two linear ordinary differential equations. In addition to the dimensionless wave number, disturbance phase velocity, and the (inner fluid) Reynold's number occurring in single-fluid studies, the viscosity and density ratios and the Froude and Weber numbers appear as important parameters for nonhomogeneous fluids. The effect of gravity is determined by the Froude number which represents the ratio of inertia to gravitational forces. The influence of surface tension is determined by the Weber number which essentially denotes the ratio of inertia to surface forces. Single-looped neutral stability maps (see Figure 1), similiar to those for homogenous fluids, and disturbance amplifications rates are presented in Reference 17.

It is essential to understand that the work of Reference 17 is an extension of the hydrodynamic instability analyses made for single fluids and, hence, gives an indication of the conditions

SINGLE-LOOPED STABILITY MAP OF FELDMAN
NEUTRAL STABILITY CURVES: WAVE NUMBER VERSUS LIQUID REYNOLDS NUMBER
GRAVITY AND SURFACE TENSION FORCES ARE NEGLECTED
LIQUID-GAS VISCOSITY RATIO = 10

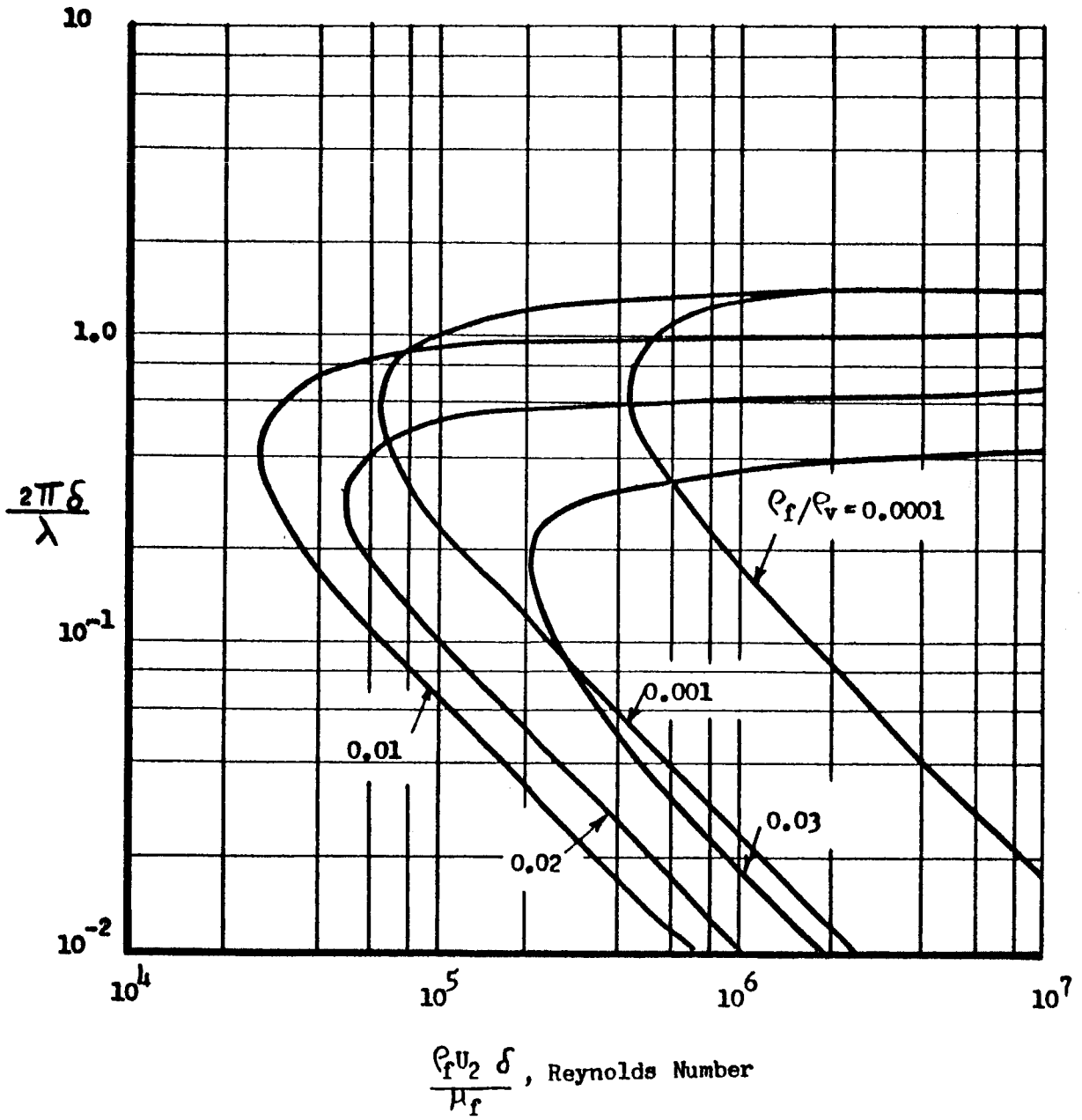

FIGURE 1

under which the interface can become wavy as a result of amplification of disturbances in the liquid film bounding a rigid plane. Considerable confusion appears in the literature as to the type of instability studied therein (see Reference 18 for example). In essence the work of Reference 17 concerns the hydrodynamic stability of a film on a surface with new constraints, due to another fluid, at its edge. Furthermore, it must be clear that these results pertain only to plane flow of two fluids under adiabatic conditions with no mass transfer. Therefore, utilization of these results for condensing annular films (as are obtained in tubes) should be made with caution.

The Kelvin-Helmholtz instability is the second possible type to influence two-phase flows. This instability arises when the different layers of a stratified heterogeneous fluid are in relative horizontal motion and is due to the interaction between the fluid media at the interface. The mathematical analysis of this instability is described in Reference 19. Basically it is also a small perturbation approach, but since attention is focused on the interface, the viscosities of the fluids are neglected. The Reynold's number, therefore, plays no important role in this type of instability. Instead a parameter $g(\alpha_1-\alpha_2)/\alpha_1\alpha_2(u_1-u_2)^2$ for fluids with discontinous velocities and densities appears as the criterion, where g is the acceleration of gravity, α_1 and α_2 are density ratios defined as $\alpha_1 = \rho_1/\rho_1+\rho_2$, and U_1 and U_2 are the velocities of the two fluids. For fluids with continous velocity and density distributions in the vertical direction, this parameter is called the Richardson number, J, and is written as $J=-(g\, d\rho/dz)/\rho(du/dz)^2$. This represents the ratio of buoyancy and inertia forces. For stability, neglecting surface tension, the disturbance wave number must be less than some value of the dimensionless parameter written in either of the above ways.

The striking aspect of the Kelvin-Helmholtz instability is then that it occurs no matter how small the velocity difference or shear of the two fluids. The instability arises by the crinkling of the interface by the shear that is present. This crinkling occurs even for the smallest differences in the velocities of the two fluids; it can occur even if the motions of both fluids are laminar. The source of the Kelvin-Helmholtz instability lies in the energy stored in the kinetic energy of relative motion of the different layers. The tendency toward mixing and instability will be greater, the greater the prevailing shear force. The only counteracting forces are inertia and surface tension.

It is important to note from the stability criterion cited above that in a zero-gravity environment the two-phase flow would be unstable to all wavelengths. In Reference 20, a similiar criterion is derived by force balances for the Kelvin-Helmholtz instability. The effect of gravity has been omitted in this work. However, growth rates for this type of instability are determined which should be of value for the present work. (See Figure 2).

The third possible type of instability is the Rayleigh-Taylor instability. This is an instability of the interface between two fluids of different densities which are stratified or accelerated towards each other. This type of instability arises from the character of the equilibrium of heterogeneous fluids. The mathematical analyses of this instability are also presented in Reference 19. They are either of a normal mode or a variational type. Studies have been made of both viscous and inviscid fluids, including and neglecting surface tension effects.

GROWTH RATE VS WAVE LENGTH FOR VARIOUS
WEBER NUMBERS (REF 20)

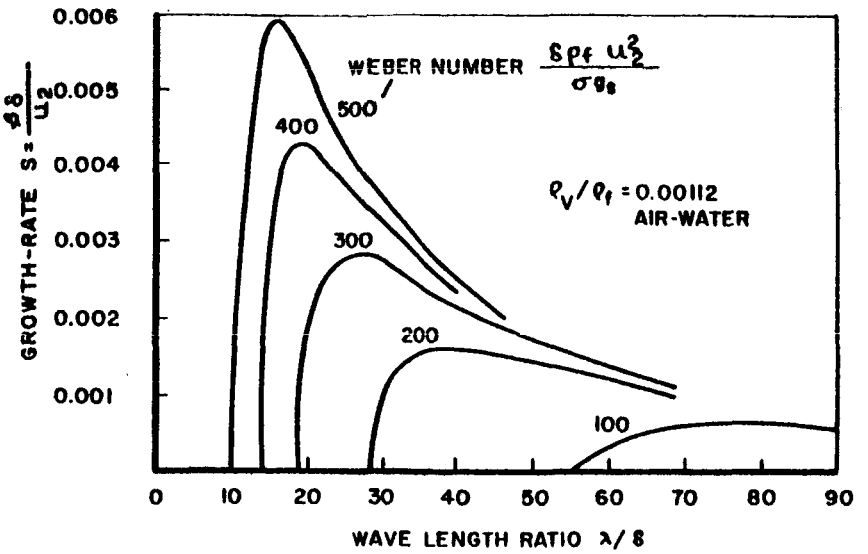

FIGURE 2

The stability in the Rayleigh-Taylor sense depends only on the relative orientation of the density gradient between the fluids and the acceleration field. For example, horizontal fluid layers in a gravitational field will be stable only if the lower fluid is heavier than the upper; this configuration is unstable (neglecting surface tension) for all wave numbers if the reverse is true. For some unstable situations modes of maximum instability exist, and the dependence of the disturbance growth rate on its wave number has been explictly determined for a number of special cases.

The last type of instability capable of influencing condenser flows is associated with having a fluid configuration in which the density variation is such that heavier fluid is above lighter fluid in a gravitational field. This is clearly a top-heavy situation which is potentially unstable. The instability creates a tendency for the fluid to redistribute itself to remedy the weakness in its arrangement. However, the natural tendency of the fluid will be inhibited by its own viscosity. In other words, it can be expected that an adverse density gradient which is maintained must exceed a certain value before the instability can manifest itself. Considerable study has been given to this type of instability where the density gradient in the fluid results from a temperature gradient. However, similiar results will be obtained if the density gradient results from concentration gradients. This type of instability is called the Bénard instability. The Rayleigh-Taylor stability applies to two fluids with an interface, whereas the Bénard stability applies to a homogeneous fluid with density gradients. In a horizontal annular condensing flow the upper part of the fluid will be subject to an adverse density gradient as a result of both thermal and concentration gradients; the lower part will be in a stable configuration. The flow on the other parts of the annulus will have the gravitational force normal to the density gradient and, hence, will be subject to conventional natural-convection phenomena. Therefore, extreme asymmetry of the flow can result from such a configuration. Note that this discussion of Bénard instability

relates to a fluid at rest. If a gas flow is superposed on such a fluid configuration, longitudinal or transverse vortex rolls result. A description of these is given in Reference 21.

The normal mode and variational analyses of the Bénard instability are presented in Reference 19. It is shown that a critical value of the Rayleigh number must be exceeded before instability occurs. (The Rayleigh number is the product of the Prandtl and Grashof numbers where the latter represents the ratio of buoyancy to viscous forces.)

It is important to note that a particular type of instability under given conditions is generally more unstable to one type of disturbance or wave than another. (Rayleigh, in Reference 21, says, "Some kinds of disturbances produce their effect much more rapidly than others.") For example, it is well known in hydrodynamic stability theory that for incompressible flows, two-dimensional disturbances (transverse waves) are more destabilizing than three-dimensional ones (oblique waves). See Reference 16. However, for compressible flows the three-dimensional waves are more destabilizing. Furthermore, for flows with body forces, longitudinal rather than transverse waves are the most destabilizing. Therefore, some study should be made to see whether each type of instability of interest is associated with distinct wave patterns. In this way it might be possible to identify the various types of instabilities or to determine the most harmful type. In the course of the experiments on film breakup described in Reference 22, two-dimensional, three-dimensional, and roll-waves were all observed.

Now that each possible type of instability has been described, the distinctions among them must be made and their relations to the problem of condensing flows must be established. First of all, note that the hydrodynamic and Kelvin-Helmholtz instabilities are fundamentally associated with fluids which are in motion; the Rayleigh-Taylor and Bénard instabilities can occur in fluids at rest. The primary factor in these is the body force action. The latter two types would not, therefore, be of consequence in a true zero-gravity environment. The hydrodynamic and Bénard instabilities can occur in homogeneous fluids as well as in heterogeneous ones, whereas the Kelvin-Helmholtz and Rayleigh-Taylor instabilities are associated only with nonhomogeneous fluids.

In a normal or reduced gravitational environment, all four types of instability are clearly possible. The Rayleigh-Taylor and Bénard instabilities most likely would not be so important as the other two types for films that have moderate motions because the body forces would be small relative to the inertia forces. The Kelvin-Helmholtz instability would most likely occur before the hydrodynamic instability because the former has been found to occur even if both fluids are in laminar motion. Near the back end of condenser tubes (and the front end of boiler tubes), the liquid layers meet and the flow velocity is very small. Under these conditions the Rayleigh-Taylor instability could be important. Work on this type of instability as well as studies of water-air, mercury-air interfaces at zero-gravity conditions (in a KC 135 aircraft) have been done at TRW and are reported in Reference 23.

In any event, it would seem that determination of the instability most probable to influence a given flow first could be qualitatively obtained by comparing the various existing stability criteria. However, it must be remembered that all the above-described analyses were for

plane flows and none included the effects of heat and mass transfer which are an inherent part of the condensing process. Therefore, at best, predictions made on this basis for two-phase annular flows are tenuous. It is, however, interesting to note that even despite the limitations of the existing stability analyses, they can be used to make some of the seemingly anomalous results obtained from the various experiments appear to be reasonable. For example, recall that in References 10 and 11 the two changes in wave structure were found. The first change, caused by the energy transmitted across the interface, certainly seems to be the Kelvin-Helmholtz instability; the second change, associated with the liquid flow rate, appears to be the hydrodynamic instability even though Dunkler did not think that the liquid Reynold's number was significant. In Reference 14 two different types of surface waves were also found. The first appeared for all liquid flow rates in consonance with the results of the Kelvin-Helmholtz stability analysis, and the second waves which occurred beyond a certain value of the liquid flow rate or Reynold's number were caused by the hydrodynamic instability. It is possible that Dunkler, who did not obtain the first type of waves until a certain amount of energy had been transmitted across the interface, had less disturbances in his experiments than did Knuth. Therefore, Knuth obtained the first waves for all liquid flow rates. These experiments tend to support the conjecture made previously herein that the Kelvin-Helmholtz and hydrodynamic instabilities are the more important pair for flows with at least moderate liquid velocities and that the Kelvin-Helmholtz instability appears first.

The waviness found in References 12 and 13 after a critical liquid Reynold's number was exceeded must have been caused by the hydrodynamic instability. The reasons why no other wave structure corresponding to the Kelvin-Helmholtz instability was reported in those papers are not clear. Either the investigators were not looking for them or the disturbances level was below that required to cause such instability. Note in Reference 13 the flow was that of a single-phase liquid external to a duct and, therefore, less disturbances were imposed on the liquid film. More careful analysis of the data of those papers might substantiate that disturbance level was low.

The conclusions of References 12 and 14 that the gas Reynold's number is unimportant as a prime interfacial stability parameter certainly are substantiated by the stability analyses, because this parameter does not appear at all. On this basis the results of Laird (Ref 15) which showed an effect in isolated regions of the gas Reynold's number remain questionable. It may be that the gas-flow turbulence level was responsible for this result. Further discussion of this point will be made subsequently.

In a zero-gravity environment the Rayleigh-Taylor and Bénard instabilities would not exist because there is no body force. It appears that the Kelvin-Helmholtz instability would be the dominant one, at least for film speeds below a rather large value (i.e., below a large Reynold's number). The reason for this conjecture, again based on the existing analyses, is that this instability can occur even if both fluids are in laminar motion, whereas the hydrodynamic type occurs when destruction of liquid laminar motion begins. Furthermore, the stability criterion for the Kelvin-Helmholtz type indicates that the flow is unstable for all wavelengths when g goes to zero. Whether, in fact, the situation is as serious as this cannot be determined without more careful study of this type of instability, including such effects

as heat, mass transfer, and viscosity.

It is known from hydrodynamic stability studies for homogeneous fluids that cooling of the layer adjacent to a rigid surface tends to stabilize it. Therefore, in a condensing flow it would seem that the layer would be less subject to hydrodynamic instability. Whether this is also true for the Kelvin-Helmholtz instability remains to be investigated. The influence of viscosity on the latter type, which has heretofore been neglected, might also be found to be stabilizing because it moderates the velocity difference at the interface.

There is one additional word of caution necessary to be added with regard to the use of existing stability analyses and that is that they all refer to essentially unbounded flow in the direction normal to the surface. In effect, the flows treated are external ones whereas for the problem at hand the flows are internal. Although, as has already been pointed out, this "geometrical" difference may be important by itself, there is another aspect which may be of even greater consequence. In an internal flow one part of the liquid layer can produce disturbances to another part. Also in the main (gas) flow there exist such disturbances in internal flows (to a greater degree than in external flows) as turbulence, regular and random sound, temperature spottiness and the like. These disturbances may cumulate in different and nonlinear ways and the theory takes no account of these. Therefore, there is some question as to whether stability analyses as described above have any meaning for internal flows. The lack of correlation of hydrodynamic stability theory with transition data for flow in shock is clearly shown in Reference 24.

Laminar internal flows are shown to become unstable at Reynold's numbers at least an order of magnitude lower than that predicted by stability theory. This is the opposite of what is meant by flow instability. The question of the validity of hydrodynamic stability analyses for normal internal flows is discussed more fully in Reference 24.

The Kelvin-Helmholtz instability may also be affected by the larger disturbances associated with internal flows.

4.1.1.2 Prediction of Condensing Film "Breakup"

The method for predicting the "breakup" time or distance from the condenser inlet to the point where liquid leaves the interface as a dispersed phase or where the liquid may bridge the tube as a plug is formulated below for an adiabatic liquid film model.

Assume a liquid-gas interface to be perturbed by disturbances of all wavelengths at a multiplicity of sources, and that the disturbance having the maximum positive growth rate dominates the interface. Since the maximum growth rate disturbance can originate at any point along the interface, it will be further assumed that only those formed at the furthest upstream distance will dominate. This assumption precludes the existence of standing waves which is reasonable since none have been observed in previous experiments. This is illustrated in Figure 3.

WAVE GROWTH ON LIQUID FILM

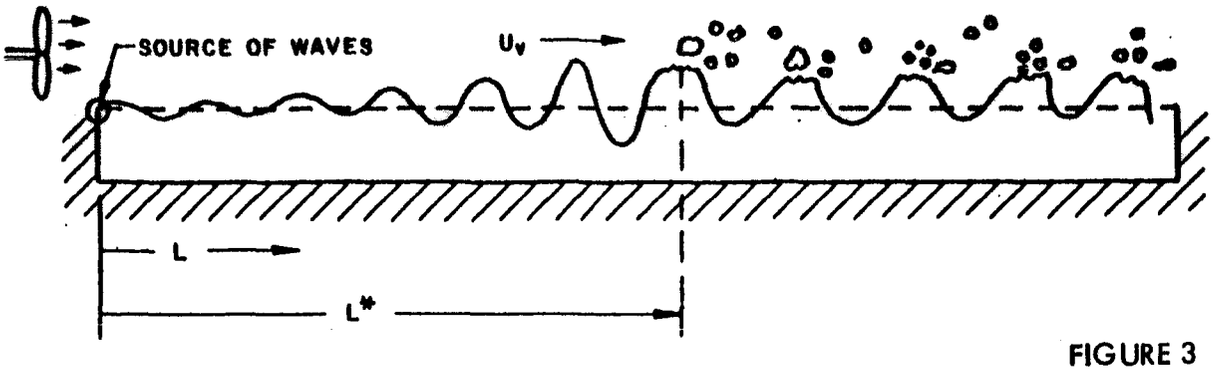

FIGURE 3

Figure 3 shows a continous formation of maximum growth rate waves at $L = 0$. L^* represents the distance at which liquid escapes from the interface. Waves of lower growth rate or waves formed at sources where $L > 0$ are eliminated from the picture. This assumption is valid if the maximum growth rate has a "steep" maximum as shown in Figure 4, curve (a). If the curve is flat as in curve (b), then the assumption becomes dubious.

GROWTH RATES IN LIQUID FILMS

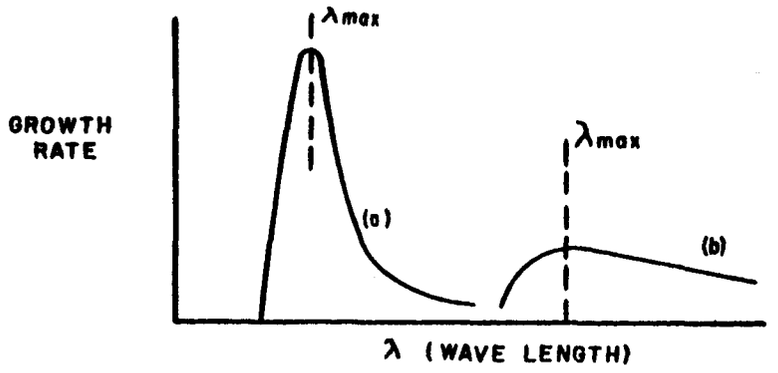

FIGURE 4

A single wave formed at $L = 0$ will appear chronologically as in Figure 5.

PROPAGATION OF A SINGLE WAVE IN A STATIONARY FLUID

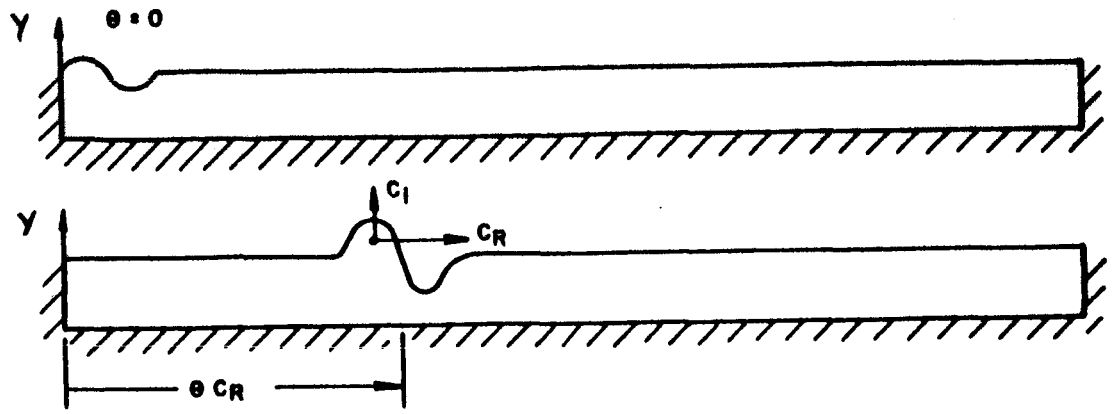

FIGURE 5

Figure 6 shows a wave as it may propagate in reality. It is simpler mathematically (for linear problems such as that of stability) to make a Fourier analysis of such a wave and consider the individual Fourier components. It is, therefore, generally assumed in stability analyses that all the waves are composed of simple harmonic waves of the form:

$$\Psi(L, Y, \theta) = f(Y)\, e^{i\alpha(L - C\theta)} \qquad \text{(Eq 1)}$$

As a result of this assumption all derived quantities, such as the velocities and amplitude, are harmonic and grow or decay exponentially. Equation 1 also defines the complex wave propagation speed $C \equiv C_R + iC_i$ whose real part, C_R, is the physical velocity of propagation of this simple wave. The imaginary part, C_i is related directly to the growth rate as will be seen later. The wave speed, C, is measured with respect to the undisturbed fluid; therefore, the wave velocity relative to a point fixed in space will vary with the velocity of the interface flow u_2 as shown in Figure 6.

PROPAGATION OF A SINGLE WAVE IN A FLOWING FLUID

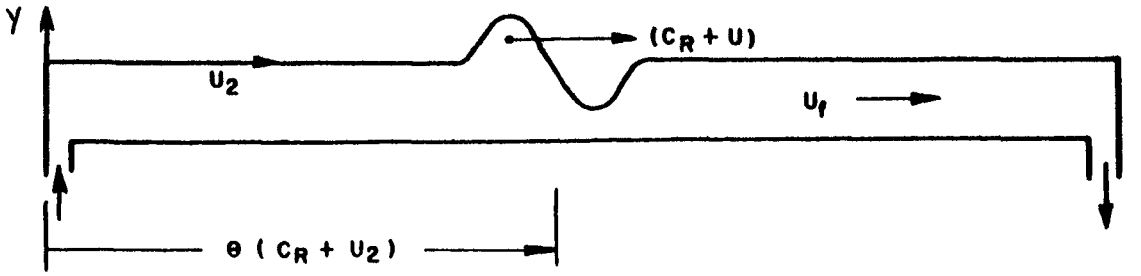

FIGURE 6

It is clear from Figure 6 that:

$$L = \theta(C_R + u_2) \qquad \text{(Eq 2)}$$

If Equation 2 is applied to a forced convection condensing process in which u_2 and C_R may be functions of length, it is more convenient to write Equation 2 in differential form as:

$$dL = d\left[\theta u_2\left(\frac{C_R}{u_2}+1\right)\right] = u_2\left(\frac{C_R}{u_2}+1\right)d\theta + \theta\left(\frac{dC_R}{du_2}+1\right)du_2 \qquad \text{(Eq 3)}$$

For adiabatic fully developed flows the wave propagation velocity and interface velocity will not vary in the downstream direction, so the second term in Equation 3 will vanish. For simplicity, this case will be considered first. Therefore, Equation 3 becomes:

$$dL = u_2\left(\frac{C_R}{u_2}+1\right)d\theta = C_R\left(1+\frac{u_2}{C_R}\right)d\theta \qquad \text{(Eq 4)}$$

Since the ratio C_R/u_2 appears as a parameter in Equation 4, it is necessary to obtain an estimate of its order of magnitude so that the "history" of a wave with a maximum growth rate (as illustrated in Figure 6), originating at $L=0$ and becoming harmful due to breakup (liquid entrainment) or flow plugging, can be determined. From Feldman's analysis of the hydrodynamic instability of a plane liquid film the ratio C_R/u_2 is plotted as a function of the property ratios of the two fluids in Figure 7. Figure 7 indicates that this ratio is approximately equal to 0.1. Therefore, Equation 4 can be written as:

$$dL = u_2 d\theta \qquad \text{(Eq 5A)}$$

If for other instabilities or flow conditions or configurations $u_2/C_R \ll 1$ then the other limiting form of Equation 4 is:

$$dL = C_R d\theta \qquad \text{(Eq 5B)}$$

The maximum value of this ratio will have to be determined from analysis or experience for the situation corresponding to annular two-phase condensing flows. In all situations other than the limiting cases (given by Equation 5A and 5B), Equation 4 must be used.

It is important to note that the time, θ, in Equations 4 and 5 depends on the growth rate of the wave, which is related to C_i. This relationship is explicitly determined as follows.

MAXIMUM WAVE CELERITY AS A FUNCTION OF PROPERTY RATIOS

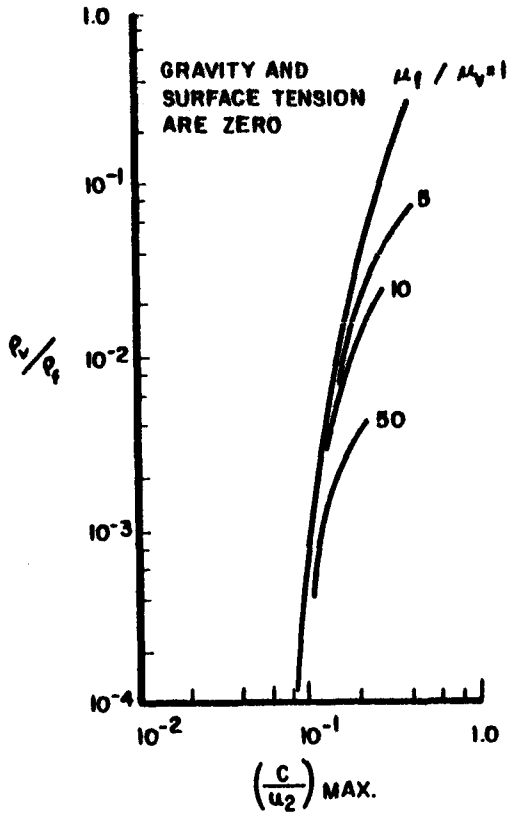

FIGURE 7

The amplification of the wave is described by the vertical velocity component of a point on the interface ($Y = b$) moving with the horizontal propagation velocity of the disturbance [$L = (c_R + u_2)\theta$]. For this case it can be found from Equation 1 that

$$v_e = -\frac{\partial \psi}{\partial L} = -i\alpha f(b) e^{\alpha C_i \theta} = \frac{dB}{d\theta} \qquad \text{(Eq 6)}$$

Differentiating Equation 6 yields

$$\frac{d^2 b}{d\theta^2} = \alpha C_i \frac{db}{d\theta} \qquad \text{(Eq 7)}$$

If δ denotes the liquid film height, then $b = B + \delta$ where B is the wave amplitude. Equation 7 can be written in terms of the wave amplitude as

$$\frac{\ddot{B}}{\dot{B}} = \alpha C_i \qquad \text{(Eq 8)}$$

upon assuming that the liquid film height, δ, does not vary with time. Integrating Equation 8 and setting the integration constant equal to zero without loss of generality gives

$$\frac{\dot{B}}{B} = \alpha C_i \quad \text{or} \quad \frac{dB}{B} = \alpha C_i \, d\theta \qquad \text{(Eq 9)}$$

It is evident from Equation 9 that αC_i is the parameter related to wave growth and, therefore, to the stability of the film.

Combination of Equations 4 and 9 yields

$$\frac{dB}{B} = \frac{\alpha C_i}{u_2(C_R/u_2 + 1)} dL \qquad \text{(Eq 10)}$$

If the limiting forms of Equation 5 had been used, the denominator term in parentheses in Equation 10 would not appear; in one case ($u_2/C_R << 1$) C_R would appear in place of u_2. In Reference 17, expressions are formulated for $C_i > 0$ (positive growth rates), $C_i = 0$ (neutral stability), C_R/u_2, and α for maximum growth rate waves. These results for hydrodynamic instability are presented in Figures 7 through 9 for the case where gravitational and surface tension effects are neglected. (For the Kelvin-Helmholtz instability the results of Reference 20 could be used).* These figures together with Equation 10 or its limiting forms are used to determine the breakup or plugging flow length. For other instabilities or configurations, of course, corresponding figures would have to be determined. However, for illustrative purposes the results of Reference 17 will be used herein with cognizance taken that these results apply explicitly to thin adiabatic liquid films with linear (Couette) velocity profiles.

MAXIMUM GROWTH RATE FACTOR AS A FUNCTION OF PROPERTY RATIOS

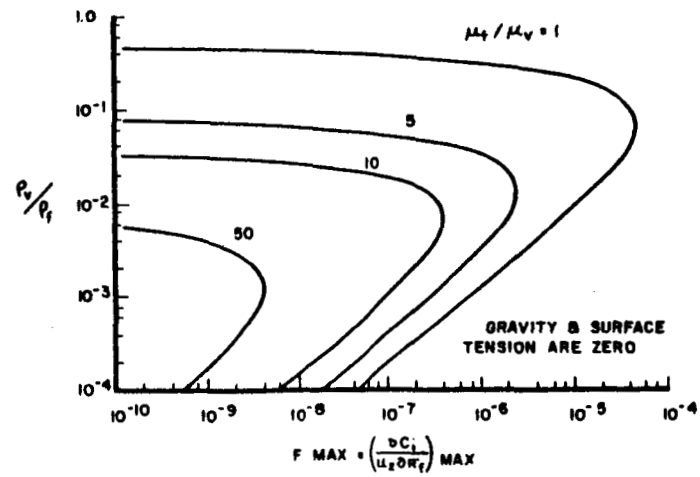

FIGURE 8

*See Figure 2

For adiabatic films the abscissa of Figure 8 is

$$\frac{\partial C_i}{\partial Re_f} = u_2 F_{max} \qquad \text{(Eq 11)}$$

where

$$F_{max} = f\left(\frac{\rho_v}{\rho_f}, \frac{\mu_f}{\mu_v}\right)$$

Intergration of Equation 11 yields

$$C_i = u_2 F_{max} Re_f + K$$

where K is an integration constant. When $C_i = 0$, $Re_f = Re_{fn}$ where Re_{fn} is the Reynold's number for neutral stability. Therefore

$$K = -u_2 F_{max} Re_{fn}$$

and

$$C_i = u_2 F_{max}(Re_f - Re_{fn}) \qquad \text{(Eq 12)}$$

If Equation 12 is substituted into Equation 10 there is obtained

$$\frac{dB}{B} = \frac{\alpha F_{max}(Re_f - Re_{fn})}{(C_R/u_2 + 1)} dL \qquad \text{(Eq 13)}$$

Replace $\alpha = 2\pi/\lambda$ by its dimensionless form used in Figure 9, $\alpha' = \frac{2\pi\delta}{\lambda}$ so that Equation 13 becomes

$$\frac{dB}{B} = \frac{\alpha' F_{max}(Re_f - R_{fn})}{(C_R/u_2 + 1)} \frac{dL}{\delta} \qquad \text{(Eq 14)}$$

MAXIMUM GROWTH RATE WAVE LENGTH AS A FUNCTION OF PROPERTY RATIOS

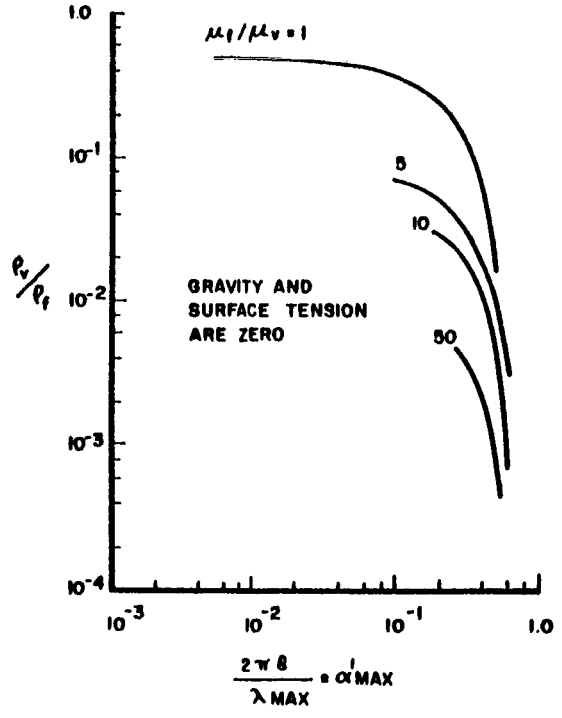

FIGURE 9

To find the breakup or plug flow length, Equation 14 must be integrated. If L^* denotes the point where the waves lead to unfavorable phenomena such as liquid entrainment and flow plugging, then the integration limits are $L=0$ to $L=L^*$. Similarly, $B = B_o$ to $B = B^*$ where B_o is the initial wave amplitude and B^* is the amplitude at which either entrainment or plugging occurs. To determine explicitly B^*, the amplitude for tearing of the interfacial waves can be obtained from experiments, whereas for plugging it is clear that the wave amplitude plus the film thickness must be of the order of one-half the flow passage diameter.

For the case of liquid entrainment it has been shown in References 22 to 25 that the wave heights approach the magnitude of the average liquid film thickness. Photometric measurements of the wave profile reported in Reference 25 are reproduced in Figure 10. This figure indicates that near the point of liquid entrainment $B^*/\delta = 0.81$. Another such figure derived in a similiar way (Figure 4c of Reference 25 shows that $B^*/\delta = 0.974$.

Figure 11 taken from Reference 25 shows maximum net wave height measurements (2B) versus film thickness. These measurements are limited to conditions for which no liquid is entrained. The upper part of the curve represents the point of incipient entrainment at which

$$\frac{2B^*}{\delta} = \frac{0.020}{0.010} \quad \text{or} \quad \frac{B^*}{\delta} = 1$$

WATER-AIR WAVE PROFILES (REF 26)

$\Gamma = 49.0 \times 10^{-4}$ lb/sec-in.

$\mu_f = 2.14 \times 10^{-5}$ slugs/Ft-sec.

$Re_f = 342$

$\delta = 0.0079$ in.

$$2\frac{B^*}{\delta} = \frac{0.015 - 0.0022}{0.0079}$$

$$\frac{B^*}{\delta} = 0.81 \text{ (computed)}$$

FIGURE 10

AIR-WATER MAXIMUM WAVE HEIGHT VERSUS FILM THICKNESS (REF 25)

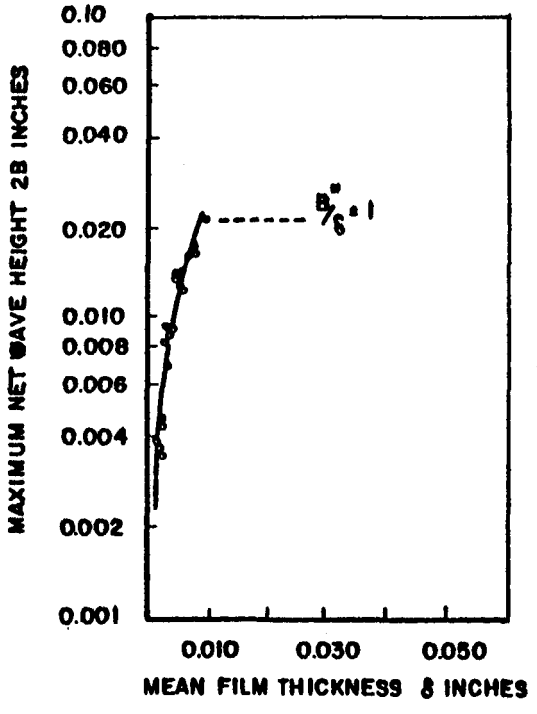

FIGURE 11

Other evidence of this sort is also available. It should be noted that these data were taken for the annular downflow in a vertical tube, and, hence, are more appropriate to the present work. However, these data were obtained for the liquid film application to rocket nozzles; therefore, the range of parametric values may not be analogous.

For the other end of the integration range it is necessary to know the initial wave amplitude B_o. Reference 27 states that $\ln B^*/B_o$ reaches a constant value for the breakup of moving liquid sheets. (This configuration is again not the same as the one of interest herein, but is used merely to obtain some orders of magnitudes from existing data.) Reference 28 theoretically predicts values for this ratio from which B_o can be determined when B^* is known.

For the other undesirable case of flow plugging, assume that flow plugging will occur when $B \approx (D/2) - \delta$. Therefore, for this case the upper integration limit is

$$B_s^* = \frac{D}{2} - \delta$$

which will occur when $L = L_s^*$. If this length is less than that for entrainment, L^*, slugging will actually take place in the flow passage. Alternate criteria for slugging may also be developed. For example, if the size of the entrained droplets as computed from Reference 29 are of the order of passage dimensions, then slugging can also occur.

Now that the integration limits have been established. Equation 14 can be integrated to give

$$\ln \frac{B^*}{B_o} = \frac{\alpha' F_{max} (Re_f - Re_{fn})}{(C_R/u_2 + 1)} \frac{L^*}{\delta} \qquad \text{(Eq 15)}$$

Since the concern here is with the maximum growth rate wave, the maximum values of α' and C_R/u_2 should be inserted in Equation 15. These can be evaluated from Figures 7, 8 and 9 which, of course, are limited to a specific configuration and instability type as discussed previously. According to these figures F_{max}, α'_{max} and $(C_R/u_2)_{max}$ are functions of property ratios alone; therefore, for a given combination of fluids at a certain pressure and temperature these quantities are constants. Also, as was previously indicated, the ratio B^*/B_o reaches a constant value for liquid film breakup.

Equation 15 can be rewritten as

$$\frac{L^*}{\delta} = \frac{\ln B^*/B_o \left[(C_R/u_2)_{max} + 1\right]}{\alpha'_{max} F_{max} (Re_f - Re_{fn})} \qquad \text{(Eq 16)}$$

or

$$\frac{L^*}{\delta} = \frac{E}{(Re_f - Re_{fn})} \qquad \text{(Eq 17)}$$

where E is a constant for a given set of property values μ_f/μ_v and ρ_v/ρ_f and is explicitly defined as

$$E = \frac{\ln B^*/B_o \left[(C_R/u_2)_{max} + 1\right]}{\alpha'_{max} F_{max}} \qquad \text{(Eq 18)}$$

To obtain an idea of how Equation 17 can be used to find the breakup length L^* and to indicate the data required to determine this length for the problem under consideration, use will be made of all existing data even though the configurations and ranges of conditions of the various sources are not consistent. Thus, if air-water systems are considered at atmospheric pressure and temperatures with $\mu_f/\mu_v = 54.1$ and $\rho_v/\rho_f = 0.0012$, then from Figure 7, for hydrodynamic instability of thin plane film, $(C_R/u_2)_{max} = 0.1$ and $\alpha'_{max} = 0.6$ from Figures 7 and 9. Note that this corresponds to a maximum growth rate wavelength-to-film thickness ratio of about 10 which corresponds to the visual experimental observations made in a tube with annular flow reported in Reference 30. From Reference 28 $\ln B^*/B_o = 12$ and from Figure 8, $F_{max} = 4 \times 10^{-9}$. Therefore, the magnitude of E is

$$E = \frac{12(0.1 + 1)}{0.6\,(4 \times 10^{-9})} = 5.5 \times 10^9$$

This calculation is for film breakup for which liquid drops are entrained. As already pointed out, the integration limits (and therefore $\ln B^*/B_o$) would be different for slugging conditions. As a check on the above calculation note that Equation 17 indicates that L^*/δ is a function of Re_f . Data are plotted in terms of these quantities from eight different sources (primarily for annular flows) in Figure 12. Table I describes the test conditions in detail. Figure 12 indicates that the data lie approximately on a 45 degree line. The film thickness, δ , therefore, plays no role in the breakup length. This is consistent with the model used in deriving Equation 17. Thus, Equation 17 can be empirically adjusted to the form $L^* u_2 \rho_f / \mu_f = 1.6 \times 10^6$. If it is assumed that $Re_{fn} \ll Re_f$, then Equation 17 can be written as

$$\frac{L^* u_2 \rho_f}{\mu_f} = E = 5.5 \times 10^9$$

The value (5.5×10^9) predicted by the method developed herein does not agree with that indicated by experiments (1.6×10^6). The lack of agreement between the predicted and experimental results should not be too disturbing because the predictions were calculated essentially from the work of Reference 17 for hydrodynamic instability of plane adiabatic thin films in Couette flow. In the experiments the flows were mainly annular with heat transfer in some cases, and the Kelvin-Helmholtz instability could also have influenced the film breakup. Further, the analysis of Reference 17 which was based on the theory of small perturbations loses accuracy as wave amplitudes become sufficiently large. If the disagreement between predictions and reality persists after more appropriate data for both calculations and experiments have been obtained, the predictions would have to be based on a higher-

BREAKUP LENGTH VERSUS REYNOLDS NUMBER

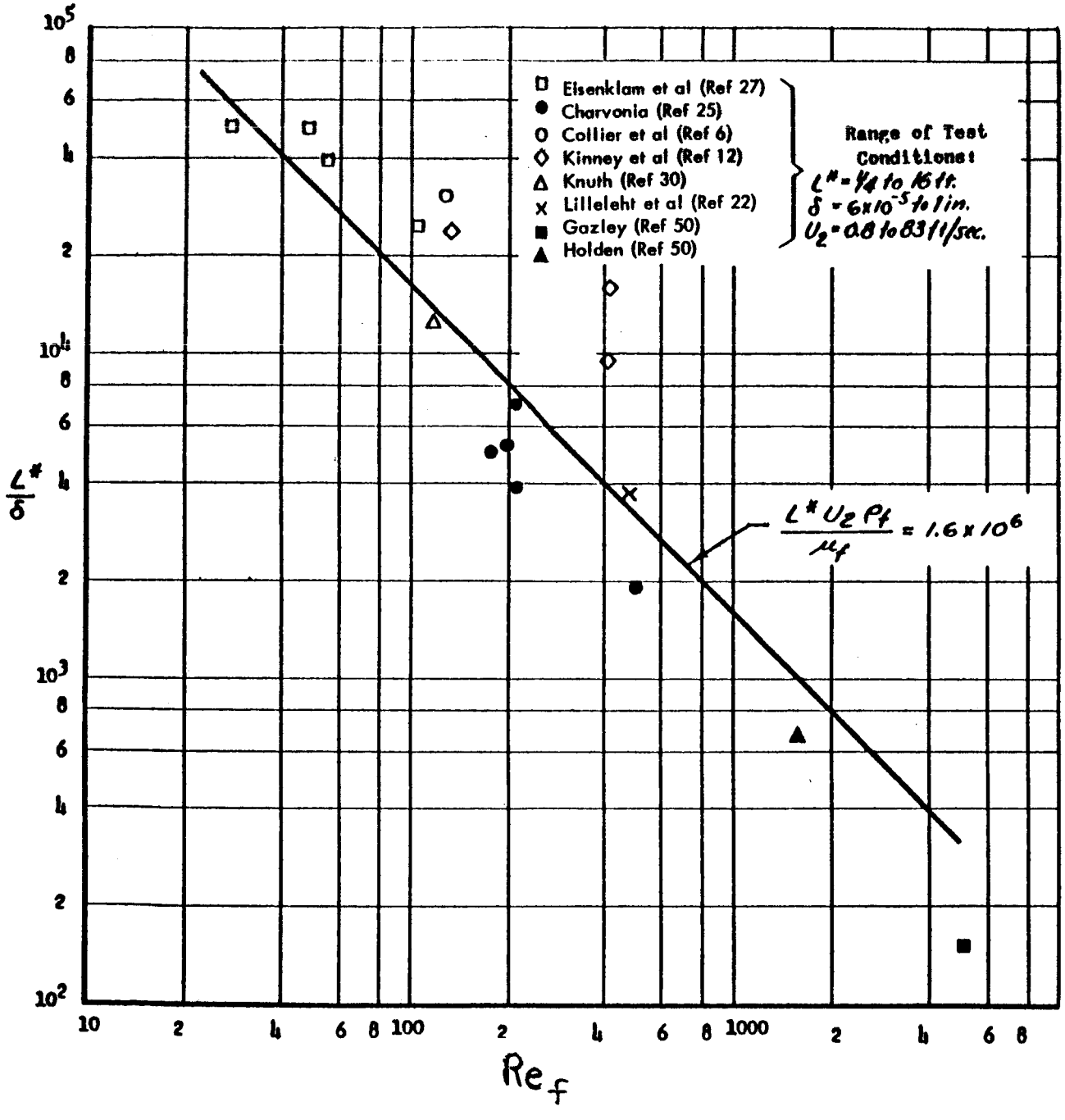

FIGURE 12

TABLE I

FILM BREAKUP TEST DATA

Source	Test Description	Air Velocity U_v ft/sec	Mean Liquid Velocity U_f ft/sec	Interface Velocity U_2 ft/sec	Instability Length L^* ft	Type of Instability	Film Thickness δ ft	W_f	R_f	$\frac{L^*}{\delta}$
1. Eisenklam et.al.	Sheets of liquid ejected from nozzles		81.3 (2480 cm/sec)		0.338 (10.3 cm)	Breakup	1.36×10^{-5} $\frac{(8.3 \text{ microns})}{2}$	35	104	2.48×10^4
2.			58 (1770 cm/sec)	$U_2 \approx U_f$	0.39 (11.9 cm)	Breakup	1×10^{-5} $\frac{(6.1 \text{ microns})}{2}$	13.1	54.5	3.9×10^4
3.			82.6 (2520 cm/sec		0.309 (9.4 cm)	Breakup	0.623×10^{-5} $\frac{(3.3 \text{ microns})}{2}$	16.7	48.3	4.95×10^4
4.			59 (1800 cm/sec)		0.253 (7.7 cm)	Breakup	0.507×10^{-5} $\frac{(3.1 \text{ microns})}{2}$	6.9	28.2	4.98×10^4
5. Charvonia	Annular two-phase flow - Horizontal	132			2.33	Breakup	0.471×10^{-3}	0.944	178	4.96×10^3
6.		162			2.33	Breakup	0.454×10^{-3}	1.22	195	5.14×10^3
7.		112			2.33	Breakup	0.605×10^{-3}	0.786	210	3.86×10^3
8.		45			2.33	Breakup	1.21×10^{-3}	1.12	500	1.93×10^3
9.		193			2.33	Breakup	0.333×10^{-3}	2.61	210	7×10^3
10.										
11. Collier et.al.	Annular two-phase flow - Vertical-up	260	2.04	4.08	10	Breakup	0.333×10^{-3}	2.16	129	3×10^4
12. Kinney et.al.	Annular two-phase flow - Horizontal			17.5	4	Observed Surf Dist. Near Cool. loss	1.667×10^{-4} (0.002 in)	19.8	135	2.4×10^4
13.				21		"	4.16×10^{-4} (0.005 in)	71.4	415	9.59×10^3
14.				30		"	2.5×10^{-4} (0.003 in)	87.2	415	1.6×10^4
15. Knuth	Annular two-phase flow - Horizontal			3	5.06	Near Point of Liquid Breakup	4.16×10^{-4} (0.005 in)	1.45	118	1.21×10^4
16. Lilleicht et.al.	Annular two-phase flow - Horizontal	23.6		1.61	11.666	Onset of Roll Waves	3.15×10^{-3}	3.17	480	3.7×10^3
17. Gazley		≈ 12		0.801	10	Hydrodynamic Rough-rapid Wave Form.	6.66×10^{-2} (≈ 0.8 in)	16.6	5060	1.5×10^2
18. Holden		≈ 10		0.666	16	"	2.5×10^{-2} (≈ 0.3 in)	4.3	1580	6.4×10^2

order theory to account for the fact that the amplitudes near breakup are large. Some study of the growth of waves with large amplitudes has already been made (Reference 31) and it has been found therein that when the wave amplitude has grown sufficiently it remains constant, i.e., the growth rate goes to zero. If this were so in the present problem, it would imply that L^* (predicted) should be less than L^* (experimental) for from Equation 17 it can be seen that if F_{max} (which is related to the growth rate) decreases, L^* increases. Clearly this is another aspect of the problem which should at least be kept in mind.

The calculation method described herein appears to be more plausible, however, if comparison is made with results more closely analogous to the conditions of the theoretical model. For example, for the special case of a single-phase boundary layer $\rho_v/\rho_f = 1$ and $\mu_f/\mu_v = 1$. Then according to Reference 32 for laminar-turbulent transition on a flat plate

$$\left(\frac{L u_\infty \rho}{\mu}\right)_{transition} = 2.8 \times 10^6$$

This number is, of course, of the same order of magnitude as that experimentally determined herein, as is to be expected. This also further substantiates the previous discussions that indicate the work of Reference 17 is directly related to hydrodynamic instability.

In summary, it can be stated that the above derivation is general, i.e., it can be applied to any configuration and instability type. It was applied to a specific problem herein merely for illustrative purposes. To extend the applicability to non-adiabatic flows such as are of interest in condensing problems, the second term of Equation 3 must be dealt with. However, on the assumption of fully developed flow, this term can be shown to be of little significance and, again, only the basic data such as α', C_R/u_2 etc. must be found for the application of the method to this case.

By applying the growth rates of Reference 20 (see Figure 2) to a mathematical treatment similar to the one already presented, it can be shown that the Kelvin-Helmholtz instability can be expressed in terms of a Weber number based on breakup length, namely,

$$\frac{L^* \rho_f u_2^2}{\sigma}$$

If we are consistent with our original premise that the maximum growth rate wave dominates the interfacial breakup, then we can assume that whichever instability, hydrodynamic or Kelvin-Helmholtz, gives the smaller breakup length, that will be the one of interest. This is rational since the greater the growth rate, the smaller the length. These assumptions are, of course, subject to experimental verification.

4.1.1.3 Stability of Condensing Films

Condensation introduces additional complexities into the mechanics of film stability. Condensation requires some modification in the boundary conditions used in the development of the stability equations of References 17 and 20. Also δ, Re_f, W_f and u_2 are

BREAKUP REYNOLDS NUMBERS VERSUS CONDENSATION VELOCITY RATIO

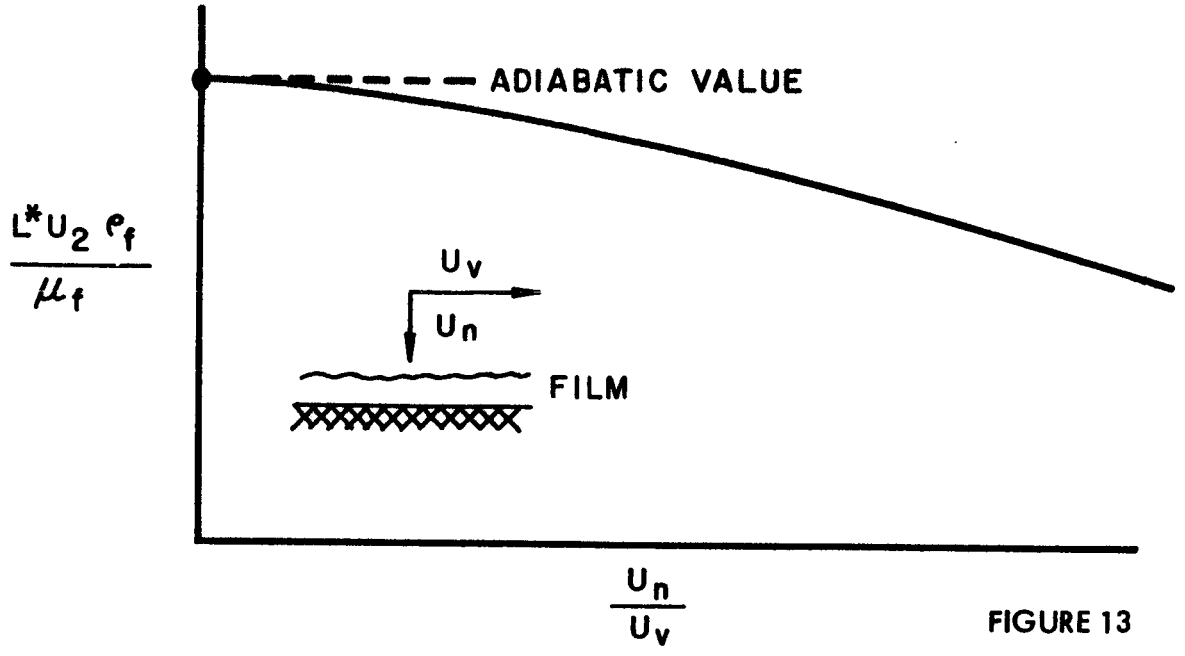

FIGURE 13

functions of length L for the case of condensation and are thus considered variables during the integration for breakup length.

The boundary equation for the vapor-liquid interface contains an equality of normal, shear, and surface tension forces. Condensation contributes an additional shear and normal stress term created by the vapor velocity normal to the interface, u_n, which depends on the magnitude of the heat flux. These stresses are,

Condensation normal stress:

$$\Delta P_m = \frac{\rho_v u_n^2}{2} \quad * \qquad \text{(Eq 19)}$$

Condensation shear stress:

$$\tau_m = \rho_v u_n u_v \qquad \text{(Eq 20)}$$

To determine the effect of these quantities on the growth rate factors (C_i or S) will require detailed analytical investigations.

The effects of condensation on film stability can be investigated empirically by plotting the "breakup" Reynold's number versus the ratio u_n/u_v as in Figure 13. When this quantity approaches zero, we are near adiabatic conditions.

* $Q/A = u_n \rho_v h_{vf}$

A designer desiring to apply the "breakup" Reynold's number to a condensing film must determine the interface velocity, u_2. Normally the vapor velocity, u_v, is the known quantity. The ratio u_f/u_v, the mean film velocity to the mean vapor velocity, is called the slip and is determined by an involved momentum transfer analysis which will not be covered in this report. The results of two investigations will be cited which should suffice, namely:

Reference 21:

$$\frac{u_f}{u_v} = \left(\frac{\rho_v}{\rho_f}\right)^{\frac{1}{2}} \quad \text{(Eq 21)}$$

Reference 24:

$$\frac{u_f}{u_v} = \left(\frac{\rho_v}{\rho_f}\ \frac{1}{2\alpha'''}\right)^{\frac{1}{2}} \quad \text{(Eq 22)}$$

where α''' is the volume fraction occupied by the vapor which approaches one for most two-phase flow systems under consideration. For thin films a linear velocity profile can be assumed. Thus, $u_f = u_2/2$

4.1.2 Horizontal Two-Phase Flow

Two-phase phenomena are generally complex and this is more the case when heat transfer is also considered. It is possible, however, to make certain general and specific observations for the case at hand, namely, the forced convection wetting condensation of mercury in horizontal tubes. For this case, the general adiabatic two-phase flow observations and data should be applicable. In particular, flow regime can be identified and the appropriate pressure drop and inventory correlations applied. Such an approach was successful for the case of Refrigerent-22 condensing in horizontal tubes (Ref 33). In this instance, the Martinelli-Nelson approach was used to predict pressure drop to within ±30%. Similar ability to predict pressure drop is expected for most of our range of operations as the primary regime anticipated is that of annular flow. This regime should be amenable to the Martinell-Nelson equations.

In terms of the fluid mechanics problem, the effect of a heat transfer is to cause an apparent vapor velocity normal to the wall. This has two consequences. There is a momentum change with length for the fluid passing through the pipe and, in addition, the flow configuration is altered as compared to the same flow rates for each phase without any heat addition. Because visual observations are so difficult when there is heat addition, there are very few such observations.

One of the most striking characteristics of a two-phase flow is that, in general, the phases do not move at the same velocity. The gas phase usually moves more rapidly than the liquid phase. Because of this, it has been found convenient to speak of a slip velocity ratio. If this ratio is specified, then it is possible to determine the density of the mixture in the pipe

from the flow rates of each of the phases. The slip velocity ratio is related to the density in the following manner: The continuity equation on each phase yields

$$w_v = w_T x = \frac{u_v A_v}{v_v}$$

$$w_f = w_T(1-x) = \frac{u_f A_f}{v_f} \qquad \text{(Eq 23)}$$

A_v and A_f are the cross-sectional areas of a pipe occupied by the vapor and a liquid, respectively. If A_p is the cross-sectional area of the pipe, then A_v/A_p is the fraction occupied by the gas. The static quality X_s is the ratio of the weight of vapor in a section of pipe to total weight of liquid and vapor in that section. For an arbitrary length of pipe, the static quality becomes

$$X_s = \frac{A_v/v_v}{A_v/v_v + A_f/v_f} .$$

When Equation 23 is substituted then

$$X_s = \frac{w_o(x/u_v)}{\frac{w_o x}{u_v} + \frac{w_o(1-x)}{u_f}} .$$

Thus, on re-arranging,

$$\frac{x}{1-x} = \frac{u_v}{u_f}\left(\frac{x_s}{1-x_s}\right) . \qquad \text{(Eq 24)}$$

Particularly at low pressure, the vapor phase normally moves with many times the velocity of the liquid phase, so the static quality is much lower than the flowing quality.

Several different experimental methods exist for determining the static quality and therefore the slip. One consists of suddenly isolating a section of pipe in which the flow is taking place and measuring how much liquid is present. Another method is to use a collimated gamma ray source and measure the attenuation in passing through the pipe. If the flow configuration is simple enough, a photograph can often yield the desired information.

When two phases flow in a horizontal pipe they can be distributed in the pipe in a number of different configurations. These configurations are called flow regimes and the analysis of any two-phase flow problem begins by specifying what the flow regime is.

Figure 14 illustrates the flow regimes that can exist in a horizontal pipe while Figure 15 shows a flow map that allows one to determine what the flow regime is when the pipe size and the flow rates of the two phases are know. The data of an additional reference (Ref 34) has been placed on this curve. It should be stressed that the divisions shown as lines in Figure 15 should really be bands. In addition, it should be stressed that this map applies only in fully developed flow for a wetting fluid without heat addition. The coordinates for this map are the ones suggested in Reference 35, while the data used to place the divisions are largely from References 36, 37 and 38. Insofar as most of the data were taken on pipes approximately one inch in diameter with air and water at low pressure, the placing of these lines must be regarded as tentative. Several of the flow regimes illustrated in Figure 14 are combined in the map of Figure 15. This has been done because the same analysis for the pressure drop and density applies for each of the groups of flow regimes.

HORIZONTAL PIPE TWO-PHASE FLOW REGIMES

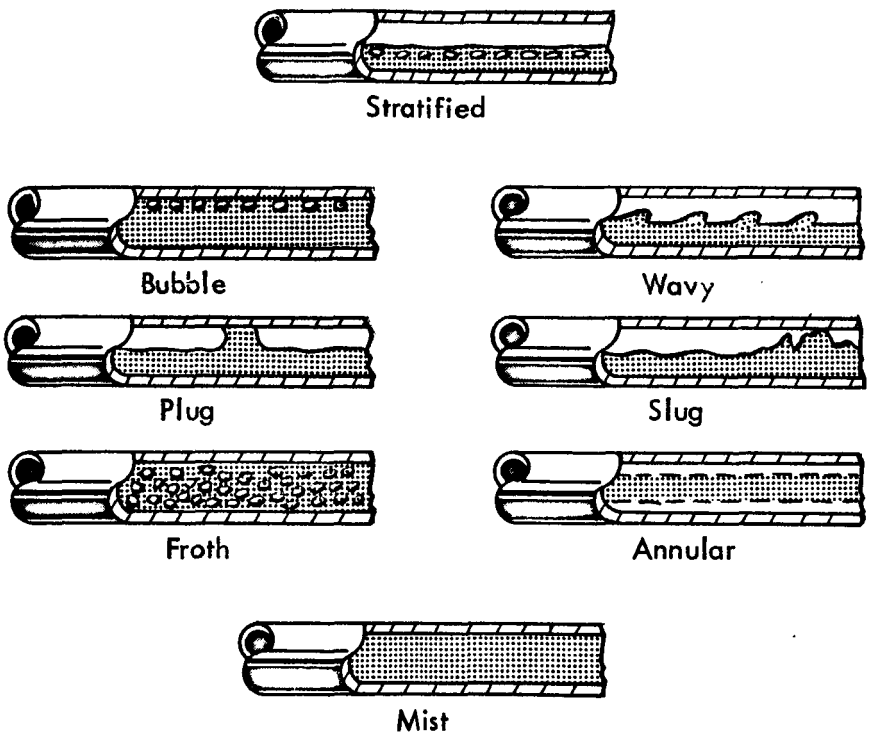

* For critical flow

FIGURE 14

Fairly complete empirical analysis of flow in large horizontal pipes is reported in Reference 37.

The major portion of any condensing rig is in the annular region but, depending on the tilt and the discharge end connections, it may go into the slug or stratified regime. To have stratified flow, of course, the tube exit quality must be greater than zero. A typical condensing run is plotted in Figure 15, which shows that annular flow is expected from 100% to about 5%

HORIZONTAL PIPE TWO-PHASE FLOW REGIME MAP FOR
ADIABATIC WETTING FLUIDS

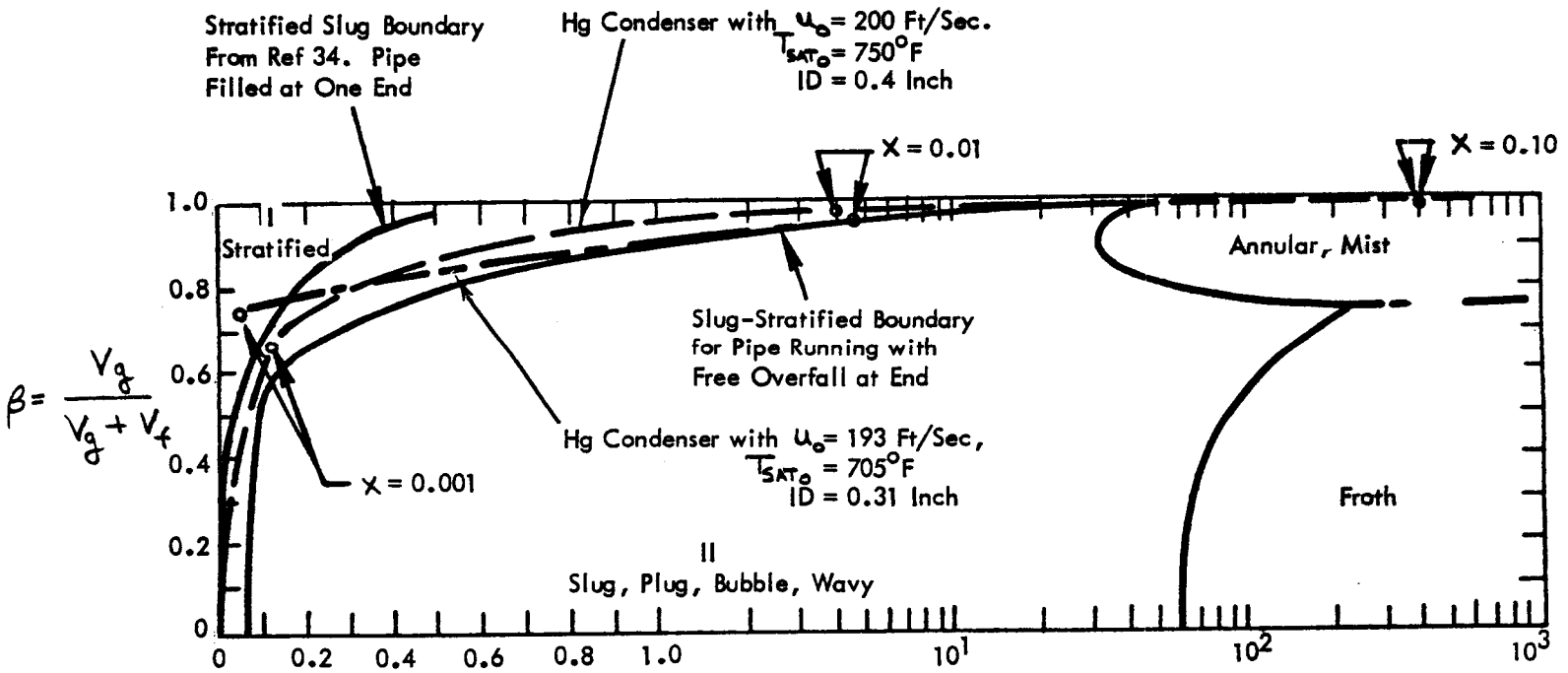

FIGURE 15

quality or until the vapor velocity is less than 10 ft/sec. (see Appendix C). For the constant diameter tube, this will not occur until the last several inches of the condensing section. At this point, stratified and/or slug flow would exist, depending on end conditions. Some pressure pulsations could occur even though the pressure drop in this region is expected to be essentially insignificant.

End conditions might determine the flow regime if one has an exit quality greater than zero, since the condensing run passes between the two slug-stratified transition limits shown, one transition being for a filled exiting pipe (Ref 38 and 39) and the other for an unfilled exiting pipe (Ref 34).

4.1.2.1 Annular Mist and Foam Flow in a Horizontal Pipe

Martinelli and others (Ref 40, 41, 42, 43) have developed the most general correlation available for calculating the pressure drop and density in a two-phase flowing system. Though there are some difficulties and internal inconsistencies in the analysis, it can be said for most of the region in which it is supposed to be valid that the Martinelli method predicts the pressure drops to within ± 30%. In the remainder of this section, the Martinelli method will be explained and its limitations pointed out.

Martinelli found in his original experiments that the pressure drop in two-phase flow is essentially independent of the details of the flow configuration so long as:

1. the flow is steady, and

2. there are no radial gradients in pressure in the tube, i.e., the static pressure drop in the liquid is equal to the static pressure drop in the vapor.

Essentially it is assumed, then, that an annular, annular spray or foam-flow pattern exists. Slug, wave and stratified flows are excluded from the pressure drop correlation.

To begin, Martinelli separated the various possible two-phase flows into four mechanisms. These mechanisms do not correspond directly to any particular regimes of flow but depend on whether the individual phases flowing in the pipe would be viscous or turbulent. They really should be regarded as a correlating device. These flow types or mechanisms are as follows:

1. Flow of both the liquid and the gas may be turbulent (turbulent-turbulent flow).

2. Flow of the liquid may be viscous and flow of the gas may be turbulent (viscous - turbulent flow).

3. Flow of the liquid may be turbulent and flow of the gas viscous (turbulent-viscous flow).

4. Flow of both the liquid and the gas may be viscous (viscous-viscous flow).

From the experimental data available at the time, the dividing line between the viscous and turbulent regimes was set as follows:

Flow Mechanism	Symbol	Re_{fp}	Re_{gp}
Turbulent-turbulent	t-t	> 2000	> 2000
Viscous-turbulent	v-t	< 1000	> 2000
Turbulent-viscous	t-v	> 2000	< 1000
Viscous-viscous	v-v	< 1000	< 1000

The region $1000 < Re < 2000$ is a transition region. To calculate the pressure drop which would take place in a two-phase flowing mixture, a quantity was defined which related the two-phase pressure drop to the pressure drop of either component flowing alone at its mass flow rate in the pipe. The definitions are as follows:

$$\Phi_f^2 = (\Delta P/\Delta L)_{TP} / (\Delta P/\Delta L)_f ,$$

$$\Phi_g^2 = (\Delta P/\Delta L)_{TP} / (\Delta P/\Delta L)_f .$$

The liquid and vapor fractions are defined below:

R_f = fraction of pipe area occupied by liquid,

R_g = fraction of pipe area occupied by gas.

The four quantities Φ_f, Φ_g, R_f, and R_g are just those needed to predict the pressure drop and density of a two-phase flowing system. By physical reasoning Martinelli postulated, subject to experimental verification, that they are all functions of a single variable which is defined as follows:

$$X^2 = \left(\frac{\Delta P}{\Delta L}\right)_f \Big/ \left(\frac{\Delta P}{\Delta L}\right)_g$$

(Eq 25)

This ratio can be calculated from the mass flow rates of the two components and the fluid properties. When this is done the result is

$$X = \frac{Re_{gP}^{m}}{Re_{fP}^{n}} \frac{C_f}{C_g} \left(\frac{w_f}{w_g}\right)^2 \frac{\rho_g}{\rho_f} . \qquad \text{(Eq 26)}$$

The exponents m and n and coefficients C_f and C_g are presented below:

	t-t	v-t	t-v	v-v
n	0.2	1.0	0.2	1.0
m	0.2	0.2	1.0	1.0
C_f	0.046*	16.0	0.046*	16.0
C_g	0.046*	0.046*	16.0	16.0

These values for the exponents and the coefficients are determined from the appropriate single-phase expressions for laminar and turbulent flow. Figure 16 shows Φ_{gtt} and Φ_{gvt} flow mechanisms plotted on the same curve.

Only one R_f curve, presented in Figure 16, was found to correlate the holdup data for all mechanisms. Later, in attempting to apply these results to steam-water mixtures at high pressure (Ref 42), it was found that the pressure drops were definitely over-predicted Because of this, Φ was allowed to take on an empirical pressure dependence. The low pressure Φ curves apply to Φ_{ftt}. In principle, they can be adapted for mercury condensing, but it is not recommended that they be used for the following reasons:

1. A large part of the region of interest is viscous-turbulent; for this region there are no pressure-corrected curves.

2. The two-phase pressure drop is tied to the single-phase liquid pressure drop. This view is more appropriate for boilers where 100% liquid enters and very low quality steam leaves than for condensers where vapor enters and most of the pressure drop occurs in the high-velocity range, vapor-fraction region.

If one examines the pressure sensitive Φ_{ftt} curves of Reference 42 closely, it can be seen that most of the pressure sensitivity could be eliminated by using Φ_{gtt} instead.

In the light of these considerations, it is recommended that Figure 16 be used along with a numerical integration up the tube.

* For smooth pipes

Φ_g VERSUS X FOR THE VISCOUS-TURBULENT AND TURBULENT-TURBULENT MECHANISMS AND R_f VERSUS X (FROM REF 40)

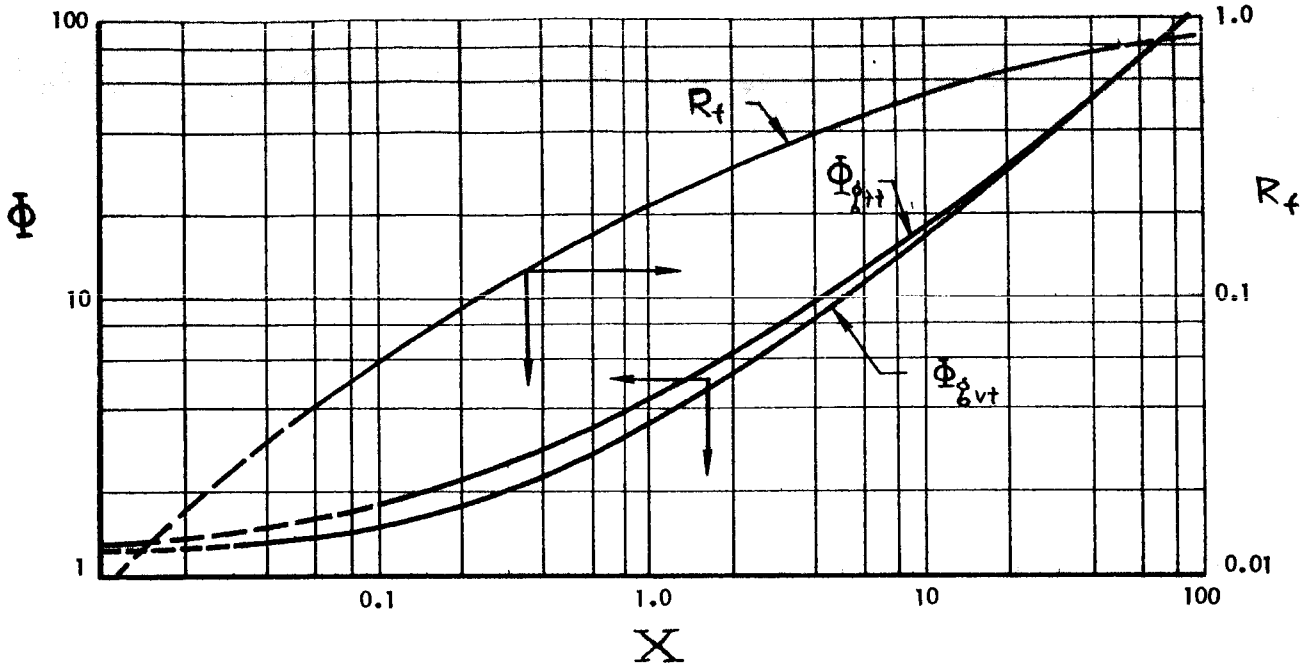

FIGURE 16

TWO-PHASE SLUG FLOW FRICTION FACTOR MULTIPLIER TO BE USED IN EQUATION 27, (FROM REF 34)

$$Fr_{MIXT} = \frac{\left(\frac{V_g + V_f}{A_P}\right)^2}{D_P g_c} \qquad \psi = \frac{f_{TP}}{f_o}$$

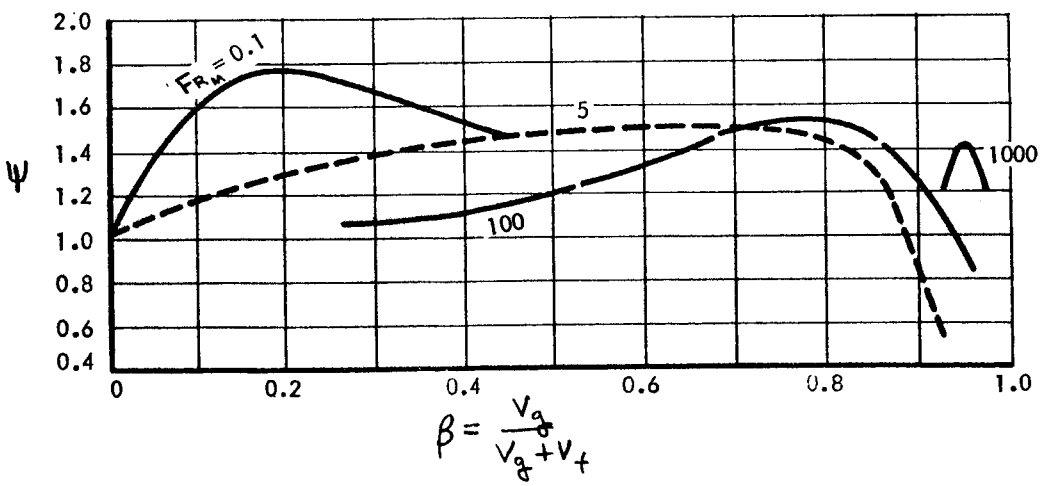

FIGURE 17

The original curves of Martinelli were taken at low pressure and should apply quite well to the case of mercury in the temperature range of 600° to 750°F. The values of X which are appropriate are very small, so it is recommended that the Φ_g curves be used because the variation of Φ_g with X in this region is very small. In fact, a constant value for Φ_g is probably adequate.

4.1.2.2 Slug, Plug and Wave Flow

This flow regime is analyzed in Reference 44 and the method proposed is based on that reference. For a straight tube the pressure drop in this regime is probably negligible.

Pressure drop is calculated from Figure 17 and the following equation:

$$\Delta P_{TP} = \frac{4f\Psi \frac{L}{D_P} \frac{(w_f + w_g)^2}{A_P^2}}{\left[\left(\frac{V_f}{V_f + V_g}\right)\rho_f + \left(\frac{V_g}{V_f + V_g}\right)\rho_g\right]} \qquad \text{(Eq 27)}$$

f = Moody friction factor

Ψ = multiplier from Figure 17.

The above equation is the usual pressure drop equation containing an arbitrarily defined mixture density.

The Reynold's number for obtaining the friction factor is defined below. The friction factor f can be obtained from the usual friction factor curve using this Reynold's number definition:

$$Re_m = \frac{4(w_f + w_g)}{\pi D_P \left[\left(\frac{w_g}{w_f + w_g}\right)\mu_g + \left(\frac{w_f}{w_f + w_g}\right)\mu_f\right]} \cdot \qquad \text{(Eq 28)}$$

To evaluate the density in slug flow, Reference 44 suggests that R_g (the fraction of the pipe filled with gas) for an absolutely horizontal pipe is

$$R_g = 0.83\left(\frac{V_g}{V_f + V_g}\right) \cdot \qquad \text{(Eq 29)}$$

This expression works well over the entire range of conditions in the slug, plug, wave flow regime of the flow regime map. It fails only when the pressure is close to the critical where the slug flow hardly exists anyway.

4.1.2.3 Stratified Flow

At very-low-volume flow rates the liquid and gas phases stratify with a smooth separation between them. As a rule, the pressure drops are very small. It has been found that usually the gas shear stress on the upper surface of the liquid is not very important in moving the liquid through the pipe, but that gravity plays the most important role. This means there is no "fully developed" flow but that for adiabatic flow the liquid level drops as the end of the pipe is approached. Thus the pressure drops are of the order of the tube diameter. The height of the liquid in the pipe and the pressure drop are both functions of the liquid of the pipe except for very long pipes.

Stratified flow is of no significance for the case of zero gravity condensing. However, tests must be run on earth and understood since a significant amount of inventory may be involved.

The most complete description of stratified flow is given by Bergelin and Gazley(Ref 38). Measurements of gas pressure drop and fluid heights were made in one-and two-inch diameter tubes, 10 and 16 ft long, for an air and water system. The gas-phase pressure drop data for the two-inch pipe was correlated by means of an apparent Reynold's number and friction factor. The friction factor is defined in the following equation:

$$-\left(\frac{dP}{dL}\right)_g = \frac{4 f w_g^2}{2 g_c \rho_g \left(\frac{\pi}{4}\right)^2 D_p^5} \qquad \text{(Eq 30)}$$

while Reynold's number is defined as

$$Re_g = \frac{4 w_g}{\pi D_p \mu_g}. \qquad \text{(Eq 31)}$$

A typical plot of friction factor versus Reynold's number is shown in Figure 18. Figure 19 gives the liquid heights in the pipe ten feet from the free overfall.

The friction factor curves of Figure 18 are somewhat misleading as the true area for gas flow is not the pipe area. If the measured liquid heights are used to find the true area available for gas flow and the "hydraulic diameter" concept is used to compute a Reynold's number, the friction factor versus Reynold's number curves all fall very close to that for a smooth pipe in both the laminar and turbulent region. When a sufficiently high Reynold's number is attained in the liquid, the interface becomes wavy and the friction factor increases very rapidly. A large fraction of the total liquid in the system is probably in that part of the system which might be in stratified flow. The typical run shown in Figure 15 indicates that whether the nappe springs free at the end or not and whether the tube runs full depends on the end connections. The difference between the full and not-full case is quite substantial. It is also not clear whether liquid inertia and vapor shear will substantially assist in carrying

FRICTION FACTOR VERSUS REYNOLD'S NUMBER FOR STRATIFIED FLOW IN A 2.065 INCH ID PIPE WITH VARIOUS WATER FLOW RATES

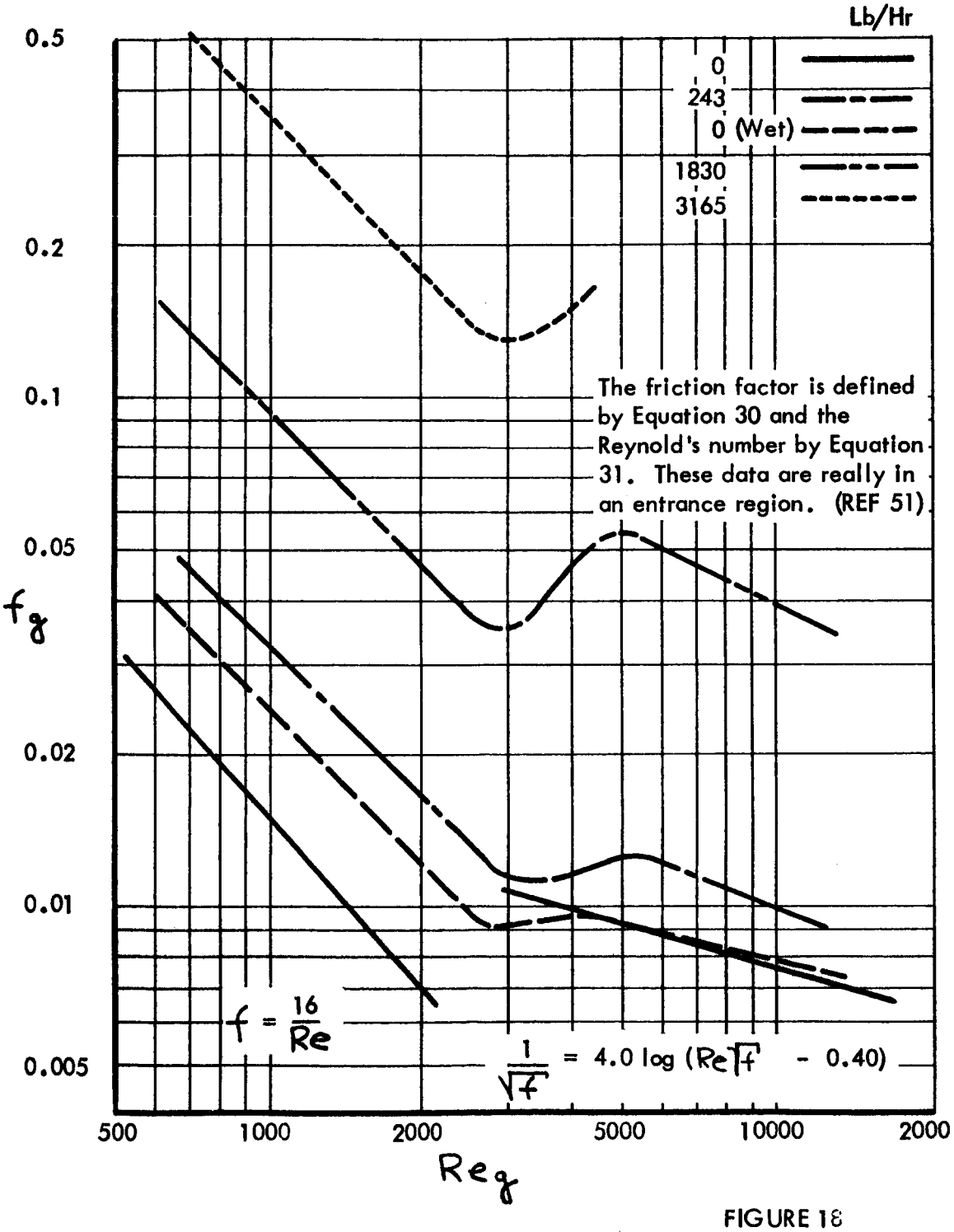

FIGURE 18

INTERFACIAL HEIGHT IN A 2.065 INCH ID PIPE WITH CO-CURRENT FLOW OF AIR AND WATER (REF 51)

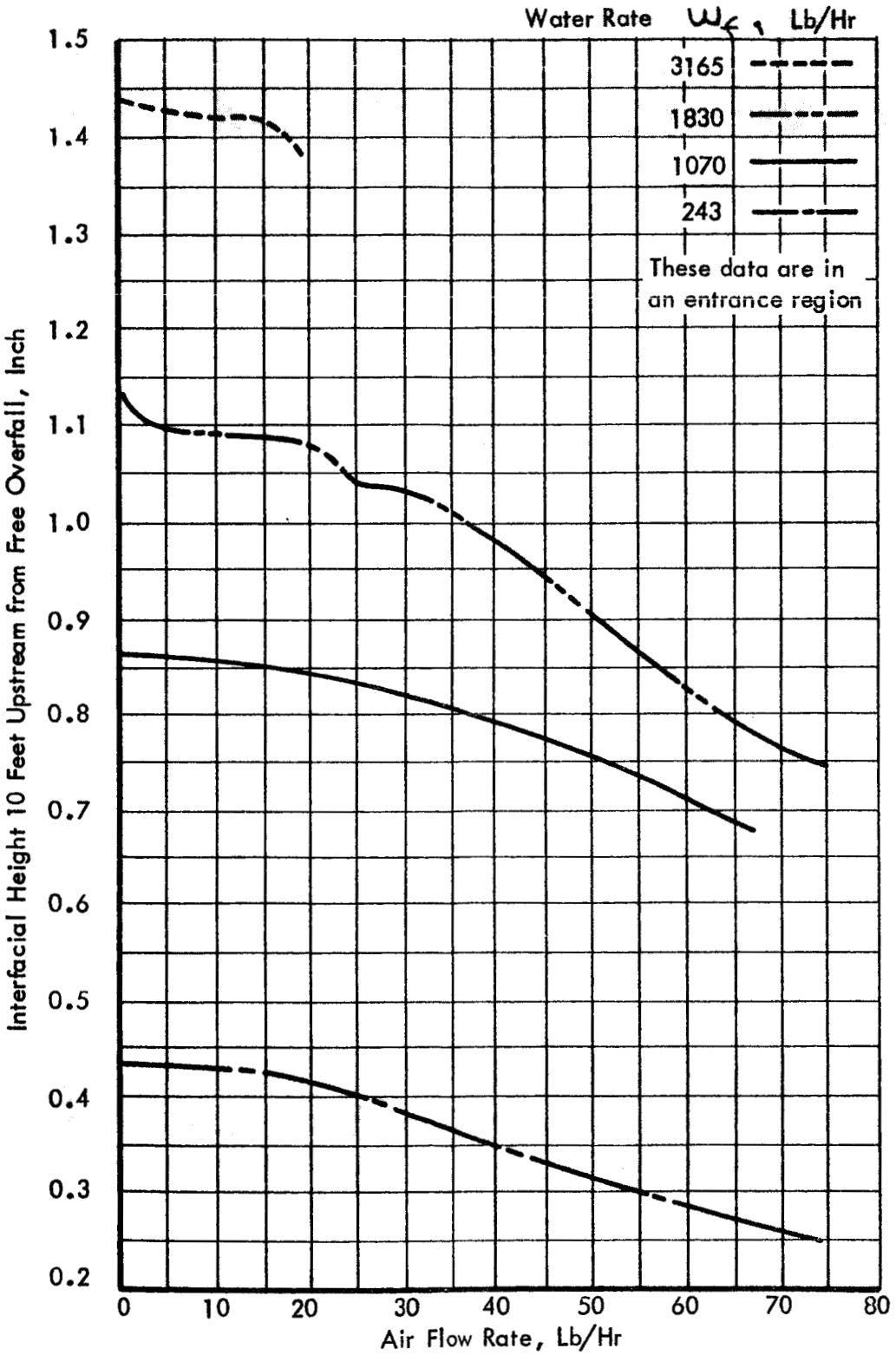

FIGURE 19

PRESSURE FLUCTUATIONS IN HORIZONTAL SLUG FLOW (FROM REF 34)
CROSS-PLOTTED FOR SMALL DIAMETERS

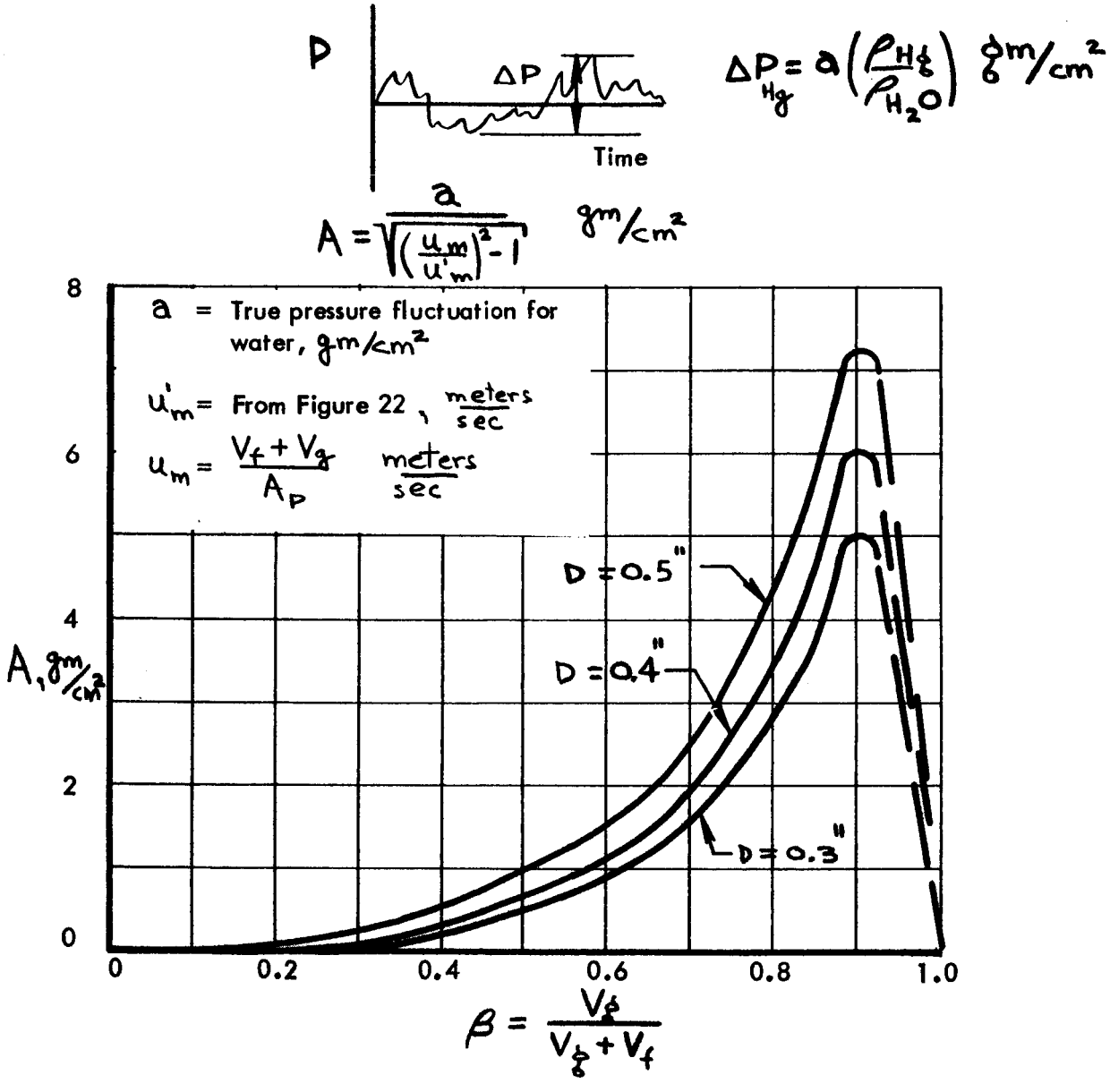

FIGURE 20

REDUCED FREQUENCY OF PRESSURE PULSATIONS AS A FUNCTION OF THE GAS CONTENT FOR THE FLOW OF WATER AND AIR IN HORIZONTAL PIPES WITH DIAMETERS FROM ABOUT 1 TO 4 INCHES (REF 34)

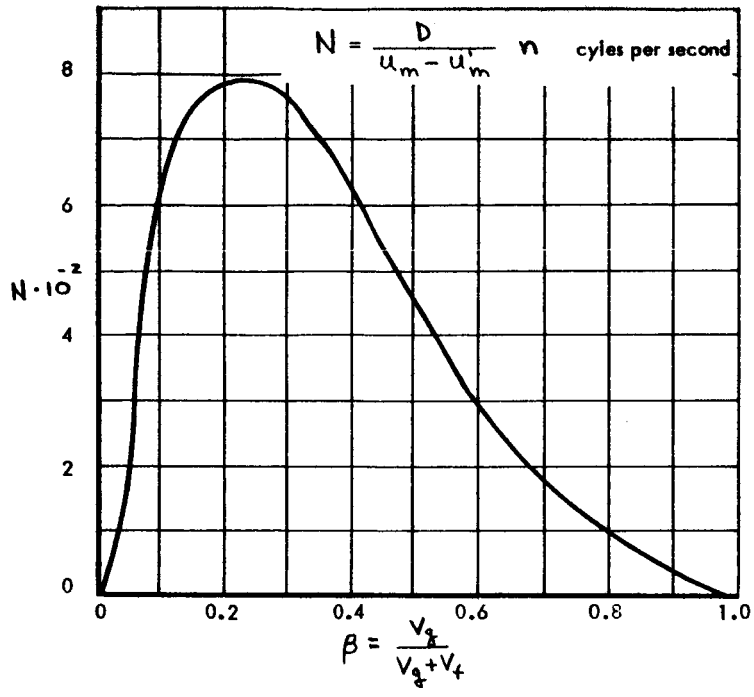

FIGURE 21

SPEED OF MIXTURE u'_m AT THE STRATIFIED FLOW LIMIT AS A FUNCTION OF GAS CONTENT AND PIPE DIAMETER (FROM REF 34)

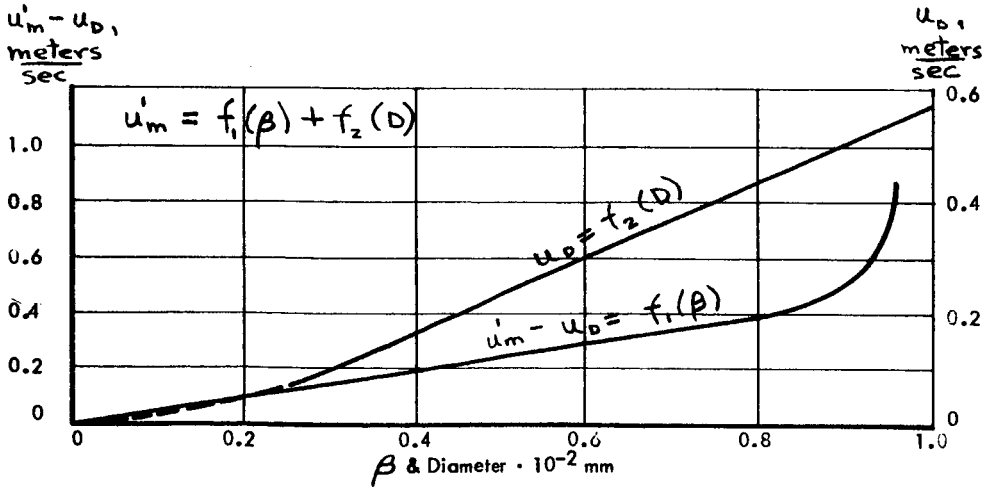

FIGURE 22

the liquid along in stratified flow.

In any case, it is desirable to have a method for estimating the density in stratified flow. Figure 19 gives this. Once stratified flow occurs, the depth is quite constant as a "dam" at the discharge limits the flow. Chato (Ref 39) found a short ramp of liquid at the beginning of stratified flow leading up to the virtually constant depth portion. This ramp is largely supported by the shear of the vapor.

The depth from Figure 19 is the depth at the discharge section. Equation 32 from Reference 39 for an air-water experiment or a rough calculation going back from the discharge will give the depth inside the tube. It is not recommended undertaking any calculation here though, unless the experiment indicates stratified flow is an important flow regime.

In Reference 39, flow regime observations were made for inlet velocities of 6 ft/sec or less and it was found that the conditions of discharge from the tube were very important in determining how much inventory there was in the tube. Tilt was also found to affect inventory tremendously, with one degree change having a significant effect.

4.1.2.4 Pressure Fluctuation Frequency and Amplitude

Both these quantities can be estimated from the adiabatic information given in Reference 34. Significant fluctuations occur only in the slug, plug, and wavy region. One will usually pass through this region, however, in the last few inches of the condenser, so the fluctuations may never develop any great amplitude. As a result, the results presented below will be conservative. In addition, the whole range of fluctuation amplitudes will (theoretically) be passed through so that one hardly knows what to expect in an experimental measurement in a condenser. Some of the data given in Reference 34 were located on the flow regime map, Figure 15, and were found to lie in the middle of the slug flow regime. The data of Reference 34 were taken without heat transfer in 1, 2, 3 and 4 inch pipes with air and water at low pressures. Pressure oscillations amplitudes, and frequencies were measured and correlated in the the manner shown in Figures 20, 21, and 22.

Pressure fluctuation amplitude may be estimated from Figure 20 where

u_m is the mixture velocity = $\frac{V_f + V_g}{A_p}$

u'_m is the stratified slug transition velocity and a function of pipe diameter and quality as given in Figure 22.

a is the fluctuation double amplitude for water. Because of the relationship of pressure drop to liquid density at constant velocity ($\Delta P \propto \rho$), it is recommended multiplying this value of a by a constant ρ_{Hg}/ρ_{H_2O} to estimate the pressure fluctuations with mercury.

Figure 20 was obtained by cross plotting and extrapolating the larger tube size data of Reference 34 to the smaller tube size range of interest.

The frequency of pressure fluctuation can be obtained from Figure 21 taken from Reference 34 directly. In Figure 21, the actual frequency, n, is obtained for a given gas content via the reduced pressure parameter N. u_m and u'_m are defined above.

4.2 Forced Convection Condensation of Non-Wetting Mercury in Zero Gravity

A drop-type flow regime is expected during the non-wetting condensation of mercury in zero gravity or with high vapor velocity. The condensed mercury is expected to condense on the surface and form a thin film (approximately 1 to 10 microns) which grows until it becomes unstable and breaks into drops (Ref 45). The drops formed have been observed in transparent tubes (Ref 4 and 5) and via the fluoroscopic observations of this program. The drops were observed to grow to a critical size and be accelerated toward the interface by vapor flowing over them.

The non-wetting property and high surface tension often encountered with mercury rarely result in stable films of pure liquid mercury in a flowing system. Droplets dispersed in a vapor phase was the flow pattern observed in all two-phase flow tests made in transparent tubes using non-wetting liquid mercury in either nitrogen gas or in mercury vapor (Ref 5). The non-wetting flow regime map of Figure 23 resulted from these tests.

In postulating either a heat transfer model or a fluid dynamic model for analytic purposes, a flow pattern involving liquid drops is therefore assumed. In condensing it is assumed that growing stationary surface drops are swept into the flowing vapor when they reach a certain critical size. The critical droplet size is determined by the vapor velocity, as shown in Reference 5. Since gas velocity will usually vary axially in a condenser, droplets of different sizes result. Figure 24 illustrates the flow pattern encountered during condenser tests.

The basic flow regime for the non-wetting condensation of mercury is then one of droplets on the wall and in the vapor stream. Droplet distribution is, of course, affected by gravity. In zero gravity a pure random drop distribution created by the mechanism described above is expected. With vertical upward and downward condensation, a significant effect on the phenomena would be expected. For example, in vertical upward flow higher velocities are required to prevent drops from falling opposite to the direction of flow. Vertical condenser design considerations were reviewed by TRW in Reference 5.

The two-phase static pressure gradient of a condenser with a flow pattern as depicted in Figure 24 can readily be obtained from the momentum equation. The two-phase static pressure gradient consists of three terms, namely,

$$\frac{dP}{dL} = \left.\frac{dP}{dL}\right|_{\substack{\text{drag of}\\ \text{transit drops}}} + \left.\frac{dP}{dL}\right|_{\substack{\text{stationary}\\ \text{drops and wall}}} + \left.\frac{dP}{dL}\right|_{\text{momentum}} \qquad \text{(Eq 32)}$$

The most difficult term to evaluate is the first term since it must encompass drops of all sizes. This can be accomplished by means of a distribution function as follows:

FLOW REGIMES FOR NON-WETTING MERCURY
FLOWING WITH NITROGEN IN GLASS TUBES

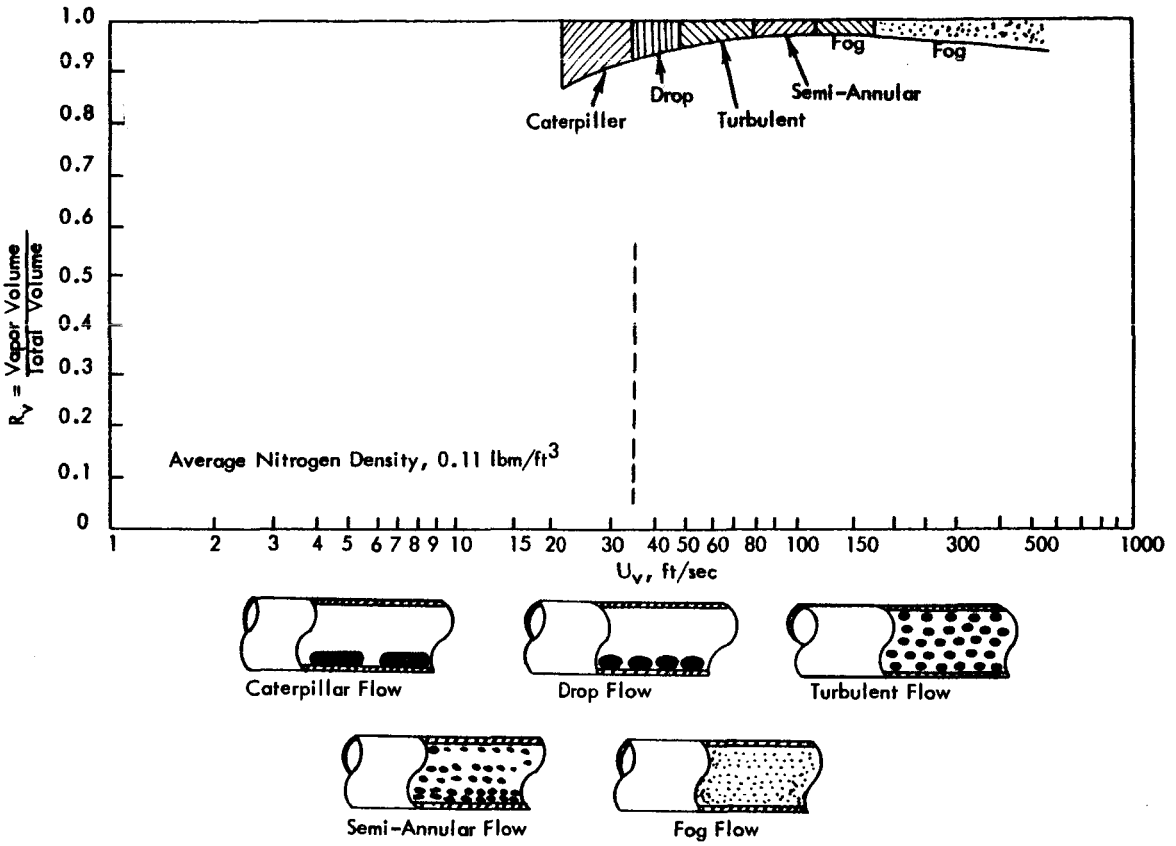

FIGURE 23

NON-WETTING MERCURY CONDENSING FLOW PATTERN SHOWING: (1) DROP ON HEAT TRANSFER SURFACE GROWING DUE TO CONDENSATION, (2) DROPS IN TRANSIT FLOWING TOWARD SUBCOOLER INTERFACE, (3) DROPS OF DIFFERENT DIAMETERS DUE TO A VARIABLE AXIAL VAPOR VELOCITY

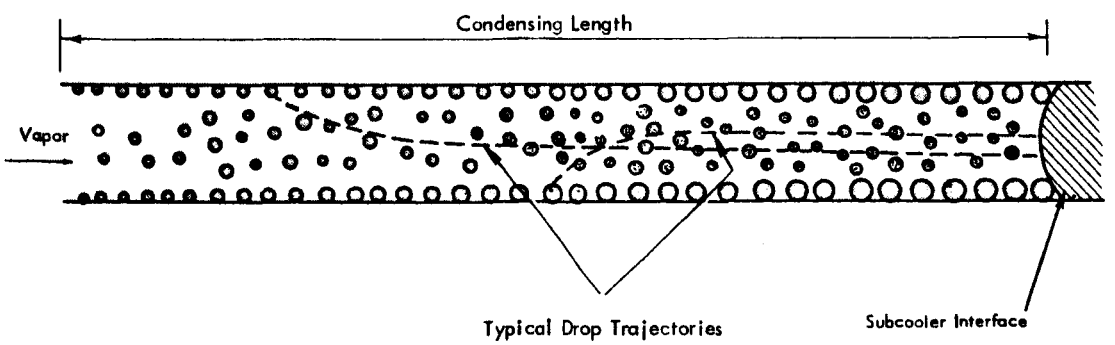

FIGURE 24

$$\left.\frac{dP}{dL}\right|_{\substack{\text{drag of}\\ \text{transit drops}}} = -\frac{2\omega^2 x^2}{\pi \xi_c D^4 \rho_v} \int_{\delta_{co}}^{\delta_c(L)} C_d N (1-\epsilon)|1-\epsilon| \delta^2 d\delta \qquad \text{(Eq 33)}$$

where N is the distribution function and $N\,d\delta$ represents the number of drops per unit volume having diameters between δ and $\delta+d\delta$ at distance L along the tube. Equation 33 is derived in Appendix B, where N is shown to be

$$N = \frac{6\rho_v}{\pi \rho_f}\left(\frac{\pi D^2 \rho_v}{4\omega}\right)\frac{1}{\delta^3 \epsilon x}\,\frac{1}{\left(-\frac{d\delta_c}{du_v}\right)} \cdot \qquad \text{(Eq 34)}$$

The term $\left(-\frac{d\delta_c}{du_v}\right)$ is evaluated by tests as described in Reference 5. For zero gravity and horizontal tubes,

$$\frac{\delta_c \rho_v u_v^2}{\sigma 2\xi_c} = 4E_\sigma \qquad \text{(Eq 35)}$$

$$\frac{d\delta_c}{du_v} = -\delta^{3/2}\left(\frac{\rho_v}{E_\sigma \sigma 2\xi_c}\right)^{1/2} \qquad \text{(Eq 36)}$$

where E_σ is a constant as evaluated by experiment and represents the amount of deformation from the action of surface forces (drag) and body forces that a stationary drop can withstand before it is entrained and transported by the flowing vapor.

The quantity ϵ in Equation 33 represents the velocity ratio of the liquid $\left(\epsilon = \frac{u_f}{u_v}\right)$ and is determined by means of the equations of motion as covered in Appendix B. In order to evaluate ϵ the following non-linear differential equation must be solved:

$$\frac{d\epsilon}{dL} = \frac{3}{4}\frac{\rho_v}{\rho_f}\frac{C_d}{\delta}\frac{(1-\epsilon)|1-\epsilon|}{\epsilon} - \frac{\epsilon}{x}\frac{dx}{dL} \cdot \qquad \text{(Eq 37)}$$

$(1-\epsilon)|1-\epsilon|$ is used rather than $(1-\epsilon)^2$ to account for proper sign in case $u_v < u_f$ which will occur in a constant diameter condenser, The coefficient of drag C_d can be evaluated by means of Figure 25 which takes into account the deformation of liquid drops due to drag.

The second term of Equation 32 is the pressure gradient induced by the "rough" surface composed of the wall with stationary growing (condensing) drops. An equation of the form,

$$\left.\frac{dP}{dL}\right|_{\substack{\text{stationary}\\ \text{drops and wall}}} = \frac{f_s}{D}\frac{(G_T x)^2}{\rho_v 2\xi_c} \qquad \text{(Eq 38)}$$

DRAG COEFFICIENTS FOR SPHERES, DISKS AND DROPS *

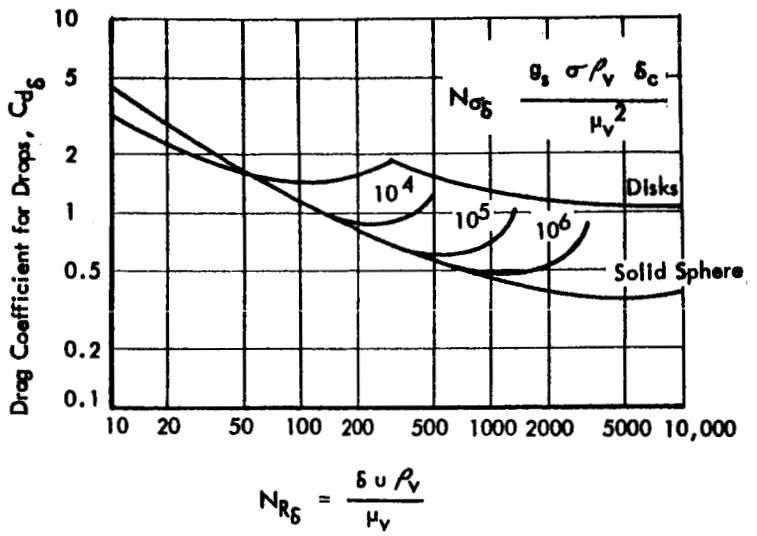

FIGURE 25

FRICTION FACTOR FOR SMOOTH AND SAND ROUGHENED PIPES AFTER NIKURADSE (REF. 48, FIGURE 84) *

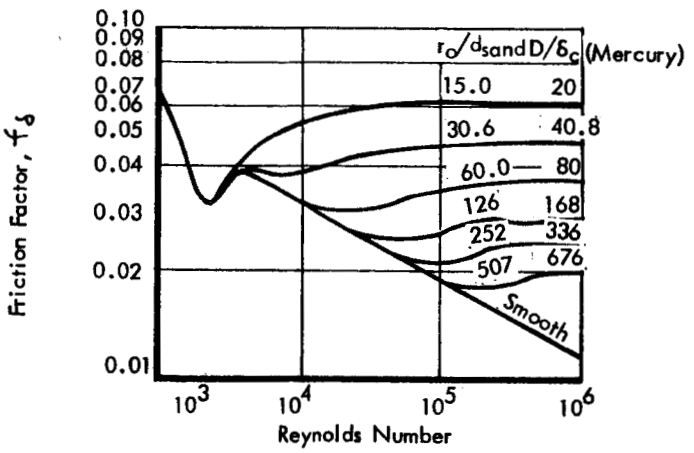

FIGURE 26

*See Hughes, R.R. and E.R. Gilliland, "The Mechanics of Drops" Chem. Engineering Progress, Vol. 48, No. 10, p 497

is recommended, where f_δ is the friction factor as produced by stationary, growing drops on the wall. As can be surmised, f_δ is a function of δ_c/D and the vapor Reynold's number $\frac{G_T \times D}{\mu_v \delta_c/D}$. This relationship is established in Reference 48 and is represented in Figure 26. δ_c/D is determined by means of Equation 35. This approach for accounting for the combined wall shear and drag of drops on the wall is based on the following factors:

1. Mercury drop populations, estimated on the basis of heat transfer considerations, are such that approximately 40% or more of the internal condensing area is covered.

2. Similar area coverage has been observed in the dropwise condensation of steam (Ref 46). With such large area coverage, Schlichting (Ref 47) has shown that spheres have the effect of a rough surface and Nikuradse's data for artifically roughened pipes, reproduced in Figure 25 may be used. In applying Figure 25 it is recommended that the equivalent sand roughness be assumed equal to the average drop size which is equal to 2/3 the maximum or critical drop size at entrainment.

The third term of Equation 32 is the pressure gradient induced by the vapor velocity changes caused by condensation and compressibility. For incompressible flow the momentum term can be calculated as follows:

$$dP \frac{\pi D^2}{4} = \frac{d(w_v u_v)}{g_c}$$

$$dP = \frac{d(G_v u_v)}{g_c}$$

$$dP = u_v \frac{dG_v}{g_c} + G_v \frac{du_v}{g_c} = \frac{G_v dG_v}{\rho_v g_c} + \frac{G_v dG_v}{\rho_v g} = 2 \frac{G_v dG_v}{g_c \rho_v} .$$

Since $G_v = x G_T$,

$$dG_v = G_T dx .$$

And for constant heat flux,

$$x = 1 - L/L_T$$

$$\frac{dx}{dL} = -\frac{1}{L_T} .$$

Thus

$$dP = \frac{2 G_T^2 dx}{g_c \rho_v}$$

$$\left.\frac{dP}{dL}\right|_{momentum} = -\frac{2G_T^2 x\,dx}{g_c \rho_v\,dL} = -\frac{2G_T^2 x}{g_c \rho_v L_T} \cdot \qquad \text{(Eq. 39)}$$

Equations 33, 38 and 39 can thus be used to predict the pressure drop during the non-wetting condensation of mercury in zero gravity. These equations are not very usable, however, and a computer simplification is required to make them so. Section 7 contains a comparison between a simplification of the theory and some data obtained.

The theory above gives a droplet size and number distribution function which could be used to calculate inventory. Consideration of the liquid on the wall is also required, of course. A major portion of the inventory will be in the low quality end, however, which is not amendable to analysis due to the influence of gravity on agglomeration.

Pressure fluctuations at the interface of a non-wetting condenser are principally due to impingement on the interface of liquid that has been picked up by the vapor or dragged along the wall. Again, the theory could be used except for the influence of gravity. The theory provides the droplet mass, velocity, and number from which momentum could be determined. The number of drops is so great, however, that the pressure pulsations would be so frequent as to be undetectable.

5.0 RIG DESIGN, INSTRUMENTATION, AND TEST PROCEDURE

5.1 Rig Design

A closed, natural circulation test loop was chosen to provide the wetting and non-wetting experimental data required. Figure 27 is a schematic representation of the test loop and Figures 28 and 29 are photographs of the rig. The use of a closed loop allowed continuous operation, although loop dynamics problems occurred as a result. Non-wetting data have been successfully obtained with the rig described below. Wetting data will be obtained with essentially the same rig, with wetting condensation induced by previously conditioning the tube.

Basically, the rig consisted of a mercury pot boiler, a heated and insulated line superheater, a horizontal condensing test section, a condensed-liquid collecting and flow metering system, and a return line to the boiler. The boiler was immersed in an electrically heated salt bath. Pressure taps were placed at 14.5 inch intervals on the replaceable test section for most of the testing and at 18 inch intervals for some of the earlier tests. The pressure measuring system consisted of mercury liquid-filled "U" tube manometers constructed from stainless steel and transparent plastic. All manometers were connected to an adjustable argon supply pressure to control the liquid mercury level. A shop air supply system provided a means for variable cooling of the condensing system.

Argon was used as a general cover gas for the system. An x-ray generator, control, fluoroscopic screen and appropriate shielding were mounted on a dolly so that the full 7.5 to 8 foot condensing length could be inspected and the condensing process thereby observed. This arrangement is illustrated in Figure 30.

The possibility of air leakage into the system was minimized by using welded bellows-sealed valves, argon cover gas(Linde Hi Purity 99.995%) and a mercury head. These features are particularly important to insure that the wetting condition is maintained, as de-wetting between mercury and metal surfaces has been observed after exposure to air (Ref 49). Maintenance of a relatively air-free system is also important to maintain a non-wetted condition. "Pseudo-wetting" was observed in experiments at TRW as a result of contamination due to air in the system. See Section 6.2.

5.1.1 Boiler

The boiler was an 8 inch diameter by 9.75 inch high stainless steel bucket partially immersed in a heat treat salt composed of 52% potassium nitrate, 40% sodium nitrite and 8% sodium nitrate. This salt melts at about 400°F and can be used in the range 500 to 1000°F. Electric immersion heaters capable of 9 kilowatt power output were used to heat the salt bath and thereby control the mercury flow rate. At mercury heights of 6, 5, and 4 inches, about 140, 118, and 93 pounds of mercury respectively, were contained in the boiler (at 700°F, ρ_f = 795 pounds per cubic foot). The salt level was maintained below that of the mercury but such that 3 pounds per minute of mercury could be evaporated at a heat flux of less than 20,000 Btu/per hour via the heat transfer area.

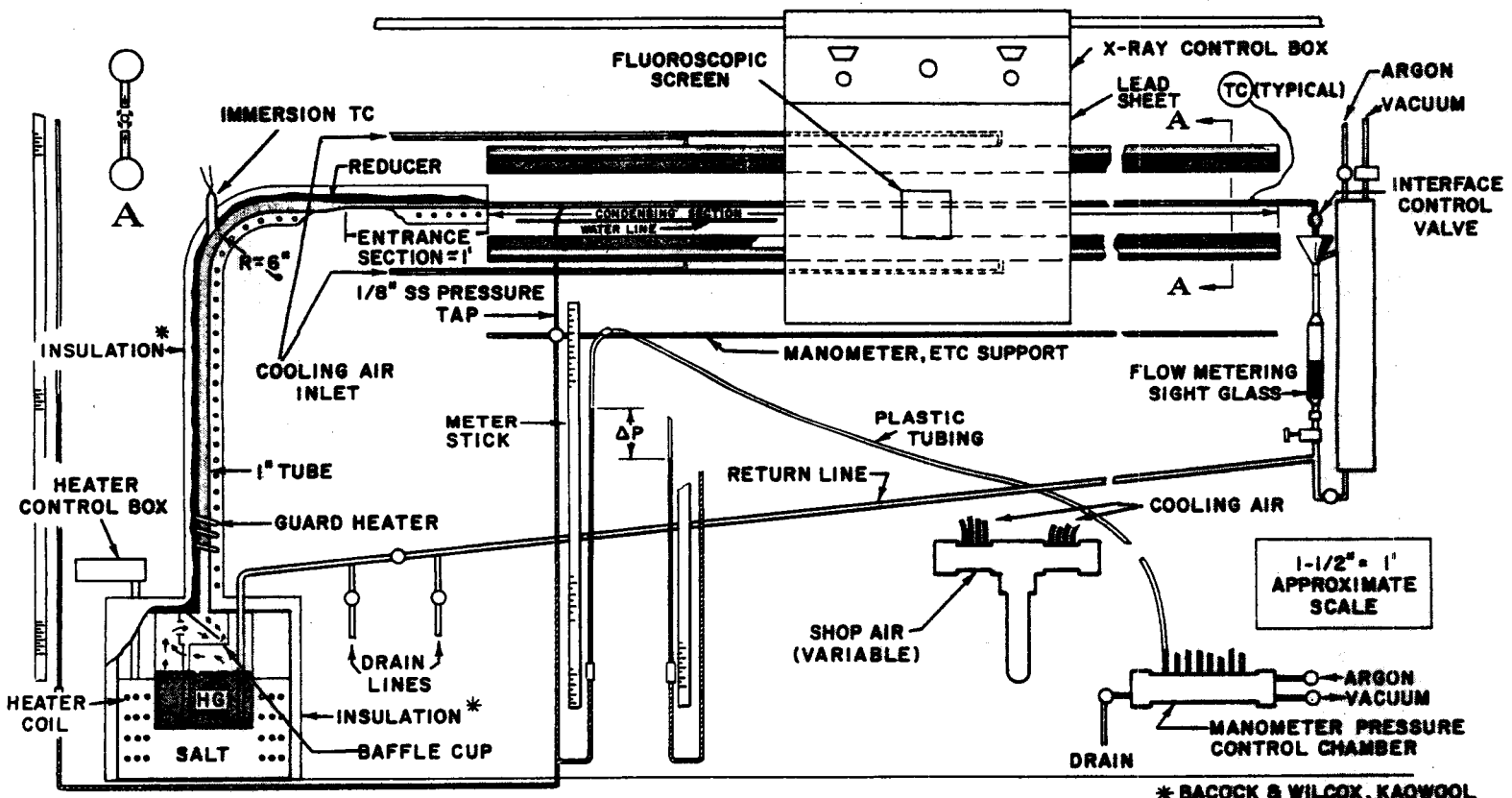

MERCURY CONDENSING TEST RIG SCHEMATIC

FIGURE 27

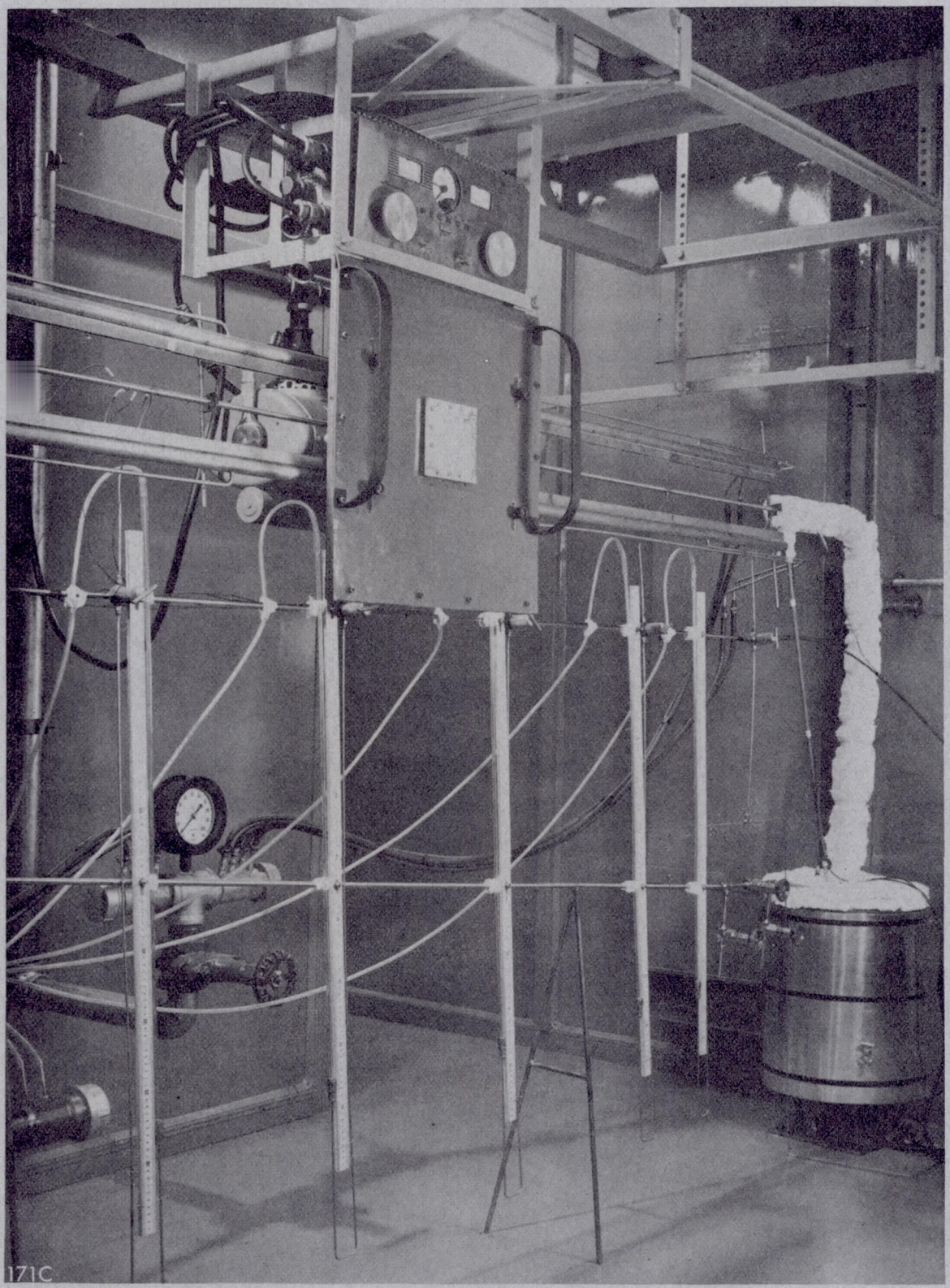

MERCURY CONDENSING TEST RIG (BOILER END)

FIGURE 28

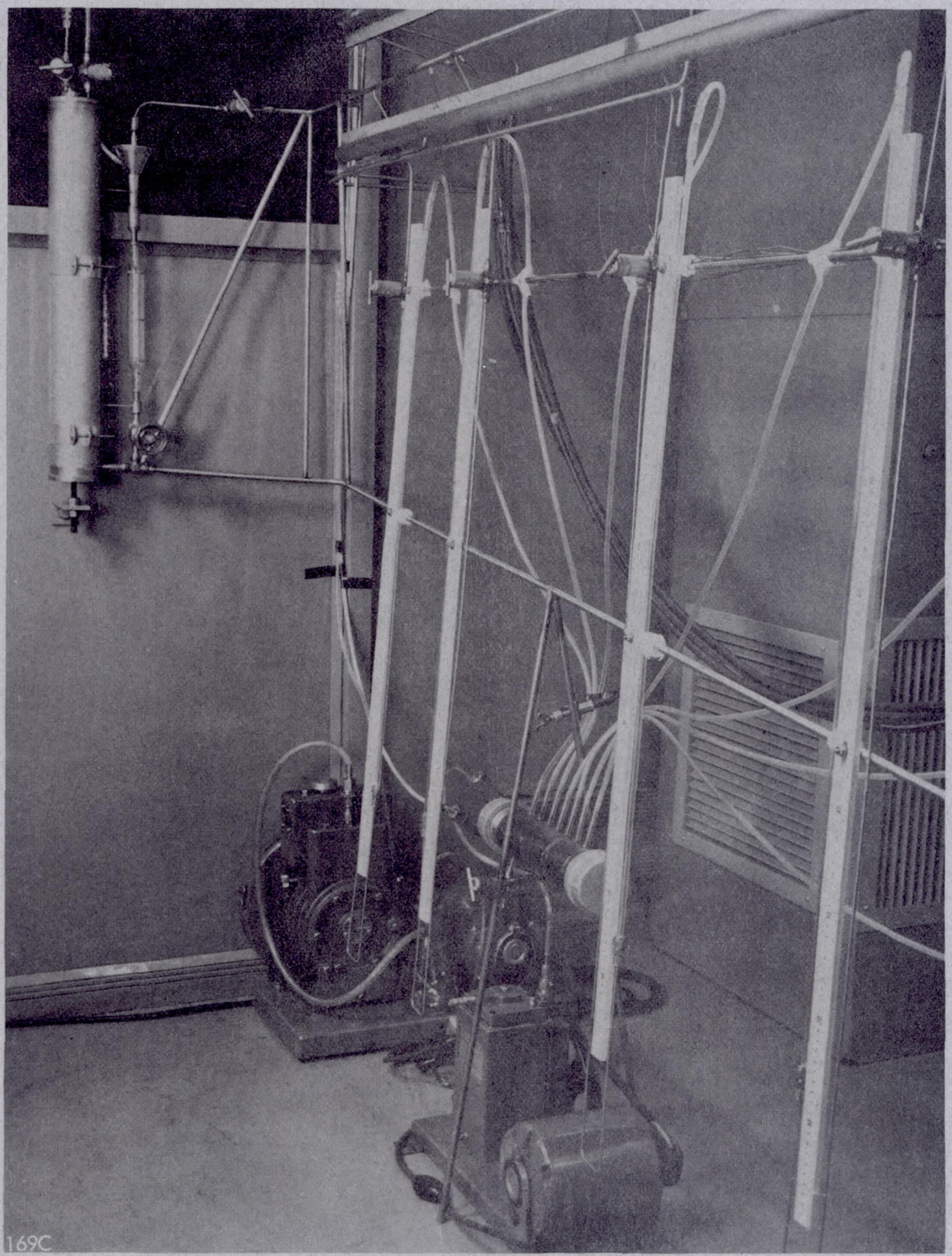

MERCURY CONDENSING RIG (FLOW METERING END)

FIGURE 29

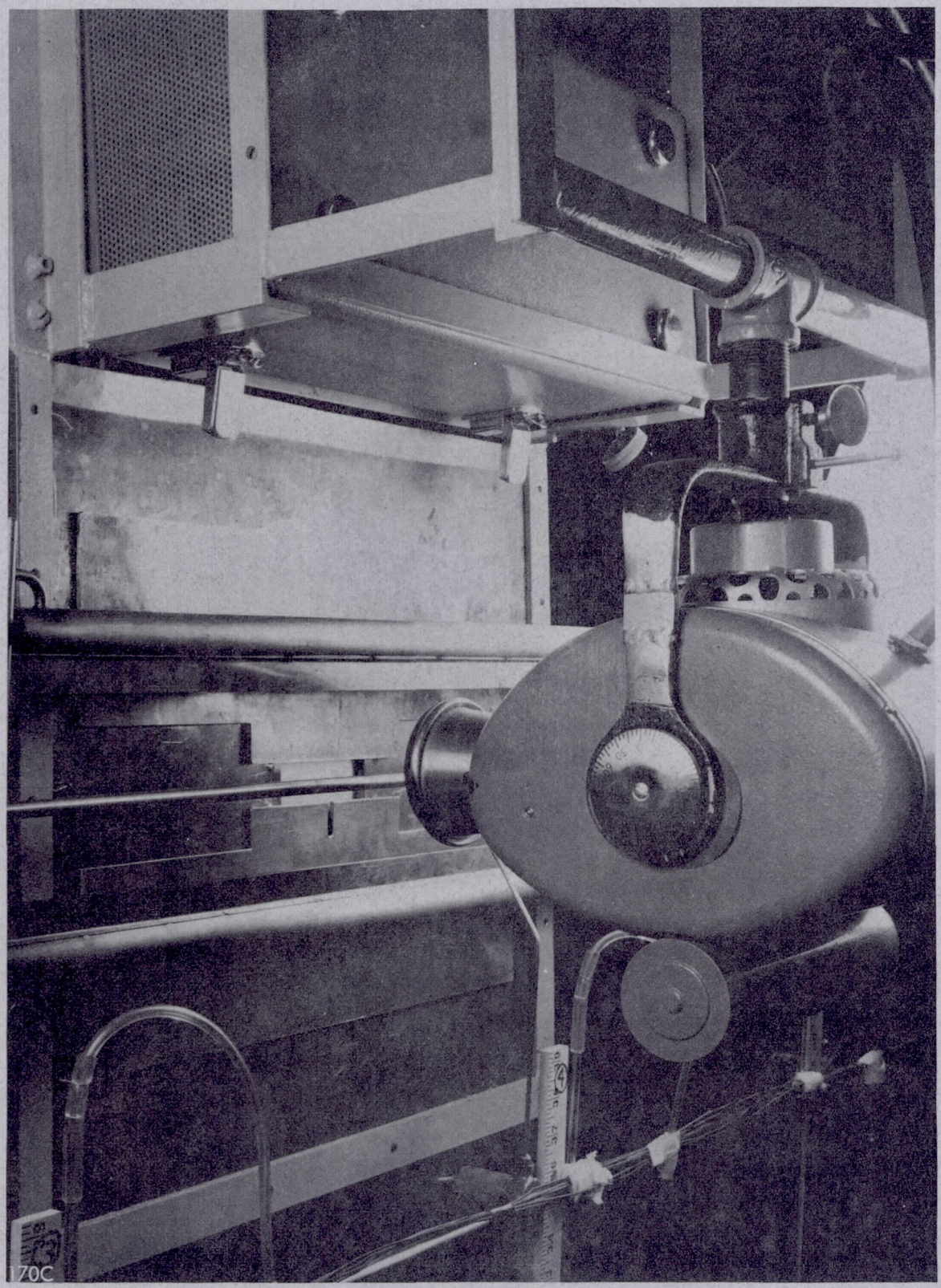

MERCURY CONDENSING RIG (X-RAY GENERATOR)

FIGURE 30

Unfortunately, flow limitations coupled with excessive salt temperatures and pressure oscillations were encountered. The flow limitations occurred at low heat transfer areas and low mercury levels and the pressure oscillations occurred at high mercury levels. Careful adjustment of the salt and mercury levels was required to avoid these problems. At heat fluxes approaching and greater than 30,000 Btu/hr-ft^2, salt temperatures were unsteady and sometimes would unpredictably start to increase. Possibly partial film boiling occurred either on the total or on only a portion of the boiling surface. Liquid level in the boiler was maintained at four inches or less to minimize the possibility of a head causing a sufficient variation in saturation temperature to result in different boiling mechanisms (i.e., nucleate, partial film and film) occurring at various portions of the boiling surface.

A baffle-cup arrangement was provided at the vapor exit of the mercury pot boiler, as shown in Figure 27, to minimize carry-over. A drain line from the baffle cup was provided for the return of liquid that dropped from the vapor. The vapor travelled from the boiler to the condensing section entrance via one-inch outside diameter by 0.035 inch wall superheater tube. Vapor velocity at the boiler exit was thus less than 20 feet per second. Several previous experiments conducted at TRW with transparent boilers and condensing sections showed no visible evidence of carry-over from pot-type boilers at this velocity.

5.1.2 Superheater-Entrance Section

The one-inch stainless steel tube exiting from the boiler rose about 4 feet vertically and was brought to a horizontal position by a 6 inch radius bend. A reducer was employed in the transition from the one-inch tube to the condensing section entrance length which is approximately one foot long. The inside diameter of the entrance section was matched with that of the condensing test section. Welding couplings were used on either side of the entrance length to avoid any weld penetration and subsequent flow interference.

The complete superheater-entrance section was heated and insulated to prevent condensation before the condensing section was entered. The heaters were electrical resistance Chromolox, KTL 1-390 WA, 4500 Watts, 120 V, 1 phase, circular immersion heater with 24 inch riser type with a stainless steel armoured protective covering. An immersion thermocouple was installed just below the bend in the one-inch tube to measure the degree of superheat.

5.1.3 Condensing Section

The condensing section geometries were described in Section 3. All test sections were horizontal within 0.5 inch over the 8 foot length (within 0.3 degrees of angle). The test section was kept straight by 12 supports tied directly to the air manifold. Each support was fixed to the test section by three screws to give nearly point contact and thereby minimize heat loss to the support. Previous to installation, each section was treated as follows:

a. cleaned with trichlorethylene,

b. steam cleaned,

c. hot air dryed.

The 1/8 inch by 0.020 inch wall stainless steel manometer taps were then welded to the bottom of the condensing section. The spacing of the local pressure manometers, from the beginning of cooling,was follows:

Test Series A		Test Series D, E, and F	
No.	Location, inches	No.	Location, inches
1 (and A)	0	1	0
2	18	A	0.5
3	36	2	14.5
4	54	3	29.0
5	72	4	43.5
6	90	5	58.0
7	102	6	72.5
		7	87.0
		8	101.5

NOTE: "A" denotes absolute pressure measurement

In welding the manometers to the condensing section, the amount of filler rod was minimized to reduce heat loss down the manometer taps. This was desirable in order that the normal mercury condensing pattern would not be disturbed by cold spots in the condensing section at the pressure taps.

To obtain system pressure level, an absolute pressure reading was obtained from the first pressure tap for the Series A tests. This reading was also used to measure local pressures. For the D, E, and F series a separate tap was provided for this pressure measurement as the series A testing showed that it was difficult to keep the first tap filled when the absolute pressure was also read from this tap. For test series E and F a cooling water line was brazed about 3/4 inch down the pressure tap to insure that the taps were filled with mercury. For the F series, however, the cooling water line was not brazed to the absolute manometer tap to minimize the localized cooling that is thus produced.

The test section was cooled by two approximately diametrically opposed air streams as shown in Section A of Figure 27. Cooling load was adjusted by varying the shop air supply between 50 to 100 psig and by adjusting the air manifold spacing from the condensing section from 1/2 to 4 inches. The heat flux available was 25,000 Btu/per hour per square foot or less, which is typical for present day direct radiator-condensers for mercury Rankine cycle space power conversion systems.

Each manifold consisted of 164 1/16 inch holes at a spacing of 3/4 inch. Parallel flow guiding strips 3/4 inch long and about 1/4 inch apart were provided along the full length of the manifold. Air entered at the top of each manifold at four locations spaced to provide an even distribution of air flow. The air entered the baffle via a partially inserted closed end tube with holes around the side. This avoided an increased flow through the jets in the immediate vicinity of the manifold air entrance.

5.1.4 Fluoroscopic Observation

An x-ray*-fluoroscopic screen combination mounted on a dolly was used to observe (1) some of the internal phenomena occurring during condensing, (2) the liquid level in the manometers, and (3) the vapor-to-liquid interface. Transportation of the assembly was possible over the full length of the condensing section. The x-rays passed through the condensing section to a 4 by 4 inch fluoroscopic sheet.

For safety a lead sheet covered the personnel side of the x-ray generator. In addition, the fluoroscopic sheet was mounted behind two sheets of 1/4 inch leaded glass and centrally mounted in a 2 foot by 2 foot by 1/2 inch lead sheet. Personnel also maintained a safe distance when the x-ray generator was operating. Victoreen, 0 to 200 milli-roentgen "Direct Reading Dosimeters" were carried by all personnel to monitor radiation pickup.

The resolution of the x-ray secreen observations was such that low-velocity mercury drops of about 0.020 inch were discernable within 0.028 inch stainless steel and 0.010 Haynes 25 tubes. Much smaller drops could be observed if an x-ray fluoroscopic combination with better resolution were employed.

5.1.5 Condensing Length Control and Return

Completion of condensing was always taken to be the point where the tube was observed on the fluoroscope to be completely full. Vapor-to-liquid interface or condensing length control was achieved by means of a high temperature welded bellows sealed needle valve in the subcooling line between the interface and the flow metering sight glass. Additional control was possible by varying the back pressure on this valve via an argon pressure source and vacuum pump combination. A plenum chamber was provided to which argon could be added or removed to maintain a pressure differential across the valve to provide controllability. The reservoir could also be used to store excess system inventory if necessary. The possible effects of argon (as a non-condensible) were reduced to insignificance by the rig operating and data taking procedures; no appreciable quantities of gas were observed via the fluoroscope, and the thermocouples inches before the interface were periodically checked to be near saturation temperature.

The mercury return line included a provision for system draining and installation of a pump to circulate the mercury with additives to promote wetting (see Section A, Appendix A).

5.2 Instrumentation and Data Accuracy

*Picker Corporation, Cleveland, Ohio, Portable X-Ray Model 6170, 110 KV Hot Shot with 40-110 KV stepless control; 1-10 ma stepless control; 110 V, 1 phase, 60 cycle power; continuous service at 3.5 ma and 110 KV; 0.5 mm focal spot; no backward radiation.

5.2.1 Pressure Measurement

Mercury-filled U-tube manometers were used to measure pressure at the condensing section locations listed in Section 5.1.3. As a result one absolute and several relative pressures were provided. Figure 27 schematically depicted these pressure taps while Figures 28, 29 and 30 are photographs of the rig and show the manometers installed.

Each leg of the U-tube manometer consisted of a 1/8 inch by 0.020 inch wall line with a welded bellows sealed valve about one foot from the test section. Closing of these valves allowed variation of system pressure without mercury spill-over. After a bend in the 1/8 inch tube, transparent plastic tubing (1/4 inch outside diameter clear plexiglass) was coupled in to allow the reading of liquid level on meter sticks. The plastic tubing (1/4 inch inside diameter "Tygon" vacuum tubing) was then continued to a manometer pressure control chamber connected to an argon supply and vacuum pump. Variation of the manometer back pressure maintained the liquid level such that it could be read on the meter stick.

The liquid level in the manometer near the condensing section was maintained by either liquid falling down into or vapor condensing in the manometer. Observation of the liquid level on the fluoroscopic screen indicated that at a relatively steady pressure level the liquid level could be 1/2 inch below the test section. For test series A and D, then, the manometer control pressure was always increased to refill the lines. Pressure levels were then read after about 30 seconds to allow the system to return to equilibrium. In this time the liquid level remained within about 1/32 inch of the test section.

For test series E and F, a water cooling line was introduced about 3/4 inch down the manometer. Subsequent fluoroscopic observations showed manometer fillage to be within 1/32 inch (0.9 millimeters of mercury) of the condensing section. Allowing for some error in reading the liquid manometer and in the relative alignment of the meter sticks, an accuracy of $\pm$ 3 millimeters of mercury in reading each local pressure is estimated if system pressure is stable. Pressure oscillations of the order of $\pm$ 5 millimeters were observed. These have been noted appropriately. The best accuracy for any pressure drop measurement would then be $\pm$ 6 millimeters or less than $\pm$ 0.12 pound per square inch plus an error due to possible tilt in the tube of $\pm$ 1.59 millimeters per foot between the pressure taps. For a 14-inch increment then, accuracy was $\pm$ 0.15 pound per square inch plus what may be noted on the data tables in Section 6.0.

To eliminate gases from the U-tube manometer, a vacuum was kept on the system for at least two hours before startup and the liquid in the metal leg of the "U" was replaced by mercury from the transparent leg which was first observed to be gas free. Errors due to gas entrainment in the manometers were thus prevented.

5.2.2 Flow Rate

Flow rate was measured by collecting and timing mercury exiting from the condensing test section in a graduated flow metering sight glass, as shown in Figure 31. Closure of the valve immediately downstream caused liquid buildup which was timed. The liquid buildup varied from to 0.84 to 1.69 pounds of mercury. Time intervals varied from 40 to 90 seconds.

GRADUATED FLOW INCREMENT SIGHT GLASS

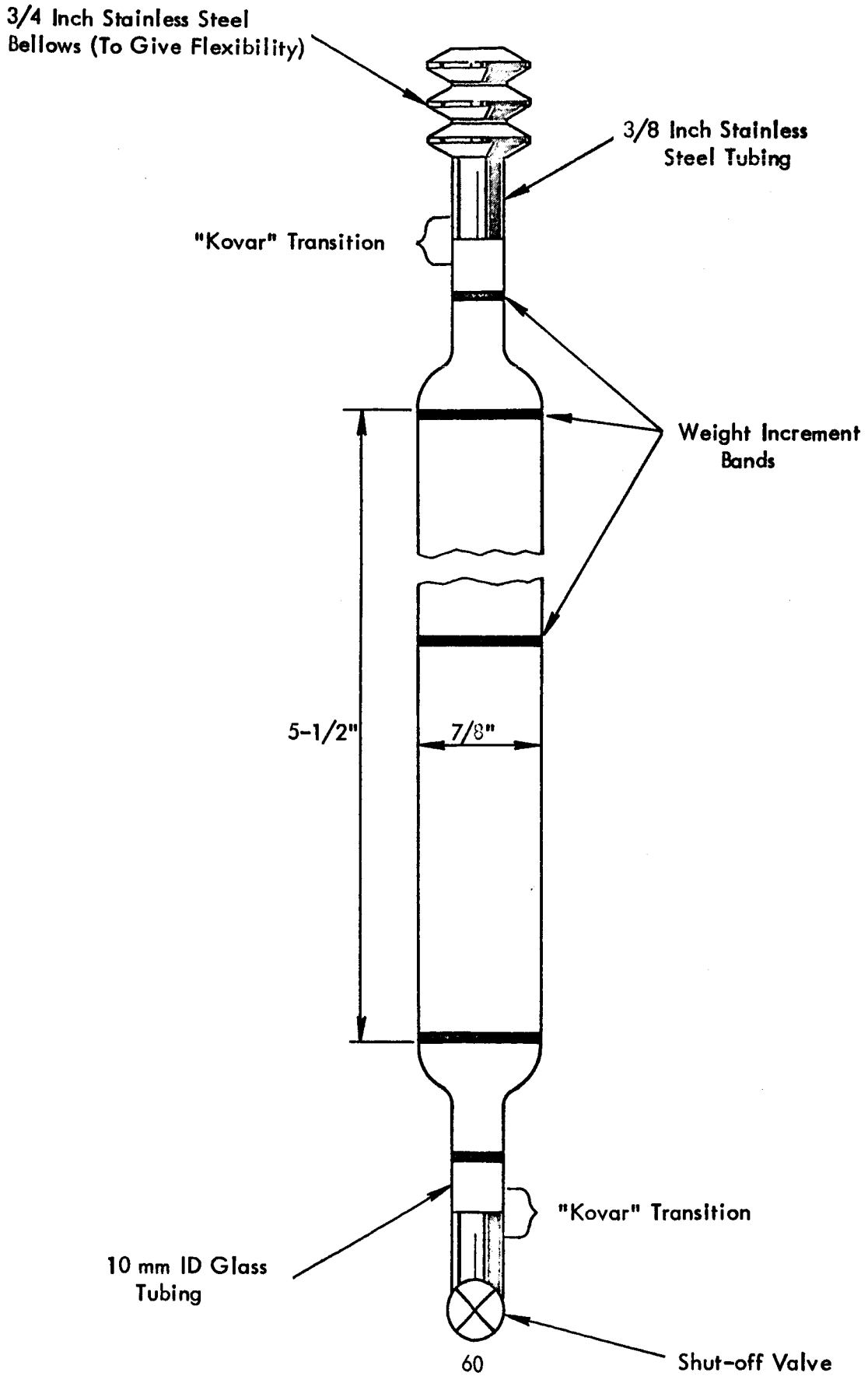

FIGURE 31

During the flow measurement, the interface control valve usually required modulation to avoid any change in subcooler inventory, thus leading to an erroneous flow rate. Interface position was observed on the fluoroscope and held to within about ± 1/4 inch. As a result, an accuracy of about ± 0.6% in flow could be introduced. The accuracy of the flow was also affected by the location in the sight glass at which time was started. At large mass increments, time was started in the very narrow lower portion of the flow metering sight glass, thereby reducing the mass increment error. The estimated accuracy for the various flow increments obtained and presented on the data sheets of Section 6 is indicated below as a function of mass increment and interface diameter:

Mass Increment, pounds	Interface Diameter, inches		
	0.397	0.319	0.2
1.67	1.1%	0.8%	0.4%
1.54	2.1	1.8	1.4
0.84	3.3	3.0	2.6

Assumptions:

(1) Interface varied ± 1/4 inch between start and finish of measurement.

(2) Liquid Level related to time to within 1/16 inch.

The accuracies are based on the assumption that interface was held between ± 1/4 inch and liquid level could be observed and related to stopwatch time to within ± 1/16 inch. Both these values are pessimistic in the sense that better accuracy than that presented was very often obtained. Whenever possible the data were obtained at the largest mass increment (which was "99 and 44/100%" of the time), thus minimizing the error in flow rate.

5.2.3 Temperature

Temperature measurements were required in the following key areas of the condensing rig:

a) One-inch upstream of the interface to provide a check for non-condensibles. (Several condensing experiments at TRW have measured tube wall temperatures hundreds of degrees below saturation due to non-condensibles.)

b) salt bath temperatures monitored for overheating and steady state,

c) superheat.

All temperatures where measured with #24 Duplex iron constantan thermocouple wires. The thermocouples were spot welded to the area of interest except for the superheat immersion probe. Superheat temperature was read out on a Thermoelectric Corporation "Minimite" with 2°F intervals over a 0 to 1000°F or 900 to 1800°F range. All other temperatures were read out on a temperature logger.

5.2.4 Vacuum Equipment

No vacuum gage as such was employed in the system. Vacuum levels are of importance when dealing with surface chemistry phenomena such as wetting and non-wetting. The vacuum pump used in the system is then worthy of description. A WM Welch Scientific Co. Duo Seal 1405 B, 0.1 micron vacuum pump was used.

5.3 Rig Operating Procedures

The procedures for startup, approaching the data point, taking point, and both emergency and normal shutdown are presented below. These procedures have been employed during the non-wetting testing and are expected to be applicable to the wetting tests. For aid in understanding these procedures reference to Section 5.1 is required.

To start testing, all manometer valves were closed and the boiler heaters, the argon supply, and the vacuum pump were turned on. After the system had been evacuated, liquid in the 1/8 inch stainless steel tube of the manometers was replaced by opening the manometer valves. All manometer valves were then reclosed. As flow began, all air manifold supports were inspected for twisting caused by thermal expansion to prevent errors in pressure readings due to gases in the liquid legs. The system was allowed to run for 15 minutes with the flow control valve open to remove gas. The cooling air supply was then turned on and the vacuum valve to the plenum was closed. The interface control valve was then closed to allow the test section to fill with mercury condensate. Before approaching the data point, all manometers were refilled with mercury condensate from the test section.

After the desired data point conditions had been determined, $T_{salt} - T_{Hgsat}$ was estimated from past experience for the desired flow. This ΔT was then added to the desired saturation temperature to obtain an estimated boiler bath temperature. The boiler temperature was adjusted to the desired level as quickly as possible by manipulating air flow and boiler heaters. When the boiler heater was within 10 degrees of desired temperature, the boiler heaters were set to produce the desired mercury flow rate and the air manifold setting and/or air flow rate were adjusted until the desired condenser pressure was reached. Condensing length was controlled by means of the interface control valve and back pressure. The mercury flow rate was periodically checked as the system stabilized and manometers were opened when stability was attained.

Before taking data, the following stability criteria were met:

1. The interface was under control near the final position for at least 15 minutes.

2. Logger boiler bath temperatures were steady (less than 3 degrees change in 15 minutes).

3. Air manifold pressure remained steady. (Pressure regulators were eventually used.)

4. Flow rate was within 5% of the desired flow.

5. No gas was observed at the interface on the fluoroscope screen and measured temperature before the interface read $\sim T_{sat}$.

6. System pressure held within 20 millimeters of the final pressure for 15 minutes and was within 10% of that desired.

Liquid level was checked to insure that the manometers were full. Manometers were read only when full and holding steady, never during a time when system pressure was increasing and manometers could not be filled to the top. Immediately after the pressure readings, the sight glass valve of the collector was closed and flow rate was read. The timer for flow rate readings was started as the mercury level passed the top of the lower reference band, allowing for buildup to the upper reference band. Careful maintenance of the interface position in the condenser was required during this time. The timer was stopped when the mercury level reached the top of the upper reference band. Bands used and buildup time were recorded.

After at least two data recordings had been made at each point and checked for similarity, preparations were made to change to the next data point. Manometer levels were carefully maintained as system pressure changed.

To terminate the test, all heaters were shut off, the flow control and return line valves were shut, and the test section was allowed to fill with liquid condensate. To prevent excessive pressure buildup in the boiler, the boiler bath temperature was reduced to below 800°F before shut down. All manometers were then refilled to 800 mm, the x-ray was shut off, the vacuum valve on the collection pot was opened, and the closed-off section of the system was then evacuated.

The procedure established for emergency shut down consisted of four steps:

1. Shut off all heaters and the x-ray as quickly as possible.

2. Shut manometer valves.

3. Shut flow control and return line valves but leave the air manifolds on.

4. Take any possible steps to correct the situation.

All safety procedures that have been established for mercury, x-ray, and fire hazards were observed throughout the tests.

6.0 EXPERIMENTAL RESULTS

6.1 Non-Wetting Condensing Data

Experimental non-wetting data are presented in Tables II, III, IV and V. The absolute pressure at each local position is presented. Pressure tap location is identified by distance from the beginning of the air cooling which is where the test section inlet insulation and guard heaters end. For example, P_{54} is the pressure 54 inches from the beginning of condensation. Actually the absolute pressure for the zero distance only was measured and all others were measured relative to this location and to each other, as described in Section 5.2.1. Because relative pressures were measured, a correction was required across the vapor-to-liquid interface only. Pressures measured by the first pressure tap in the liquid portion of the tube have been corrected by substracting a head of one-half the test section tube diameter. For the 0.319 inch data then, a correction of -4 millimeters was required. The accuracy of each pressure measurement is discussed in Section 5.2.1. System oscillations caused pressure fluctuations which were recorded and are presented in the data tables.

Flow rate was calculated from the mass increment and collection times presented. Flow accuracy as a function of mass increment collected and tube diameter is estimated in Table II. For the Series A, D, and E data, two corresponding sets of pressure and flow data were obtained at approximately the same system pressure level and flow rate (e.g., A-3 and A-4). For the F series tests the two sets of pressure profiles were recorded and the flows were averaged and associated with each pressure profile.

To give an indication of the superheat existing, the measured inlet temperature is presented along with the saturation temperature (T_{sat}) corresponding to the test section inlet pressure (P_o). Superheat is then ($T_{sat} - T_o$). Condensing length (L_c), the approximate axial length of the interface (L_I), and the distance from inlet (L') at which globules were fluoroscopically observed on the tube bottom are also given. L_I and L' were not obtained for the A, D, and some of the E series data.

Table II contains some data (W series) obtained during the "pseudo-wetting" experienced with the stainless steel 0.319 inch tube, described in Section 6.2.

Figures 32, 33and 34 summarize the range of flows and saturation levels covered by the data. Details pertinent to the apparatus, instrumentation, and operating and data taking procedures were presented in Section 5.3.

6.2 "Pseudo-Wetting" Investigations

During initial testing of the 0.319 inch inside diameter condenser tube (A series), partial wetting was observed in the low quality region of the tube after about 70 hours of operation tion. The observations were made on the fluoroscope screen. Figure 35 shows sketches of the appearance of wetting and non-wetting condensing on the fluoroscope screen.

The argon cover gas was replaced by an air cover in an attempt to obtain more data on the

TABLE II

MEASURED DATA DURING NON-WETTING CONDENSATION OF MERCURY IN A 316 STAINLESS STEEL AND HAYNES 25 TUBE SERIES A AND W (0.319 inch ID by 8 feet long)

No.	Hg Collected, lb	Time, Sec.	w lb/min.	P_0, mm Hg	P_{18}, mm Hg	P_{36}, mm Hg	P_{54}, mm Hg	P_{72}, mm Hg	P_{90}, mm Hg	P_{102}, mm Hg	T_0 °F	T_{sat0},* °F	L_c In.,
A-1	1.60	65.0	1.48	933	910	880	859	856	870	864	750	694	94
A-2	↓	65.0	1.48	936	906	877	856	848	863	859	754	695	↓
A-3		60.5	1.59	999	976	948	930	925	943	939	763	702	
A-4		61.0	1.57	993	971	942	923	925	935	931	765	701	
A-5		51.0	1.88	900	857	811	785	775	784	780	757	691	
A-6		50.0	1.92	895	855	812	790	783	790	789	755	690	
A-7		38.0	2.52	916	890	802	776	757	794	872	782	692	
A-8		30.8	3.12	1546	1496	1434	1409	1410	1429	1522	832	750	
A-9		32.0	3.00	1384	1333	1267	1241	1237	1269	1319	813	737	
A-10		32.0	3.00	1466	1386	1317	1293	1291	1311	1377	806	743	
A-11		54.2	1.77	639	581	525	504	506	526	569	692	657	
A-12		55.2	1.74	648	584	528	505	505	527	549	686	658	
A-13		50.0	1.92	796	761	715	694	694	711	760	706	678	
A-14		52.0	1.85	826	774	728	708	708	736	742	702	682	
A-15		52.8	1.82	1536	1492	1467	1452	1449	1464	1495	759	749	
A-16		52.5	1.83	1608	1560	1536	1522	1522	1522	1566	761	754	
A-17		45.0	2.13	932	877	829	807	802	807	824	714	694	
A-18		47.0	2.04	818	752	697	675	670	685	696	706	680	
A-19		48.0	2.00	1034	987	947	931	929	929	950	721	705	
A-20		49.0	1.96	1026	982	939	927	924	934	940	720	704	
A-21		42.5	2.26	1134	1081	1030	1010	1007	1020	1033	737	765	
A-22		42.5	2.26	1106	1054	1005	986	984	996	1007	737	712	
A-23		45.0	2.13	854	779	716	689	688	708	730	716	685	
A-24		44.5	2.15	828	758	696	669	669	686	707	713	682	
A-25		46.2	2.08	996	962	908	881	882	896	919	725	701	
A-26		46.0	2.08	1030	974	929	909	905	919	937	724	705	
A-27		75.2	1.28	927	900	874	860	855	860	860	710	693	
A-28		75.8	1.27	914	887	865	851	848	852	852	708	692	
A-29		70.0	1.37	719	678	640	620	617	615	618	686	668	
A-30		72.0	1.33	645	606	572	555	551	556	555	676	658	
A-31		73.2	1.31	442	378	317	284	283	287	299	654	623	
A-32		73.0	1.31	432	361	300	271	270	287	300	657	620	
A-33		43.6	2.20	1404	1360	1322	1300	1295	1302	1308	771	739	
A-34		44.0	2.18	1354	1311	1272	1250	1246	1256	1267	772	734	
A-37		86.5	1.11	596	568	543	529	526	531	537	682	650	
A-38		88.0	1.09	590	560	537	521	520	527	543	680	649	
A-39		77.6	1.24	551	506	468	453	453	463	471	676	642	
A-40		78.0	1.23	519	476	438	422	422	430	440	672	637	
A-41		75.0	1.28	430	365	303	276	276	293	307	662	620	
A-42		74.4	1.29	411	345	278	246	246	262	273	660	615	
A-43		39.7	2.42	1549	1502	1457	1433	1428	1430	1429	766	750	
A-44		40.0	2.40	1559	1512	1469	1445	1443	1448	1448	764	751	
A-45		50.3	1.91	1263	1220	1184	1158	1160	1163	1189	743	726	
A-46		51.3	1.87	1267	1224	1191	1175	1176	1188	1195	743	727	
W-1		58.5	1.64	1042	1000	968	951	948	948	944	728	706	
W-2		55.8	1.72	1030	988	967	958	953	945	945	718	705	
W-3		50.0	1.92	1021	981	959	951	937	939	945	726	704	
W-4		45.5	2.11	1013	967	945	924	919	909	923	725	703	
W-5	↓	44.8	2.14	1030	990	954	937	933	928	931	727	705	↓

*Not measured but obtained from P_0 and saturated temperature-pressure relationship.

Note - All data taken when system was stable and therefore accuracy of pressure should be as described in Section 5.2.1.

Subscript of P's denotes distance of manometer tap from the beginning of cooling.

TABLE III
MEASURED DATA DURING NON-WETTING CONDENSING OF MERCURY IN A HAYNES 25 TUBE
SERIES F (0.319 Inch ID by 8 Feet Long)

No.	Hg Collected, lb	Time, Sec.	$\dot{m}$ lb/min	P_0, mm Hg	$P_{14.5}$, mm Hg	$P_{29.0}$, mm Hg	$P_{43.5}$, mm Hg	$P_{58.0}$, mm Hg	$P_{72.5}$, mm Hg	P_{87}, mm Hg	$P_{101.5}$, mm Hg	T_0, °F	T_{sat0},* °F	L_1, In.	L', In.	L_c, In.	±p+ mm Hg
F- 1	1.69	59.6	1.70	941	897	865	844	815	815	817	821	720	695	2	72	94	0
F- 2		59.6	1.70	918	871	838	818	781	844	847	855	720	693	2	72	94	0
F- 3		43.0	2.36	744	646	551	463	369	344	344	342	710	672	1/2	80	94	1
F- 4		43.0	2.36	748	650	553	458	378	350	353	354	710	671	1/2	80	94	1
F- 5		46.5	2.18	877	795	717	660	598	586	593	602	725	675	1/2	65	94	0
F- 6		46.5	2.18	867	785	723	663	613	593	598	608	725	687	1/2	65	94	0
F- 7		45.9	2.21	981	916	853	806	765	753	764	772	732	699	1/2	65	94	0
F- 8		45.9	2.21	967	909	847	802	763	757	764	769	732	697	1/2	65	94	0
F- 9		52.8	1.92	1344	1308	1287	1275	1265	1271	1276	1279	764	733	1	36	72	0
F-10		52.8	1.92	1341	1309	1289	1279	1259	1265	1275	1270	764	732	1	36	72	0
F-11		83.8	1.21	974	969	957	946	936	935	936	930	715	698	3-1/2	48	94	0
F-12		83.8	1.21	972	966	956	944	934	934	933	927	715	698	3-1/2	48	94	0
F-13		79.8	1.27	963	942	916	910	923	921	922	922	715	697	3-1/2	34	72	0
F-14		79.8	1.27	964	941	915	910	921	920	921	921	715	697	3-1/2	34	72	0
F-15		81.8	1.24	966	954	950	948	944	945	945	946	715	697	3	19	53	0
F-16		81.8	1.24	966	956	952	952	949	950	950	950	715	697	3	19	53	0
F-17	0.84	60.0	1.69	967	930	906	894	884	887	883	884	730	698	-	-	72	1
F-18	0.84	60.0	1.69	987	942	914	900	885	886	886	888	730	700	-	-	72	1
F-19	1.69	55.4	1.83	968	930	904	892	881	880	880	880	730	698	-	-	72	1
F-20		55.4	1.83	961	921	897	879	874	874	879	876	730	697	-	-	72	1
F-21		57.6	1.76	1569	1548	1535	1529	1519	1515	1524	1524	792	752	2-1/2	41	72	0
F-22		57.6	1.76	1565	1541	1527	1516	1509	1509	1509	1509	792	751	2-1/2	41	72	0
F-23		57.0	1.78	1555	1524	1515	1505	1502	1498	1498	1498	800	750	2-1/2	41	72	0
F-24		57.0	1.78	1571	1543	1533	1519	1511	1510	1510	1505	800	752	2-1/2	41	72	0
F-25		44.1	2.30	975	898	830	778	715	701	704	706	794	698	1	72	72	1
F-26		44.1	2.30	965	887	805	752	687	673	680	676	794	697	1	72	72	1
F-27		85.2	1.19	616	585	570	544	535	533	548	541	685	653	3	58	94	1
F-28		85.2	1.19	624	598	580	555	544	537	549	540	685	654	3	58	94	1
F-29		85.9	1.18	968	953	938	928	916	916	919	911	714	698	6	48	94	0
F-30		85.9	1.18	970	954	940	927	917	916	917	911	714	698	6	48	94	0
F-31		80.5	1.26	1527	1514	1502	1491	1482	1492	1492	1486	760	748	6	36	94	0
F-32		80.5	1.26	1529	1515	1502	1491	1481	1481	1480	1474	760	748	6	36	94	0
F-33		57.6	1.76	989	941	903	881	846	842	846	842	740	700	6	-	94	0
F-34		57.6	1.76	994	944	910	884	856	853	857	850	740	701	6	-	94	0
F-35		51.7	1.96	975	926	898	879	872	871	877	872	740	698	2	-	72	0
F-36		51.7	1.96	976	928	897	882	873	874	877	873	740	698	2	-	72	0
F-37	1.57	55.7	1.69	1520	1497	1477	1464	1443	1442	1443	1435	783	747	6	-	94	0
F-38	1.57	55.7	1.69	1520	1504	1484	1467	1448	1444	1445	1437	783	749	6	-	94	0
F-39	0.84	24.2	2.08	635	533	426	320	198	128	128	154	733	656	1/2	80	94	0
F-40	0.84	24.2	2.08	636	539	434	331	202	125	122	137	733	656	1/2	80	94	0
F-42	1.69	76.8	1.32	1557	1546	1538	1531	1530	1532	1532	1530	772	750	5	25	53	0
F-43	1.57	51.2	1.84	785	734	697	675	663	664	669	667	726	677	3	37	72	0
F-44	1.57	51.2	1.84	797	746	706	583	570	565	566	561	726	679	3	37	72	0

+Approximate oscillation of pressure readings.

*Not measured but obtained from P_0 and saturated-temperature relationship.

Note - Subscript of P's denotes distance of manometer tap from the beginning of cooling.

TABLE IV
MEASURED DATA DURING NON-WETTING CONDENSING OF MERCURY IN HAYNES 25 SPINEL-COATED TAPERED TUBE
SERIES D (0.4 to 0.2 Inch ID by 7 Feet Long)

No.	Hg Collected, lb	Time, Sec.	w lb/min	P_0, mm Hg	$P_{14.5}$, mm Hg	$P_{29.0}$, mm Hg	$P_{43.5}$, mm Hg	$P_{58.0}$, mm Hg	$P_{72.5}$, mm Hg	P_{87}, mm Hg	T_0, °F	T_{sat0},* °F	Lc, In.
D-15	1.6	48.5	1.98	1546	1536	1519	1509	1506	1489	1493	780	749	82
D-16	↓	48.1	2.00	1546	1536	1521	1511	1505	1494	1511	780	749	↓
D-17		68.0	1.41	812	795	779	761	760	756	781	706	680	
D-18		68.0	1.41	800	790	775	757	757	754	780	700	678	
D-19		46.0	2.09	810	779	754	721	712	710	784	714	679	
D-20		45.2	2.12	815	787	760	725	715	708	788	714	680	
D-21		37.2	2.58	1552	1527	1505	1485	1470	1464	1517	808	750	
D-22		37.4	2.57	1538	1510	1487	1467	1452	1445	1498	808	748	
D-23		32.5	2.95	1549	1517	1494	1468	1448	1442	1516	806	750	
D-24		33.0	2.91	1552	1520	1496	1470	1454	1449	1525	806	750	
D-25		35.0	2.74	1064	1016	984	942	914	919	1051	750	708	
D-26		39.0	2.46	790	739	698	642	593	583	735	712	677	
D-27		38.4	2.50	817	771	730	678	635	625	755	712	680	
D-28		43.0	2.23	781	746	715	682	671	700	-	718	675	72
D-29		43.2	2.22	788	754	725	694	676	702	-	718	677	72
D-30		55.8	1.72	777	760	757	755	715	-	-	698	675	48
D-31	↓	57.6	1.67	771	757	754	752	759	-	-	695	674	48

*Not measured but obtained from P_0 and saturated temperature-pressure relationship.

Note - Subscript of P's denotes distance of manometer tap from the beginning of cooling.

MEASURED DATA DURING NON-WETTING CONDENSING OF MERCURY IN A HAYNES 25 TUBE
SERIES E (0.397 Inch ID by 8 Feet Long)

No.	Hg Collected, lb	Time, Sec.	w lb/min.	P_0, mm Hg	$P_{14.5}$, mm Hg	$P_{29.0}$, mm Hg	$P_{43.5}$, mm Hg	$P_{58.0}$, mm Hg	$P_{72.5}$, mm Hg	P_{87}, mm Hg	$P_{101.5}$, mm Hg	T_0 °F	T_{sat0}* °F	L_1 in.	L'	L_c in.	±p± mm Hg
E-1	1.6	78.0	1.23	594	589	582	574	574	568	572	564	748	650	-	-	94	0
E-2		76.0	1.26	582	580	571	563	563	557	560	552	750	648	-	-	94	0
E-3		80.0	1.20	597	595	602	592	587	582	587	587	764	650	-	-	72	1
E-4		83.0	1.16	592	594	594	579	589	584	589	589	760	650	-	-	72	1
E-5		71.3	1.34	607	617	621	620	616	616	611	606	778	652	-	-	48	1
E-6		71.4	1.34	643	648	650	648	643	646	647	646	778	657	-	-	48	1
E-7		85.8	1.12	1057	1055	1053	1043	1040	1037	1033	1033	825	708	-	-	94	0
E-8		86.0	1.12	1047	1045	1042	1040	1041	1039	1038	1033	825	707	-	-	94	0
E-9		50.0	1.92	600	590	577	560	558	556	544	536	696	650	-	-	94	0
E-10		51.0	1.88	609	605	596	586	585	579	587	580	698	652	-	-	94	0
E-11		49.8	1.93	613	607	593	576	572	565	566	560	702	653	-	-	94	0
E-12		49.0	1.96	600	594	581	564	558	551	556	550	702	650	-	-	94	0
E-13		48.8	1.97	593	589	583	578	584	579	579	578	702	650	-	-	72	1
E-14		48.8	1.97	591	589	588	572	585	580	580	579	702	649	-	-	72	1
E-15		40.4	2.38	607	603	583	554	550	540	542	537	788	652	-	-	94	1
E-16		40.0	2.40	597	601	604	559	553	545	549	540	783	650	-	-	94	2
E-17		42.6	2.25	1042	1035	1034	1017	1014	1008	1015	1010	811	707	-	-	94	1
E-18		40.2	2.38	1062	1056	1043	1029	1026	1021	1032	1027	809	708	-	-	94	2
E-19		80.0	1.20	1561	1571	1570	1564	1564	1563	1560	1554	760	750	16	-	95	3
E-20		74.0	1.30	1535	1541	1541	1537	1537	1539	1537	1532	760	749	16	-	95	3
E-21	1.48	45.0	1.97	1057	1057	1054	1042	1042	1037	1036	1030	740	708	8	-	95	2
E-22	1.48	44.2	2.01	1056	1049	1042	1030	1030	1029	1026	1017	740	708	8	-	95	2
E-23	1.60	71.0	1.35	1040	1040	1039	1036	1036	1031	1026	1024	714	707	11	-	72	0
E-24	1.60	71.4	1.34	1042	1041	1041	1036	1036	1036	1023	1021	714	707	11	-	72	0
E-25	1.60	77.0	1.25	1059	1056	1054	1045	1045	1046	1046	1053	719	708	8	-	53	0
E-26	1.60	78.2	1.23	1042	1041	1039	1030	1027	1028	1028	1031	719	707	8	-	53	0
E-27	1.60	80.0	1.20	1531	1525	1523	1516	1521	1523	1525	1525	760	749	-	-	53	3
E-28	1.60	81.2	1.18	1536	1538	1538	1534	1536	1536	1539	1541	760	749	-	-	53	3
E-29	1.48	47.2	1.88	1048	1045	1043	1035	1037	1030	1031	1031	752	707	5	-	72	0
E-30	1.48	48.0	1.85	1043	1042	1041	1032	1035	1033	1027	1027	752	707	5	-	72	0
E-31	1.60	48.2	1.99	1051	1049	1047	1038	1043	1035	1034	1035	760	708	5	-	72	0
E-32	1.60	49.4	1.94	1053	1050	1050	1042	1046	1042	1042	1042	760	708	5	-	72	0
E-33	1.60	54.0	1.78	1564	1568	1568	1566	1564	1572	1571	1571	825	750	6	16	53	2
E-34	1.60	55.0	1.75	1567	1565	1563	1557	1556	1555	1557	1557	825	751	6	16	53	2
E-35	1.60	54.8	1.75	1550	1550	1557	1551	1554	1554	1561	1561	842	750	6	16	53	6
E-36	1.60	55.4	1.73	1564	1559	1554	1555	1555	1548	1559	1550	842	750	6	16	53	6
E-37	1.69	52.2	1.94	1062	1062	1062	1062	1057	1058	1059	1060	722	708	5	19	53	1
E-38		51.7	1.96	1067	1070	1071	1067	1062	1065	1068	1064	722	708	5	19	53	1
E-39		58.9	1.72	1563	1561	1555	1548	1548	1541	1541	1540	766	750	6	32	94	2
E-40		57.3	1.77	1569	1569	1564	1552	1551	1546	1551	1551	766	750	6	32	94	2
E-41		48.3	2.10	1520	1516	1496	1491	1500	1493	1486	1486	760	749	6	32	94	3
E-42		49.7	2.04	1525	1519	1517	1510	1513	1512	1505	1490	760	750	6	32	94	3
E-43		44.9	2.26	1065	1068	1058	1052	1059	1059	1054	1044	742	708	5	22	72	8
E-44		45.3	2.24	1070	1073	1067	1055	1065	1062	1065	1065	742	708	5	22	72	8
E-45		86.9	1.166	606	603	591	583	583	581	581	580	665	651	5-1/2	41	94	0
E-46		87.6	1.158	601	592	579	573	573	573	575	572	665	651	5-1/2	41	94	0
E-47		52.3	1.94	1040	1042	1040	1029	1023	1026	1030	1021	738	706	3-1/4	18	53	2
E-48		53.8	1.885	1053	1052	1047	1044	1037	1042	1051	1052	738	706	3-1/4	18	53	2
E-49		57.7	1.758	1541	1535	1526	1523	1523	1519	1521	1516	782	750	7-1/2	35	94	0
E-50		59.6	1.700	1546	1546	1538	1531	1531	1525	1524	1516	782	750	7-1/2	35	94	0
E-51		59.9	1.692	1554	1547	1542	1532	1532	1529	1529	1527	784	750	7-1/2	35	94	0
E-52		59.6	1.70	1556	1554	1552	1549	1552	1554	1542	1539	784	750	7-1/2	35	94	0

*Not measured but obtained from P_0 and saturated temperature-pressure relationship.

±Approximate accuracy of pressure readings.

Note - Subscript of P's denotes distance of manometer tap from the beginning of cooling.

FLOW, PRESSURE AND CONDENSING LENGTH DATA POINT COMBINATIONS OBTAINED FOR THE HORIZONTAL CONDENSATION OF MERCURY IN A HAYNES-25 0.397 INCH BY 8 FOOT LONG TUBE (SERIES E)

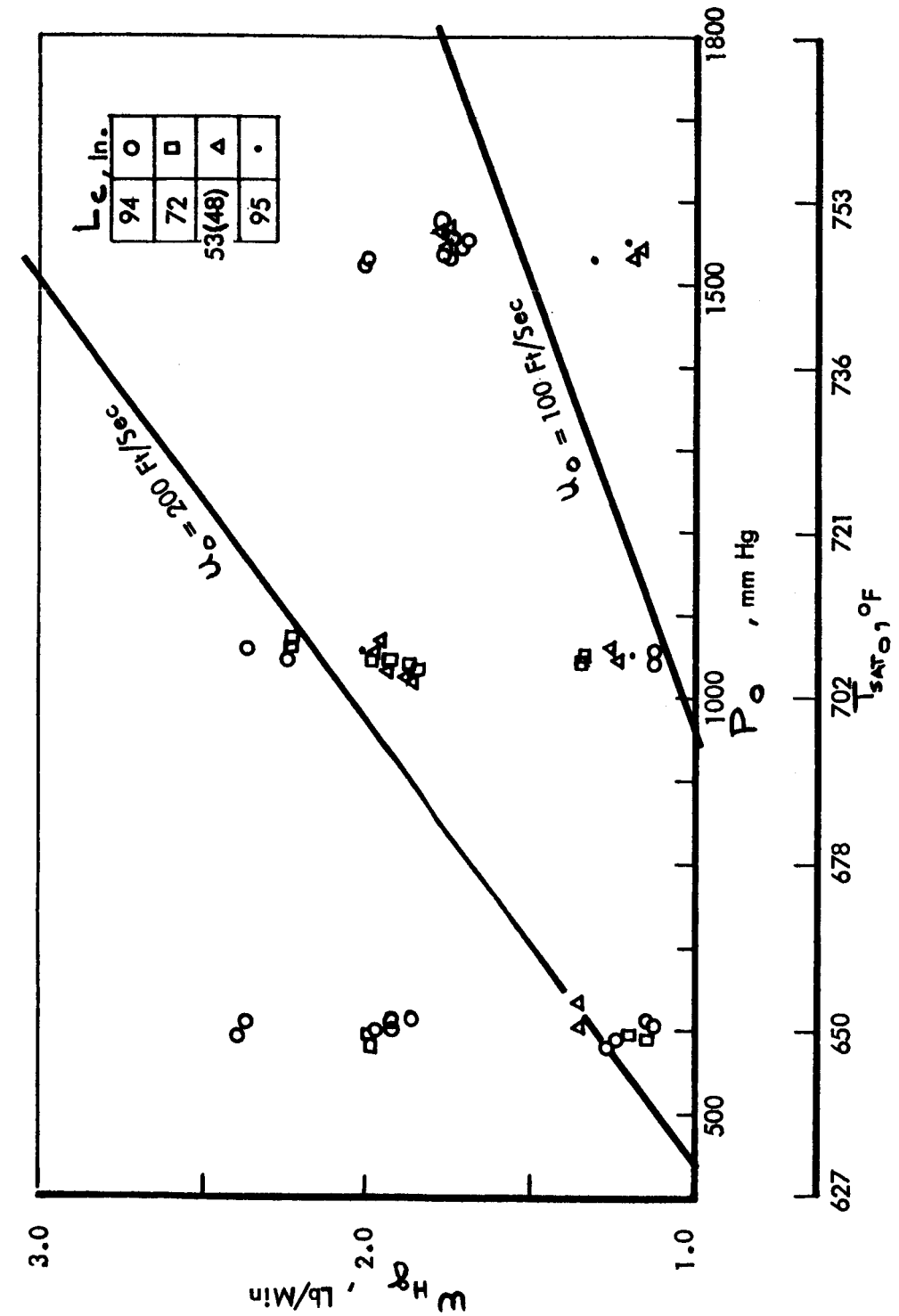

FIGURE 32

FLOW, PRESSURE AND CONDENSING LENGTH DATA POINT COMBINATIONS OBTAINED FOR THE HORIZONTAL CONDENSATION OF MERCURY IN A HAYNES-25 SPINEL COATED 0.4 TO 0.2 INCH ID BY 7 FOOT LONG TAPERED TUBE (SERIES D)

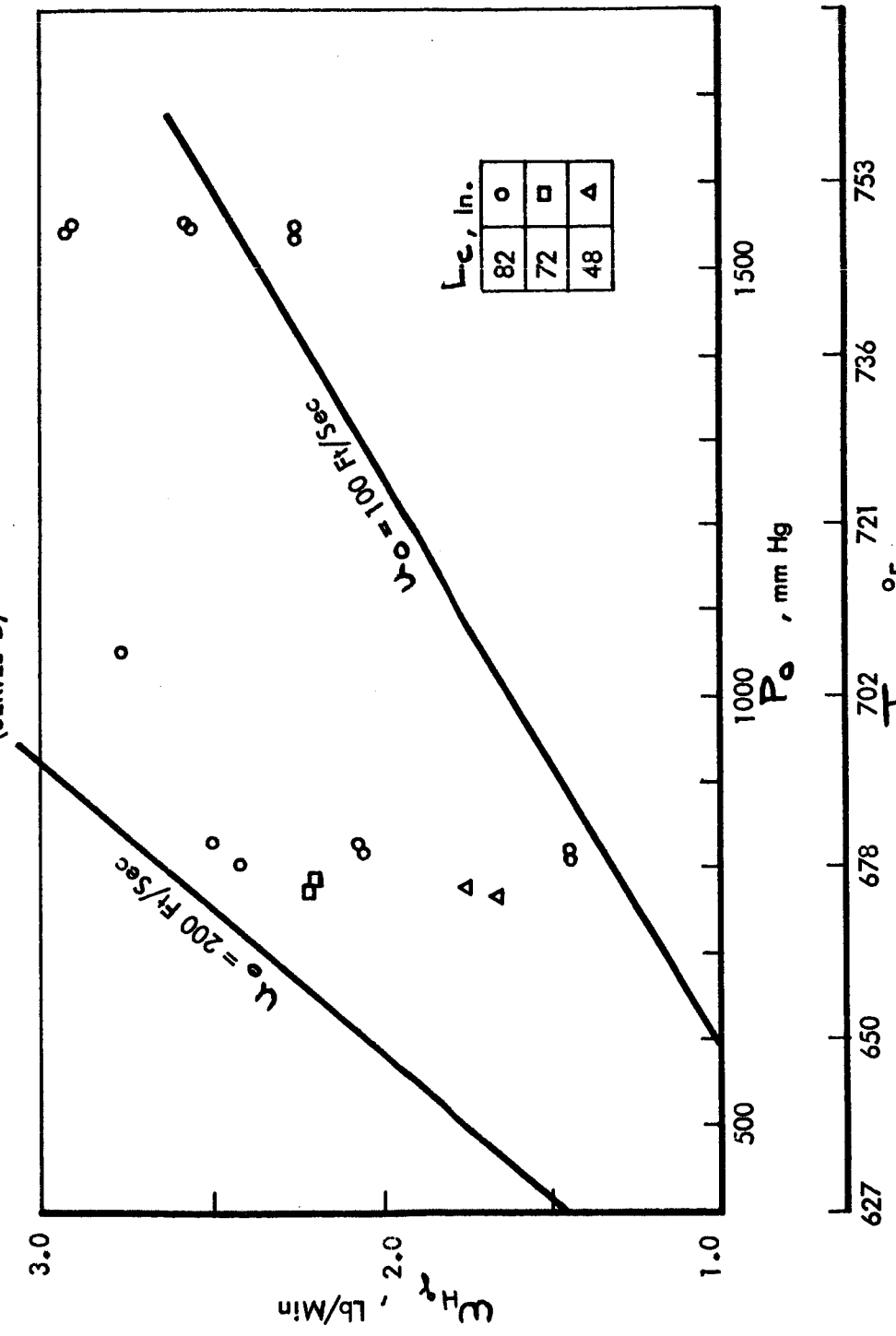

FIGURE 33

FLOW, PRESSURE AND CONDENSING LENGTH DATA POINT COMBINATIONS OBTAINED FOR THE HORIZONTAL CONDENSATION OF MERCURY IN A HAYNES-25 AND A STAINLESS STEEL 0.319 INCH BY 8 FOOT LONG TUBE (SERIES A & F)

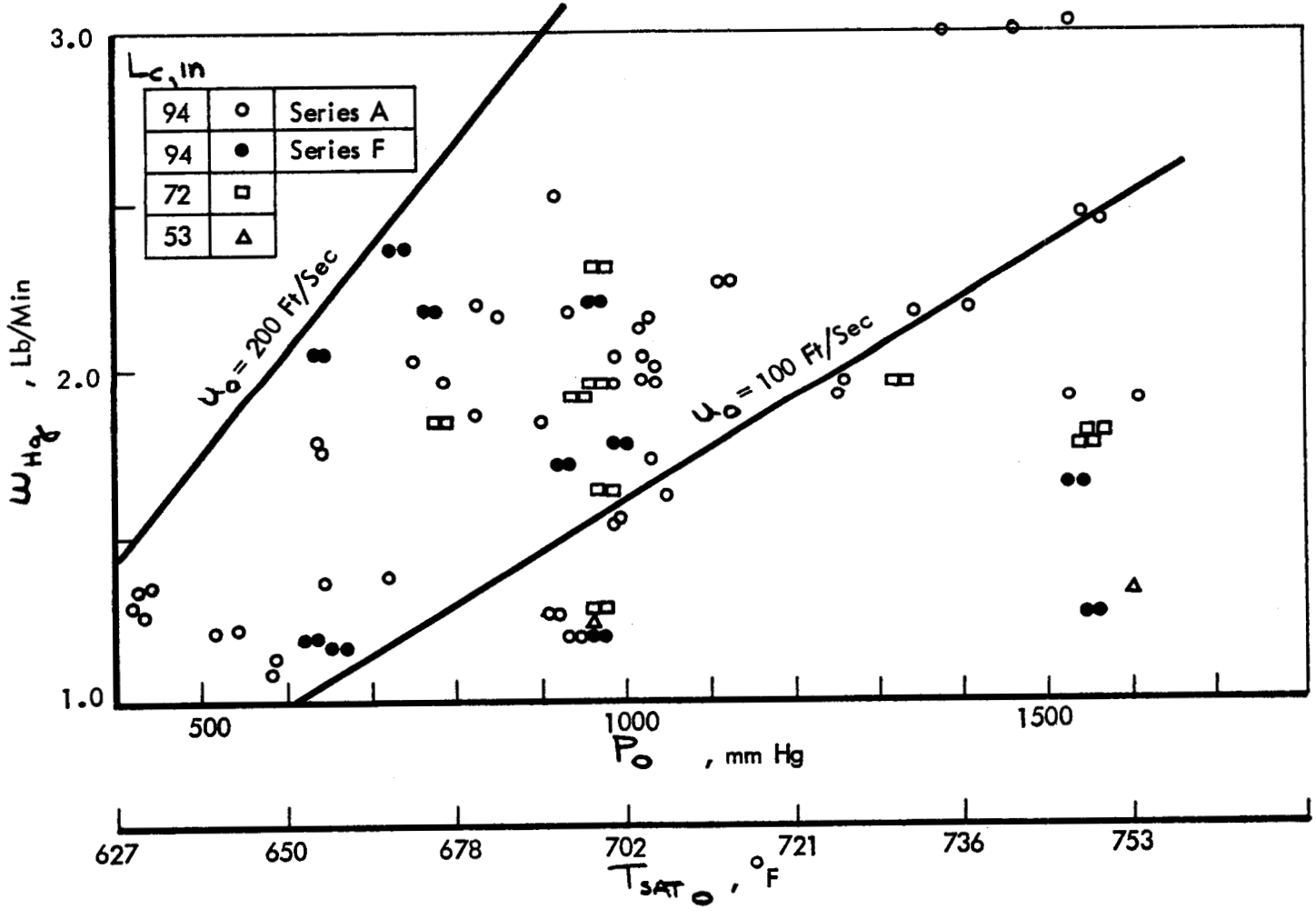

FIGURE 34

SKETCHES OF FLUOROSCOPIC OBSERVATIONS DURING CONDENSATION OF MERCURY IN A HORIZONTAL 316 STAINLESS STEEL TUBE

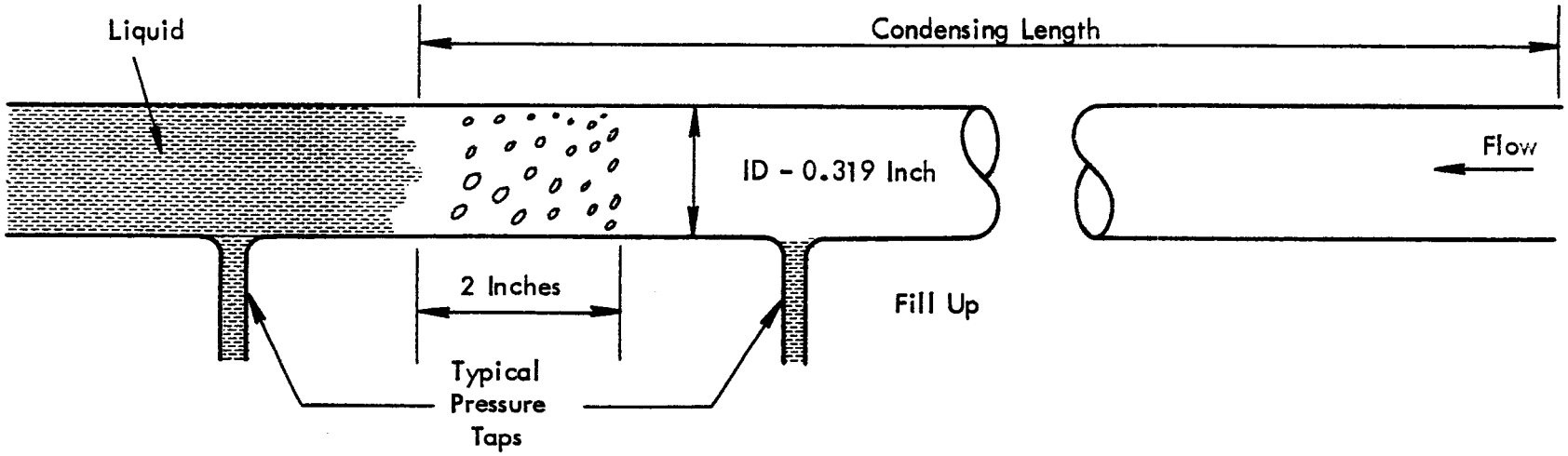

(a) Non-Wetting

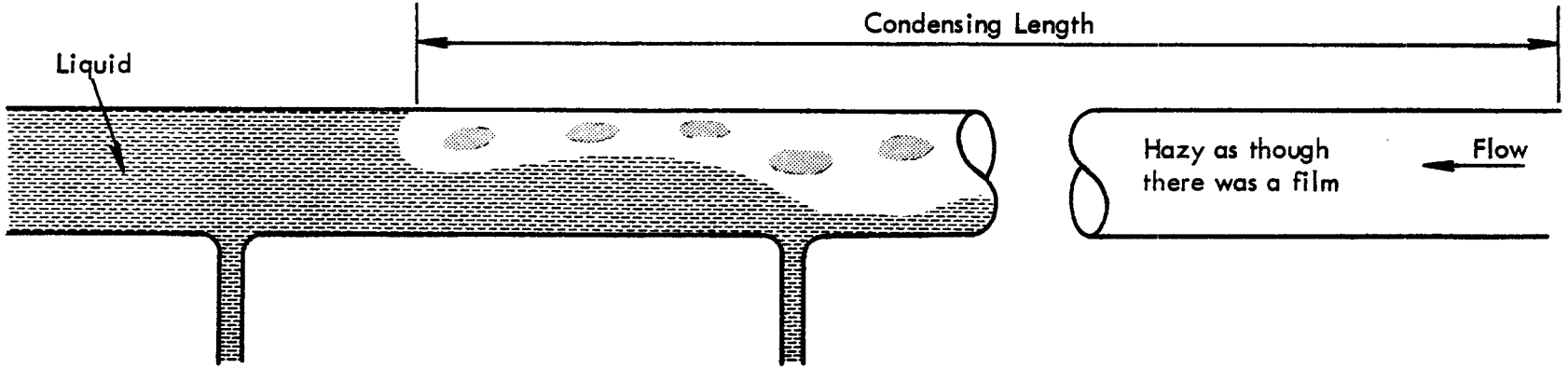

(b) Pseudo-Wetting

FIGURE 35

non-wetting condensing of mercury. Further testing, however, showed that wetting still existed and progressed with time. Since the existence and development of the wetting is of basic interest, observations were made and data taken for several days before termination of this test. The above performance will be compared with the performance of tubes with wetting condensing promoted by additives. Figure 36 compares pressure profiles during the wetting and non-wetting conditions and compares each with Martinelli theory (See Section 4.2).

Continuing with the non-wetting testing, a 0.397 inch inside diameter by 8 foot Type 304 stainless steel condensing tube was installed in the rig. An air cover gas was maintained in order to maximize the non-wetting testing time. Contrary to our expectations, wetting was noted within several hours. Similar results were obtained with the 0.4 inch to 0.2 inch inside diameter by 7 foot Haynes-25 tapered tube. These results are very unusual when one considers that de-wetting between mercury and metal surfaces has been observed after exposure to air (Ref 49). Introduction of air into the loop was expected to create this type of contamination and thereby cause the mercury to de-wet the surface.

The premature wetting obtained can be attributed to "pseudo-wetting" between mercury saturated contaminants or crud and contaminant on the surface. The problem was to determine the cause of the "pseudo-wetting" and how it could be prevented. In order to continue the testing and insure that sufficient non-wetting testing time would be available, the following specific areas were investigated:

1. the causes of the premature (or "pseudo-wetting") wetting,

2. methods for eliminating premature wetting once obtained,

3. steps required to insure that non-wetting data could be obtained continuously for at least a period of two weeks.

To expedite this investigation three minature versions (Minirigs) of the full scale test rig were made. A sketch of the rig is presented below.

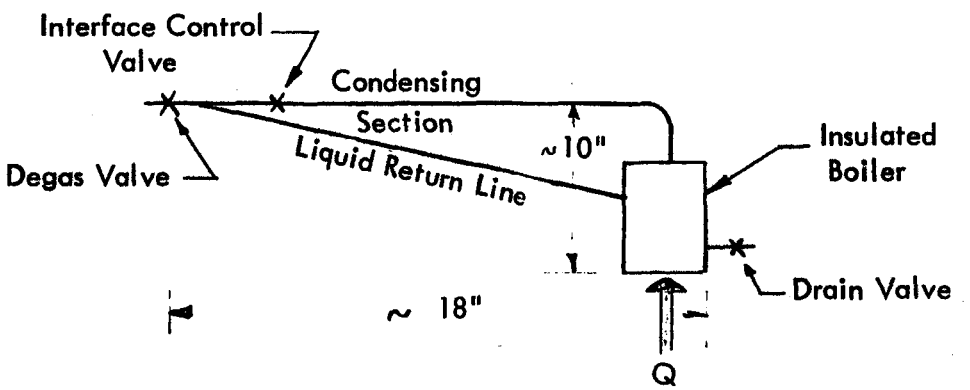

COMPARISON OF MEASURED VARIATION OF PRESSURE WITH LENGTH WITH MARTINELLI FOR THE COMPLETE WETTING AND NON-WETTING CONDENSATION OF MERCURY IN A 0.319 INCH ID, 316 STAINLESS STEEL HORIZONTAL TUBE

● Run A-26; w = 2.08 lb/min (No wetting observed)
■ Run W-4; w = 2.11 lb/min (Wetting* observed)
▬ Martinelli: See Appendix C

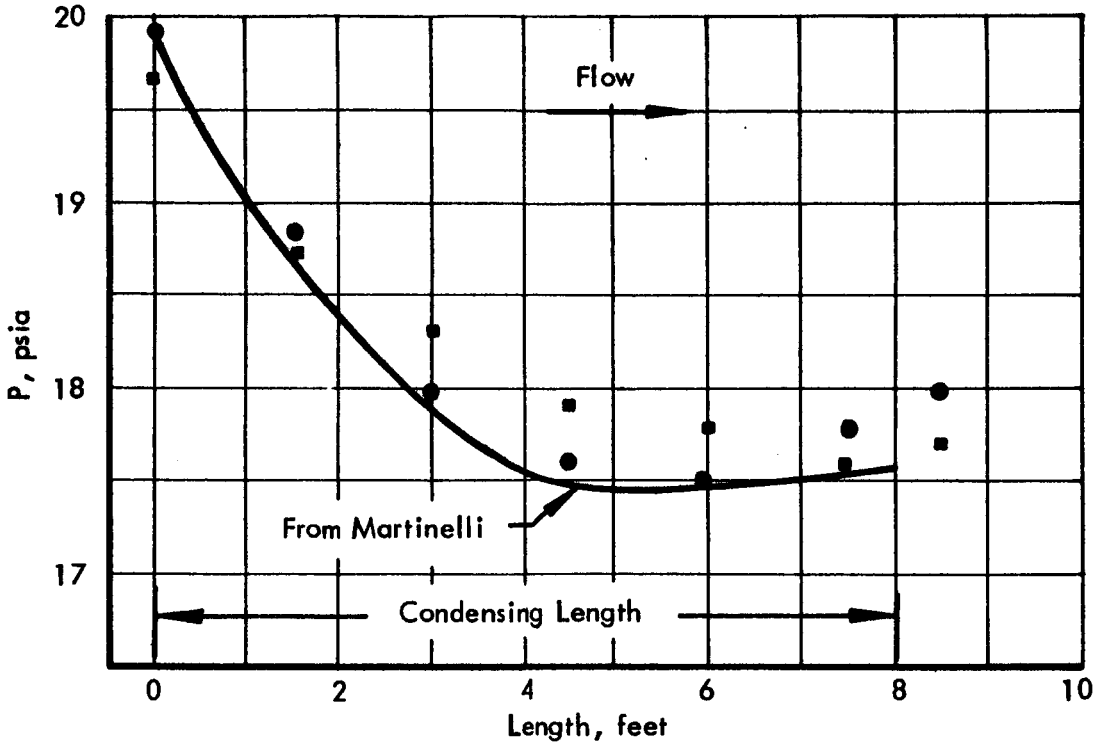

*Probably pseudo-wetting

FIGURE 36

Operation of the rigs was fluoroscopically observed to detect any significant changes in wetting in the condensing section. Table VI summarizes the operation of the rigs and compares the operation with the full-scale rig.

The three Minirigs were run a total of about 1000 hours. All three rigs were purposely dirtied, then cleaned, and the condensing section was replaced and rerun to determine if non-wetting operation were possible after the rig had been contaminated. Minirig No. 1 was contaminated by introduction of air after operation for about 500 hours. No wetting was observed on the fluoroscope screen during the 500 hours operation whereas the introduction of the air caused some wetting. A cleaned but otherwise untreated Haynes-25 type material was used in the condensing section after the rig was cleaned. Non-wetting operation was achieved for about 150 hours.

Minirig No. 2 was contaminated by using dirty mercury and large amounts of air. The rig was cleaned and a Haynes-25 type material spinel-coated tube was installed in the condensing section. A green spinel coating is formed by high temperature ($\sim$ 1750°F) exposure in a wet hydrogen atmosphere. Non-wetting operation was obtained for about 100 hours. The rig was shut down and argon back filled over night and during weekends. Minirig No. 3 was also dirtied with dirty mercury and air. The rig was cleaned and a stainless steel spinel-coated tube was installed in the condensing section. Due to poor cleaning the spinel coating was not uniform, however, and possibly caused the wetting that was noticed upon initial startup. A Haynes-25 type material spinel-coated tube was then used in the condensing section. Non-wetting operation was obtained for about 160 hours.

As a result of the Minirig testing the following procedures are now required to prevent pseudo-wetting while obtaining non-wetting mercury condensing data.

1. Air-mercury exposure in the rigs must be minimized.

2. When necessary, rig components should be cleaned with a dilute (20%) nitric acid solution followed by water.

3. A Haynes-25 type material tube treated in a wet hydrogen atmosphere should be used to provide non-wetting condensation for about 100 hours if (1) and (2) are heeded.

4. Rig shut down should be minimized but if necessary a high purity argon cover gas should be used.

6.3 Reduced Data

A digital computer program has been developed for the local and over-all reduction of constant tube diameter data. Data inputs are total condensing length, flow rate, absolute pressure level, local pressure readings and geometry. Average local and over-all saturation pressures are then calculated and thermodynamic properties are calculated according to Reference 50.

Local and over-all measured two-phase pressure drop (ΔP_{TP}) is calculated, corrected for vapor momentum recovery to give total two-phase pressure drop (ΔP_{TPT}), and divided by the vapor-only pressure drop (ΔP) for the same geometry and temperature. Vapor velocity is assumed to vary linearly with length in the data reduction. The ratio $\Delta P_{TPT} / \Delta P_G = \Phi_g^2$ can then be used for experimental correlation and comparison with Martinelli (see Section 4.1.2). In addition, local liquid and vapor Reynold's numbers are calculated and the appropriate X term calculated according to the equations of Section 4.1.2. An additional term $Re_a \, (v_g/v_l)^{1.25}$ is calculated as this combination has successfully correlated over-all two-phase pressure data at TRW (Ref 3, 5).

The computer program cannot presently handle the tapered tube data. Additional correlating parameters calculatable from the inputs can be easily included. The computer program is obtainable from either NASA or TRW.

TABLE VI

PSEUDO-WETTING OPERATING HISTORIES

	Test Rig	Previous History T/S	Previous History Rig	Hg	Material T/S	Material Rig	Cleaning Procedures	Vacuum Time, hr	Operating Life, hr	Comments
Full Size $600 < T_{T/S} < 750°F$	Test Series A 0.319 in. ID x 8 ft	As purchased	As purchased	Not distilled	316 ss	316 ss	Trichlorethelene except collection pot which had nitric acid, acetone, & water	12	> 0	No wetting observed.
									30–40	Manometer broke and air may have entered during ~10–20 hour exposure.
									~ 70	Wetting noticed in tube via X-ray and sight glass.
									~ 80	Air introduced into system through Hg in boiler to cause condensing surface to become oxidized and therefore non-wetting; ~60 hour exposure to air.
	Test Series W								> 80	Air cover maintained. Wetting continued to progress.
	0.397 in. ID x 8 ft	As purchased	Same Rig	Same Hg	304 ss	Same Rig	T/S only - Trichlorethelene	1/2	~2	Wetting noticed via X-ray and sight glass.
	0.4 in. to 0.2 in. tapered x 7.5 '	As purchased	Same Rig	Same Hg	HS-25	Same Rig	T/S only - Trichlorethelene	1/2	~2	Wetting noticed via X-ray and sight glass.
										Rig was dismantled and boiler dissected. Surface crud with Hg adhering could be scraped off with finger. After Hg evaporated, brownish dust or powder remained.
Mini-Version of full size test rig No. 1 $600 < T_{T/S} < 750°F$ $700 < T_{HTR} < 800°F$		As purchased	As purchased	Not distilled; Bottom of Hg from full scale	316 ss	316 ss	Blew hot air through.	1 hr with boiler at 400°F	> 0	No wetting.
									~2	Tube shows signs of spotty coating; heavier on top.
									~3	No wetting.
									3–490	Run continuously with only three shutdowns and back filled with argon. No wetting observed.
									490	Air admitted to rig and rig started. Some wetting noticed immediately. Drops irregular and about two times previous size. Rig allowed to run all night.
									508	Next morning. No wetting and tube walls appear cleaner than before air was admitted.
									532	Same as above. Rig shut down for change.
	Changed T/S Tube	As purchased	Same Rig	distilled	HS-25	Same Rig	Rig-nitric acid & distilled H_2O. T/S-nothing. After cleaning system filled with argon.	3	> 0	Degas valve leaked; therefore system could not be run at $T_{sat} < 680°F$. Some air sucked into system. Valve inards show evidence of crud.
									114	System has been run continuously. Some drops on wall indicate wetting but interface was not sloppy. 90°F.
									138	Same as above. Leak rate too high. Shut down.

TABLE VI (Continued)

PSEUDO-WETTING OPERATING HISTORIES (Continued)

	Test Rig	Previous History		Hg	Material		Cleaning Procedures	Vacuum Time, hr	Operating Life, hr	Comments
		T/S	Rig		T/S	Rig				
Mini-Version of full size test rig No. 2		As purchased	As purchased	Not distilled; used Hg from full scale	316 ss	316 ss	Trichlorethelene and distilled H_2O baked to eliminate liquid	1	> 0	No wetting.
									25	No wetting. Air introduced while cooling from 600 to 300°F. Restarted and no wetting observed in first hour.
									30	Slight indication of wetting.
									47	Some wetting. Air introduced again while hot. Restarted. More wetting observed.
									53	Shut down for weekend with air passing through mercury in boiler; 64 hours.
									53-92	Rig run - heavy wetting observed. Test terminated.
	Changed T/S Tube	HS-25 spinel 1830°F; 20% wet; H_2 for 1 hr	Same Rig	Distilled	HS-25 spinel	Same Rig	20% nitric acid. T/S - none	2	> 0	No wetting.
									100	System run with shut down and back filled with argon overnight and weekend. No wetting.
Mini-Version of full size test rig No. 3		As purchased	As purchased	Not distilled; Same as No. 1	316 ss	316 ss	Trichlorethelene and distilled H_2O baked to eliminate liquid	1	> 0	No wetting.
									24	Air introduced to hot system. Upon restart wetting noticed.
									53	Wetting. Shut down for weekend. Restarting, no wetting observed at first. After about 1/2 hour wetting began. More air introduced into system and heavy wetting observed for about 1 hr after which wetting diminished. Air was introduced for 2 hrs with boiler at 400°F. System restarted and wetting observed.
									150	Heavy wetting. Test terminated.
	Changed T/S Tube	316 spinel; poor	Same Rig	Distilled	316 ss spinel	Same Rig	20% nitric acid Oakite, Freon. T/S - nothing	17-total; final 1/2 hr with torch (~900°F)	> 0	Wetting with sluggish mercury flow.
									24	Wetting continued. Rig shut down.
	Changed T/S/Tube	HS-25 spinel	Same Rig	Distilled	HS-25 spinel	Same Rig	Dilute nitric acid dilute Oakite, Freon 113, distilled H_2O	1/2	> 0	Slight wetting noticed. No wetting after 1/2 hour.
									160	No wetting. Shut down. Air admitted. Restarted.
									165	Heavy wetting and slugging observed. Shut down.

7.0 COMPARISON OF DATA WITH THEORY

The theory available for comparison with mercury condensing data is presented in Section 4, "Theory and Analysis." At this time comparison between the data and theory is incomplete. The comparisons available are nevertheless presented, although a more extensive comparison is to be expected in the final report.

Section 4.2 presents a method for predicting pressure drop during the non-wetting condensing of mercury with low Froude numbers (i.e., when the ratio of gravity to inertia forces is small). The most difficult phenomenon to account for in the non-wetting pressure drop prediction is the effect of drops in transit. A rather complex computer solution is required for the complete solution. To provide a check on the theory, the equations were made amenable to hand calculation by means of several simplifying assumptions. Figures 37 and 38 compare the pressure profiles actually obtained with the profiles predicted by the theory of Section 4.2 simplified by means of the following assumptions:

1. Droplet drag can be determined from the Stokes equation,

$$C_d = \frac{24}{Re_\delta} = \frac{24\,\mu_v}{\delta \times G_T\,|1-\epsilon|} .$$

2. Slip can be assumed to vary linearly with droplet size from zero to nearly one, or

$$\epsilon = \frac{\delta_c - \delta}{\delta_c - \delta_{\epsilon=1}} .$$

3. The effect of the axial vapor velocity variation with length was neglected and Equation 37 became a linear differential equation.

4. Only drops having slips from $\epsilon = 0$ to $\epsilon = 0.96$ were considered.

The limit of $\epsilon = 0.96$ is effectively a correlating adjustment.

The low pressure gradient at the inlet of the 0.397 inch inside diameter tube data of Figure 38 is tentatively attributed to the increased cooling effect caused by the two water-cooled pressure taps used at the inlet during these tests. Otherwise the theory appears to correlate quite well with the data.

Section 4.1 describes the application of Martinelli's data to the prediction of condensing pressure drop. A comparison with wetting and non-wetting data was felt to be useful; this is presented in Figure 36. Both non-wetting and pseudo-wetting pressure data are presented for the 0.319 inch inside diameter tube. Appendix C presents the sample calculations made to determine the pressure curve shown in Figure 36.

COMPARISON OF SIMPLIFIED THEORY WITH DATA FOR THE NON-WETTING CONDENSING OF MERCURY

Run - A-26
W = 2.08 lb/min
ID = 0.319 inch

O - Measured data

Material - Stainless steel
Horizontal

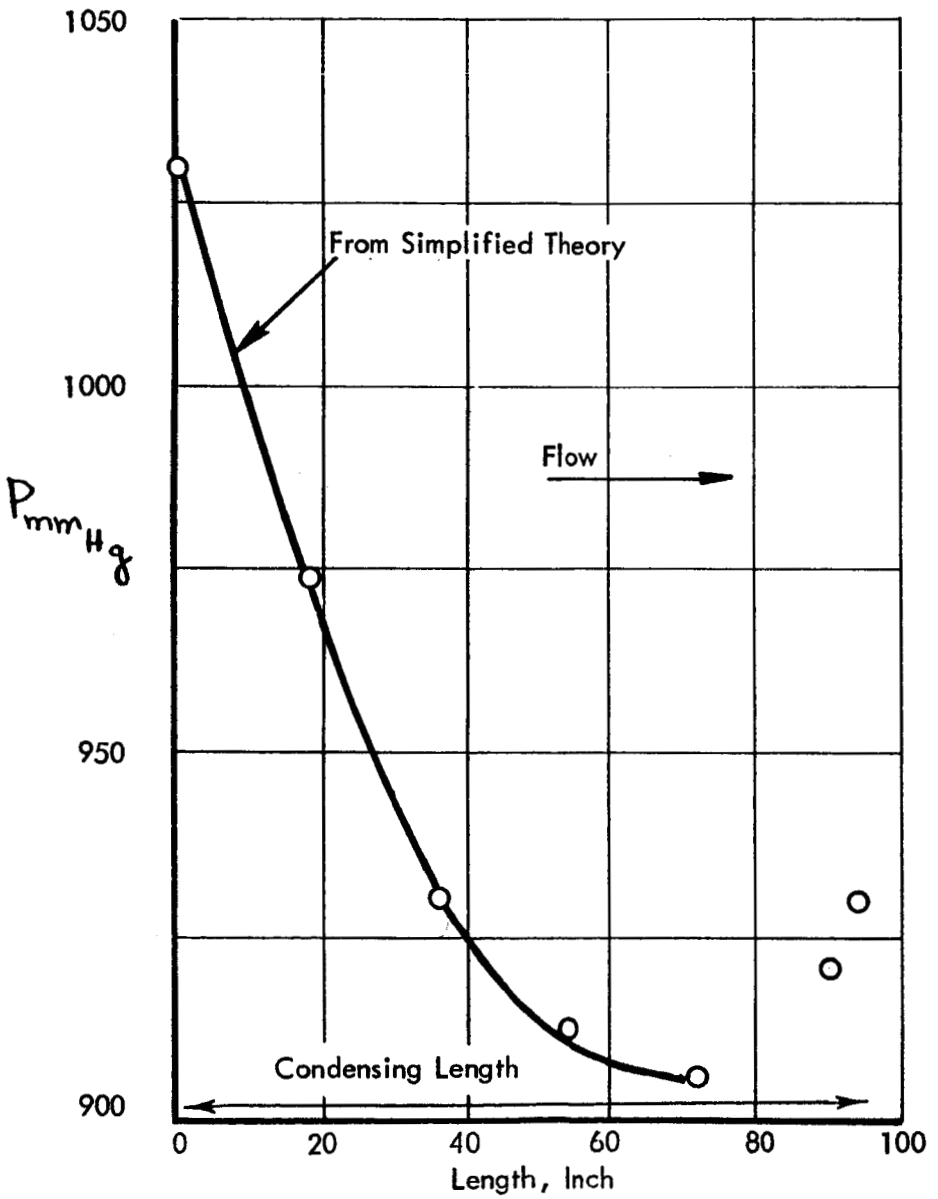

FIGURE 37

COMPARISON OF SIMPLIFIED THEORY WITH DATA FOR THE NON-WETTING CONDENSING OF MERCURY

Run - E-15
W - 2.38 lb/min
ID - 0.397 inch

Material - Haynes 25
Horizontal

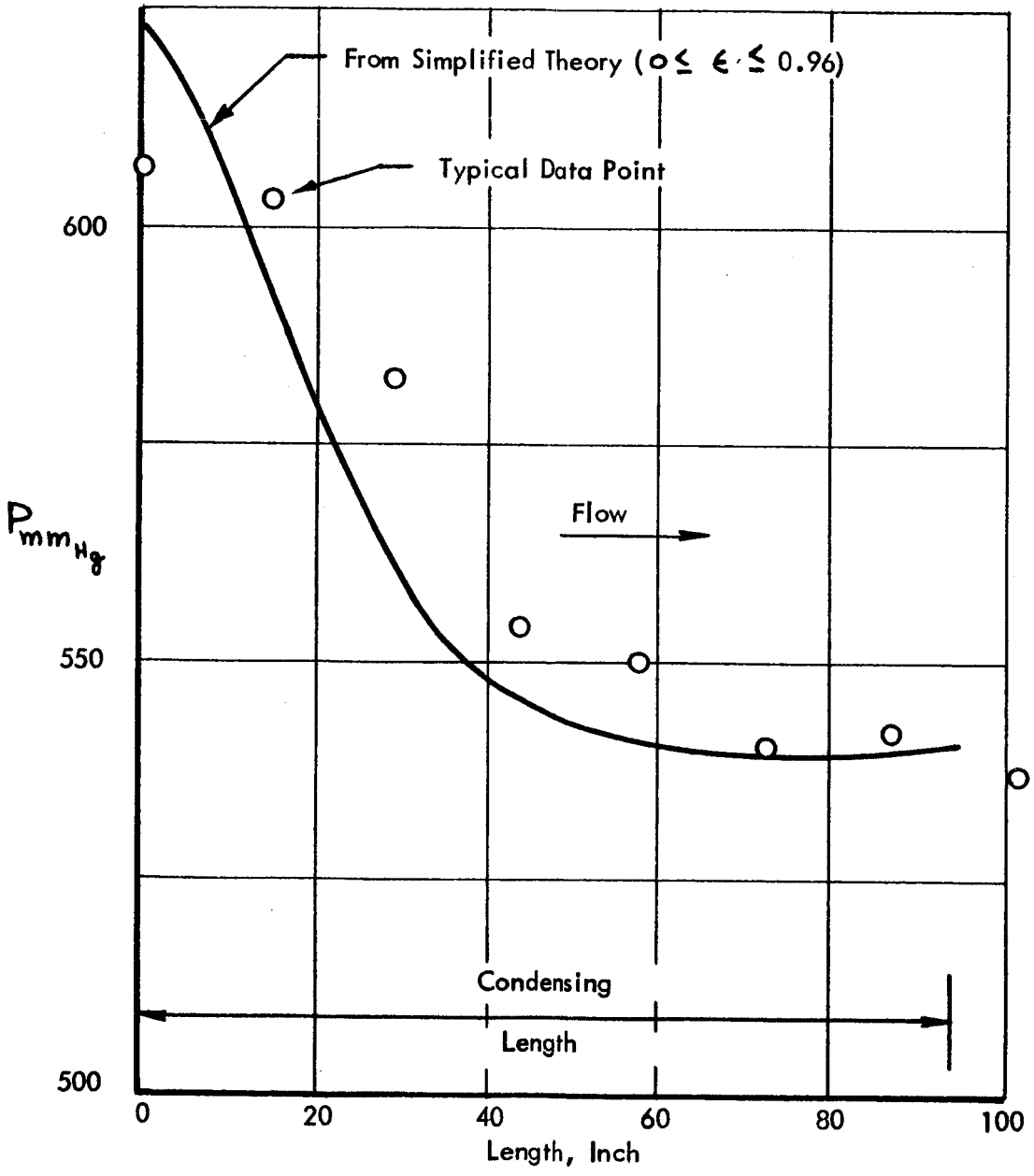

FIGURE 38

APPENDIX A

WETTING AND NON-WETTING CONDENSING

The general consideration of interfaces between solids and either liquid and/or vapor is not simple. Considerations are required of surface roughness, non-homogeneity, and contamination. Contamination may include very lightly held, physically absorbed molecules or thin oxide layers. These phenomena are summarized by Bikerman in Reference 52.

The case of non-wetting mercury can be attributed to surface contamination (oxides) and/or adsorbed gases. An example of the effect of adsorbed gases and/or surface contaminations is the fact that mercury has been shown to wet glass that was heated under a vacuum (Ref 53). Similarly metal that is normally non-wetting, such as stainless steel, when broken in mercury to give immediate exposure to the mercury is immediately wetted.

With sufficient time and temperature mercury will dissolve adsorbed gases and remove the oxide surface coating. In the interim, however, the surface will be non-wetting and non-wetting condensation will occur. Non-wetting data were thus obtained from tubes that were cleaned according to procedures commonly used for cleaning mercury Rankine cycle space power systems. These procedures include sufficient exposure to oxygen to allow some form of oxygen contamination. The oxygen pressure required to produce contamination is far lower than the best obtainable vacuum for most metals of engineering importance.

Wetting condensation can be obtained by using magnesium and titanium additives to remove contaminants. (Ref 54, 55) Both magnesium and titanium are "getters" of oxygen and break down oxide films as well as remove adsorbed gases. As a result, a clean metal surface is left for the mercury to wet. Actually, however, mercury containing titanium forms a titanium intermetallic of some sort (iron, carbon, or nitrogen, and even mercury) which serves as a barrier to mercury contact with the metal, and mercury wets this intermetallic. (Ref 56). If the titanium intermetallic should be eroded, the clean metal surface remains and should cause wetting condensation.

Wetting condensation can thus be maintained as long as oxygen and other contaminants are kept from the surfaces. To prevent reversion to non-wetting, the surfaces to be preserved should be exposed to mercury vapor and/or liquid only. As a poor alternative an inert gas cover such as very high purity argon might be used.

Another form of wetting has been obtained in TRW experiments and can readily be observed by placing contaminated mercury in a glass cup. A non-uniform and spotty mercury-like substance will adhere to the glass. This form of wetting is pseudo-wetting in that it is really wetting between mercury-soaked contaminants and the contaminated glass wall. Section 6.2 discusses the actual occurrence of "pseudo-wetting" during test. An obvious problem thus exists. When "wetting" appears, is it actual wetting or not and how do wetting and pseudo wetting compare. This is a surface chemistry problem beyond the scope of this contract but certainly worthy of consideration.

APPENDIX B
NON-WETTING DROP MODEL DERIVATIONS

DROP DISTRIBUTION FUNCTION

Flow Rate

Let $N(\delta, L)d\delta$ be the number of drops per unit volume, having diameters between δ and $d\delta$, at distance L.

The mass of one drop of diameter δ is $\frac{\pi\delta^3}{6}$.

The mass of fluid per unit voulme, contained in drops having diameters between δ and $d\delta$ at distance L, is

$$\frac{\pi\rho_f}{6} N(\delta, L)\delta^3 d\delta$$

The mass flow rate, at distance L, of fluid contained in drops having diameters between δ and $\delta + d\delta$ is then

$$\frac{\pi D^2}{4}\frac{\pi\rho_f}{6} u_f(\delta, L) N(\delta, L)\delta^3 d\delta \qquad \text{(Eq B-1)}$$

Let $u_f(\delta, L) = \epsilon(\delta, L)\, u_v(L)$ (Eq B-2)

Equation B-1 gives,

$$dw_f(\delta, L) = \frac{\pi^2 D^2 \rho_f}{24} u_v(L) N(\delta, L)\epsilon(\delta, L)\delta^3 d\delta \qquad \text{(Eq B-3)}$$

The total mass flow rate of fluid contained in drops at distance L is

$$w_f(L) = \frac{\pi^2 D^2}{24}\rho_f u_v(L)\int_{\delta_{c_0}}^{\delta_c(L)} N(\delta, L)\epsilon(\delta, L)\delta^3 d\delta \qquad \text{(Eq B-4)}$$

It is known that $d\delta_c(L)/dL$ is always positive.

Let $C_1 \equiv \frac{\pi^2 D^2 \rho_f}{24}$ (Eq B-5)

Thus,

$$w_f(L) = C_1 u_v(L) \int_{\delta_{c_0}}^{\delta_c(L)} N(\delta, L) \epsilon(\delta, L) \delta^3 d\delta \qquad \text{(Eq B-6)}$$

Sketch Showing Variation of Drop Size With Length

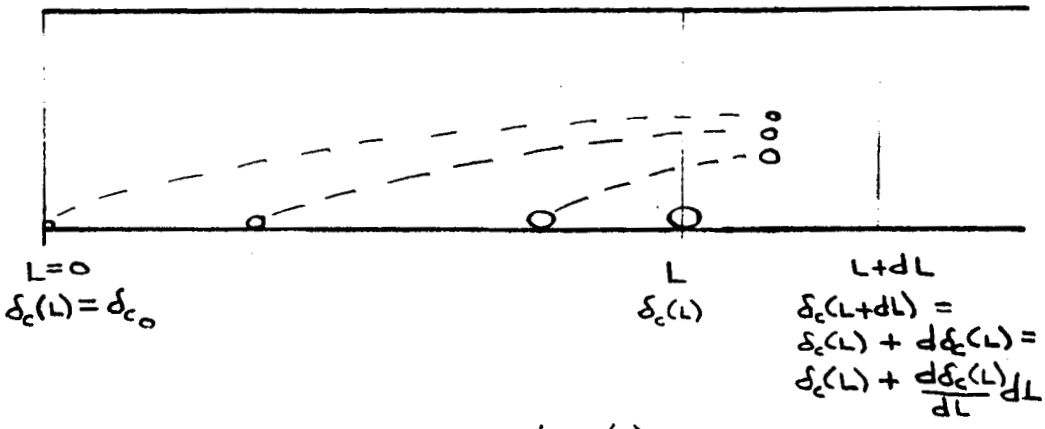

The rate of entrainment of liquid by vapor is $\frac{dw_f(L)}{dL}$.

The increase in drop flow rate between L and $L+dL$ is

$$dw_f(L) = \frac{dw_f(L)}{dL} dL$$

This increase of flow rate consists of drops having diameter between δ_c and $\delta_c + d\delta_c$ and includes all drops in this size range.

At distance $L+dL$ the mass flow rate of drops having diameters between δ_c and $\delta_c + d\delta_c$ is, from Equation B-3,

$$C_1 u_v(L) N(\delta_c, L) \epsilon(\delta_c, L) \delta_c^3 d\delta_c = \frac{dw_f(L)}{dL} dL$$

or

$$N(\delta_c, L) \epsilon(\delta_c, L) \delta_c^3 = \frac{\frac{dw_f(L)}{dL}}{C_1 u_v(L) \frac{d\delta_c(L)}{dL}} \left(= \frac{1}{C_1 u_v(L)} \frac{dw_f}{d\delta_c} \right) \qquad \text{(Eq B-7)}$$

Since δ_c, C_1, $\frac{dw_f(L)}{dL}$, $u_v(L)$ and $\frac{d\delta_c(L)}{dL}$ are all positive finite quantities the product $N(\delta_c, L) \epsilon(\delta_c, L)$ must be positive and finite. But it is known that $\epsilon(\delta_c, L) \neq 0$; therefore the values of the distribution function $N(\delta_c, L)$ must approach infinity as the drop size approaches the critical size for that particular distance L.

Continuity Relation

The mass rate of flow of drops in the size range δ to $\delta + d\delta$ is the same at all values of L provided that this size is less than the critical size in the range of L considered. In equation form,

$$dw_f(\delta, L_1) = dw_f(\delta, L_2) \qquad \delta < \delta_c(L_1) \left[< \delta_c(L_2)\right]$$

or,

$$C_1 u_v(L_1) N(\delta, L_1) \epsilon(\delta, L_1) \delta^3 d\delta = C_1 u_v(L_2) N(\delta, L_2) \epsilon(\delta, L_2) \delta^3 d\delta$$

Therefore,

$$u_v(L_1) N(\delta, L_1) \epsilon(\delta, L_1) = u_v(L_2) N(\delta, L_2) \epsilon(\delta, L_2) \qquad \text{(Eq B-8)}$$

At $L = L_c$, i.e. where $\delta = \delta_c(L)$, from Equation B-7,

$$N(\delta, L_c) \epsilon(\delta, L_c) = \frac{1}{C_1 u_v(L_c) \delta^3} \left[\frac{\frac{dw_f(L)}{dL}}{\frac{d\delta_c(L)}{dL}} \right]_{L=L_c} \qquad \text{(Eq B-9)}$$

$$N(\delta, L) \epsilon(\delta, L) = \frac{1}{C_1 \delta^3} \frac{1}{u_v(L)} \left[\frac{\frac{dw_f(L)}{dL}}{\frac{d\delta_c(L)}{dL}} \right]_{L=L_c} \qquad \text{(Eq B-10)}$$

NOTE: The quantity $u_v(L) N(\delta, L) \epsilon(\delta, L) \delta^3$ is constant for all values of L, at a fixed value of δ. It is not constant for all values of δ at a fixed vlaue of L unless $\left[\frac{\frac{dw_f(L)}{dL}}{\frac{d\delta_c(L)}{dL}} \right]_{L=L_c}$ is constant for all values of δ.

In the expression for $N(\delta,L)\epsilon(\delta,L)$, Equation B-10, the derivative $\frac{d\delta_c(L)}{dL}$ is not a directly measured quantity, However, since $dw_v(L) = -dw_f(L)$

$$\frac{d\delta_c(L)}{dL} = \frac{du_v(L)}{dL}\frac{d\delta_c(u_v)}{du_v} = -\frac{4}{\pi D^2 \rho_v}\frac{dw_f(L)}{dL}\frac{d\delta_c(u_v)}{du_v} \quad \text{(Eq B-11)}$$

Therefore, in Equation B-10,

$$\frac{\frac{dw_f(L)}{dL}}{\frac{d\delta_c(L)}{dL}} = -\frac{\frac{dw_f(L)}{dL}}{\frac{4}{\pi D^2\rho_v}\frac{dw_f(L)}{dL}\frac{d\delta_c(u_v)}{du_v}} = \frac{\pi D^2 \rho_v}{4\left[-\frac{d\delta_c(u_v)}{du_v}\right]}$$

Also,

$$\frac{1}{c_1}\frac{\pi D^2\rho_v}{4} = \frac{6\rho_v}{\pi\rho_f}$$

And,

$$\frac{1}{u_v(L)} = \frac{u_v(L_c)}{u_v(L)}\frac{1}{u_v(L_c)} = \frac{w_v(L_c)}{w_v(L)}\frac{1}{u_v(L_c)} = \frac{\frac{w_v(L_c)}{w_o}}{\frac{w_v(L)}{w_o}u_v(L_c)} = \frac{x(L_c)}{x(L)}\frac{1}{u_v(L_c)}$$

Thus, Equation B-10 becomes,

$$N(\delta,L) = \frac{6\rho_v}{\pi\rho_f}\frac{1}{\delta^3\epsilon(\delta,L)}\frac{x(L_c)}{x(L)}\frac{1}{\left[-u_{v_c}\frac{d\delta_c(u_v)}{du_{v_c}}\right]_\delta} \quad \text{(Eq B-12)}$$

Alternatively, without involving the quantity $x(L_c)$ which is known only indirectly as a function of δ:

$$N(\delta,L) = \frac{6}{\pi}\frac{\rho_v}{\rho_f}\frac{1}{\delta^3\epsilon(\delta,L)}\frac{1}{u_v(L)}\frac{1}{\left[-\frac{d\delta_c(u_v)}{du_v}\right]_\delta} \quad \text{(Eq B-13)}$$

Or, in terms of the quality at L:

$$N(\delta,L) = \frac{6}{\pi}\frac{\rho_v}{\rho_f}\left(\frac{\pi D^2\rho_v}{4w}\right)\frac{1}{\delta^3\epsilon(\delta,L)x(L)}\frac{1}{\left[-\frac{d\delta_c(u_v)}{du_v}\right]_\delta} \quad \text{(Eq B-14)}$$

DRAG ON A SINGLE DROP (of diameter δ at distance L)

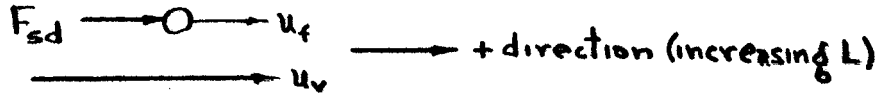

$$F_{sd} = C_d A_{sd} \frac{\rho_v (u_{rel})^2}{2 g_c} = C_d A_{sd} \frac{\rho_v (u_v - u_f)|u_v - u_f|}{2 g_c}$$

But,

$$u_v - u_f = u_v \left(1 - \frac{u_f}{u_v}\right) = u_v (1 - \epsilon)$$

$$A_{sd} = \frac{\pi \delta^2}{4}$$

$$F_{sd} = \frac{\pi}{8 g_c} \rho_v u_v^2 C_d \delta (1 - \epsilon)|1 - \epsilon| \qquad \text{(Eq B-15)}$$

$(1-\epsilon)|1-\epsilon|$ is used rather than $(1-\epsilon)^2$ to account for proper sign when $u_v < u_f$

Newton's second law of motion is

$$F_{sd} = \frac{M_{sd}}{g_c} \frac{d^2 L}{dt^2} = \frac{M_{sd}}{g_c} u_f \frac{du_f}{dL} = \frac{M_{sd}}{g_c} \left(u_v^2 \epsilon \frac{d\epsilon}{dL} + u_v \epsilon^2 \frac{du_v}{dL}\right) \qquad \text{(Eq B-16)}$$

The mass of a single drop $M_{sd} = \frac{\pi \rho_f \delta^3}{6}$

Combining Equations B-15 and B-16 yields

$$\frac{d\epsilon}{dL} + \frac{\epsilon}{u_v} \frac{du_v}{dL} = \frac{3}{4} \frac{\rho_v}{\rho_f} \frac{C_d}{\delta} \frac{(1-\epsilon)|1-\epsilon|}{\epsilon} \qquad \text{(Eq B-17)}$$

$$\frac{d\epsilon}{dL} = \frac{3}{4} \frac{\rho_v}{\rho_f} \frac{C_d}{\delta} \frac{(1-\epsilon)|1-\epsilon|}{\epsilon} - \frac{1}{u_v} \frac{du_v}{dL} \epsilon \qquad \text{(Eq B-18)}$$

But $$\frac{1}{u_v} \frac{du_v}{dL} = \left(\frac{\pi D^2 \rho_v}{4 w x}\right)\left(\frac{4w}{\pi D^2 \rho_v} \frac{dx}{dL}\right) = \frac{1}{x} \frac{dx}{dL} \qquad \text{(Eq B-19)}$$

Equation B-19 becomes,

$$\frac{d\epsilon(\delta,L)}{dL} = \frac{3}{4}\frac{\rho_v}{\rho_f}\frac{C_d(\delta,L)}{\delta}\frac{[1-\epsilon(\delta,L)]|1-\epsilon(\delta,L)|}{\epsilon(\delta,L)} - \frac{dx(L)}{x(L)dL}\epsilon(\delta,L) \quad \text{(Eq B-20)}$$

Assume C_d is a function of the Reynold's number based on drop diameter and vapor properties:

$$Re_\delta = \frac{\rho_v u_v |1-\epsilon|\delta}{\mu_v} \qquad \text{But,} \quad u_v = \frac{4w}{\pi D^2 \rho_v} x$$

$$Re_\delta = \frac{G}{\mu_v} x(L)|1-\epsilon(\delta,L)|\delta$$

The differential equation for ϵ as a function of L, for a given drop diameter δ is then,

$$\frac{d\epsilon}{dL} = \frac{3}{4}\frac{\rho_v}{\rho_f}\frac{C_d}{\delta}\frac{(1-\epsilon)|1-\epsilon|}{\epsilon} - \frac{1}{x}\frac{dx}{dL}\epsilon \qquad \text{(Eq B-21)}$$

where $x = x(L)$

and $C_d = C_d\left(\frac{G}{\mu_v}, x(L), \epsilon, \delta\right)$

For a given condenser tube, handling a given fluid, at a given flow rate per unit area, a number of solutions must be obtained for various drop diameters.

Start of Solution at $\epsilon = 0$

There is a problem in starting a step-by-step numerical solution of the differential equation (Equation B-21), because the derivative $\frac{d\epsilon}{dL}$ is infinite when ϵ is zero.

However, for small ϵ the equation has the form

$$\frac{d\epsilon}{dL} = \frac{3}{4}\frac{\rho_v}{\rho_f}\frac{C_{do}}{\delta}\frac{1}{\epsilon}$$

This equation may be put in the form

$$\frac{d(\epsilon^2)}{dL} = \frac{3}{2}\frac{\rho_v}{\rho_f}\frac{C_{do}}{\delta}$$

with solution

$$\epsilon = \sqrt{\frac{3}{2}\frac{\rho_v}{\rho_f}\frac{C_{do}}{\delta}L}$$

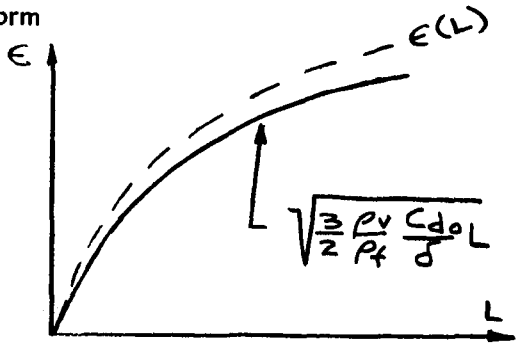

which may be used to start the step-by-step solution (see sketch)

TOTAL FORCE BETWEEN DROPS AND VAPOR (at distance L)

The total force acting on a single drop has been shown to be,

$$F_{sd} = \frac{\pi}{8\xi_c} \rho_v u_v^2 C_d \delta (1-\epsilon)|1-\epsilon| \qquad \text{(See Equation B-15).}$$

The force per unit volume on drops having diameters between δ and $\delta + d\delta$ is then,

$$dF_d(\delta, L) = F_{sd}(\delta, L)\, N(\delta, L)\, d\delta$$

$$= \frac{\pi}{8\xi_c} \rho_v u_v^2(L)\, C_d(\delta, L) N(\delta, L)[1-\epsilon(\delta, L)]|1-\epsilon(\delta, L)|\delta^2 d\delta$$

The total force per unit volume on all drops at L is

$$F_d(L) = \frac{\pi}{8\xi_c} \rho_v u_v^2(L) \int_{\delta_{co}}^{\delta_c(L)} C_d(\delta, L) N(\delta, L)\left[1-\epsilon(\delta, L)\right]|1-\epsilon(\delta, L)|\delta^2 d\delta$$

Effect on Pressure Drop

$$P + dP = P + \frac{dP}{dL} dL$$

$$dV = A\, dL$$

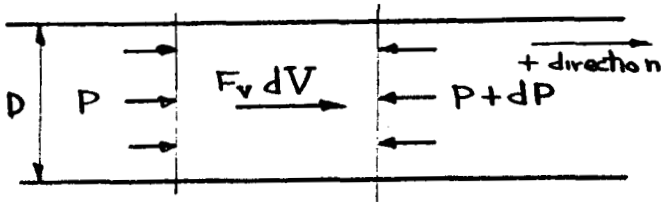

If there are no effects other than droplet drag,

$$F_v\, dV = A\, dP$$

$$F_v A\, dL = A \frac{dP}{dL} dL$$

$$\left(\frac{dP}{dL}\right)_{drag} = F_v = -F_d$$

$$= -\frac{2w^2}{\pi \xi_c D^4 \rho_v} x^2(L) \int_{\delta_{co}}^{\delta_c(L)} C_d(\delta, L)\, N(\delta, L)\left[1-\epsilon(\delta, L)\right]|1-\epsilon(\delta, L)|\delta^2 d\delta \qquad \text{(Eq B-22)}$$

The equation for the pressure drop due to drag has been written in terms of the drag coefficient $C_d(\delta, L)$ which, in view of the non-steady relative motion, is likely to be a very complicated (and perhaps unpredictable) function of local conditions. Since in an analytical treatment the drag equation must be solved first for every drop size, it is probably

better to express the pressure drop due to drag in terms of the resulting drop velocity distribution, i.e., in a form which does not explicitly involve the drag coefficient. Substituting from Equation B-17,

$$C_d(1-\epsilon)|1-\epsilon|\delta^2 = \frac{4}{3}\frac{\rho_f}{\rho_v}\delta^3\epsilon\left(\frac{d\epsilon}{dL} + \frac{1}{x}\frac{dx}{dL}\epsilon\right)$$

$$= \frac{4}{3}\frac{\rho_f}{\rho_v}\frac{\delta^3\epsilon}{x}\frac{d(x\epsilon)}{dL} \qquad \text{(Eq B-23)}$$

from the differential drag equation,

$$\left(\frac{dP}{dL}\right)_{drag} = -\frac{8\omega^2\rho_f}{3\pi\delta_c D^4\rho_v^2}\,x(L)\Big/\int_{\delta_o}^{\delta_c(L)} N(\delta,L)\,\epsilon(\delta,L)\,\frac{d}{dL}\left[x(L)\,\epsilon(\delta,L)\right]\delta^3 d\delta \qquad \text{(Eq B-24)}$$

APPENDIX C

SAMPLE CALCULATIONS FOR WETTING CONDENSING OF MERCURY

This section applies the recommendations of Section 4.1.2 to the prediction of the performance of a horizontal wetting mercury condenser. The approach used is based on a modification of the available adiabatic two-phase flow test results reviewed in Section 4.1.2.

No wetting mercury data as such are available for comparison. However, a comparison of the pressure profile resulting from the calculations below is made with some non-wetting mercury condensing data in Figure 36.

To apply the modified adiabatic relations for pressure drop and liquid (or vapor) volume fraction, consider an incremental condensing length,

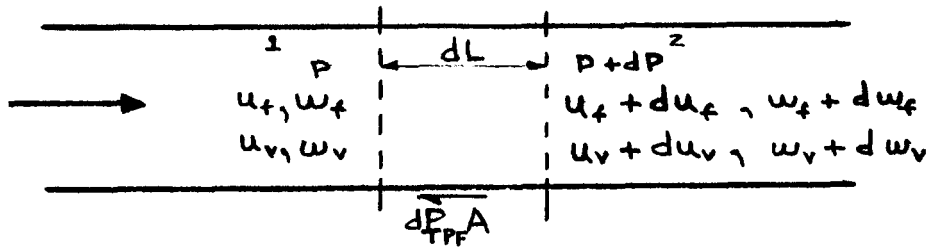

For steady state,

$$\Sigma F = \text{outflow momentum} - \text{inflow momentum}$$

$$[P-(P+dP)]A - dP_{TPF}A = (w_f+dw_f)(u_f+du_f) + (w_v+dw_v)(u_v+du_v) - w_f u_f - w_v u_v$$

or

$$-dPA = dP_{TPF}A + d(w_f u_f) + d(w_v u_v) \qquad \text{(Eq. C-1)}$$

But, also

$$w_f = \rho_f u_f A_f = \rho_f u_f R_f A \qquad \left(R_f = \frac{A_f}{A}\right)$$

$$u_f = \frac{w_f}{A R_f \rho_f} = \frac{G_f}{\rho_f R_f} \qquad \left(G_f = \frac{w_f}{A}\right)$$

Likewise,

$$u_v = \frac{G_v}{\rho_v R_v}$$

Thus

$$-dP = dP_{TPF} + \left[d\left(\frac{G_f^2}{\rho_f R_f}\right) + d\left(\frac{G_v^2}{\rho_v R_v}\right) \right]$$

also

$$G_f + G_v = G_T$$

$$G_v = x G_T$$

$$G_f = (1-x) G_T$$

Therefore,

$$-dP = dP_{TPF} + G_T^2 \left[d\left(\frac{[1-x]^2}{\rho_f R_f}\right) + d\left(\frac{x^2}{\rho_v R_v}\right) \right] \qquad \text{(Eq. C-2)}$$

Letting $\Phi^2 = \frac{\Delta P_{TPF}}{\Delta P_v}$ and using finite increments

$$P_1 - P_2 = \Phi^2 \Delta P_v + G_T^2 \left\{ \left[\frac{(1-x)^2}{\rho_f R_f}\right]_2 - \left[\frac{(1-x)^2}{\rho_f R_f}\right]_1 + \left[\frac{\bar{x}^2}{\rho_v R_v}\right]_2 - \left[\frac{\bar{x}^2}{\rho_v R_v}\right]_1 \right\}$$

But

$$\Delta P_v = f \frac{\Delta L}{D} \frac{\rho_v u_v^2}{2} = \left(\frac{0.316}{\left(\frac{D \bar{x} G_T}{\bar{\mu}_v}\right)^{1/4}} \right)^{*} \frac{\Delta L}{D} \frac{\bar{x}^2 G_T^2}{2 \bar{\rho}_v}$$

Thus,

$$P_1 - P_2 = \Phi^2 \frac{0.316}{\left(\frac{D \bar{x} G_T}{\bar{\mu}_v}\right)^{1/4}} \frac{\Delta L}{D} \frac{\bar{x}^2 G_T^2}{2 \bar{\rho}_v} + G_T^2 \left\{ \left[\frac{(1-x)^2}{\rho_f R_f}\right]_2 - \left[\frac{(1-x)^2}{\rho_f R_f}\right]_1 + \left[\frac{x^2}{\rho_v (1-R_f)}\right]_2 - \left[\frac{x^2}{\rho_v (1-R_f)}\right]_1 \right\} \qquad \text{(Eq. C-3)}$$

where

$$\Phi, R_f = f\left(\frac{G_T D}{\mu_v}, \frac{\mu_v}{\mu_f}, \frac{\rho_f}{\rho_v}, x \right)$$

The above equations are set up for the Martinelli annular or mist flow regime parameters. For different regimes $\Phi^2 \Delta P_v$ should be replaced with the two phase frictional pressure drop for the particular regime.

*This expression is called the Blasius law. (See p 81, Ref 57)

Sample calculation:

Tube inside diameter = 0.319 inch

Condensing length = 94 inch

v_v* = 3.1 cubic feet per pound

v_f* = 1.25×10^{-3} cubic feet per pound

P_o = 1030 millimeters mercury (T_{SAT_o} = 705°F)

ω = 2.08 pounds per minute (u_o = 193 feet per second)

To determine the Φ and R_f to be substituted in Equation C-3, determination of the flow regimes existing in the condenser tube is required. This is accomplished by means of the condenser line on Figure 15 which shows the variation of flow regime performance with quality for the case being considered as well as another. To introduce quality, the following relationships were used:

$$\beta = \frac{V_v}{V_v + V_f} = \frac{1}{1 + \frac{(1-x)}{x}\frac{\rho_v}{\rho_f}} \qquad \text{(Eq. C-4)}$$

$$F_{R_m} = \frac{\left(\frac{V_v + V_f}{A_p}\right)^2}{\frac{\delta}{\delta} D_p} = \frac{\left(\frac{\omega_o x}{A_p \rho_v}\right)^2 \left[1 + \frac{\rho_v}{\rho_f}\frac{(1-x)}{x}\right]^2}{\frac{\delta}{\delta} A_p} \qquad \text{(Eq. C-5)}$$

Figure 15 shows that annular flow will exist to a quality of approximately 5%, after which either slug or stratified flow will exist. Slug flow should exist because completion of condensing would fill the tube and not allow stratified flow to exist at $x = 0$.

Pressure drop and inventory may now be considered for the annular (quality varying from 100 to 5%) and slug flow regime (quality varying from 5 to 0%). Pressure fluctuations for the slug flow regime may also be investigated.

For the first 18 inch increment, assuming a linear heat flux with length,

$$X_1 = 1.0$$

$$\bar{X} = \frac{96 - 9}{96} = 0.905$$

$$X_2 = 0.809$$

*Assumed constant throughout tube. Variation in properties could be accounted for if necessary although this is not usually required except when pressure levels are low.

To define the flow regime,

$$Re_v = \frac{4\omega_T x}{\pi D \mu_v}$$

Re_{v_1} = 38,800

$\overline{Re}_f$ = 286 viscous

$\overline{Re}_v$ = 35,100 turbulent

Re_{v_2} = 31,500 turbulent.

To obtain R_{f_1} and R_{f_2}, X_1 and X_2 must be calculated. R_{f_1} is, of course, zero.

$$X^2_{vT_2} = Re_{v_2}^{-0.8} \frac{C_f}{C_v} \frac{(1-X)}{X} \frac{U_f}{U_v} \frac{\mu_f}{\mu_v}$$

$$= (31,500)^{-0.8} \frac{16}{0.046} \frac{.187}{.813} \frac{1.25 \cdot 10^{-3}}{3.1} \frac{.55 \cdot 10^{-3}}{4.27 \cdot 10^{-5}}$$

$$= 1.05 \times 10^{-4}$$

$X^2_{vT_2}$ = 0.01025.

From Figure 16,

R_{f_2} = 0.009

The average liquid volume fraction is then 0.0045. To obtain Φ, calculate

$\overline{X}_{vT}$ = 0.00664.

From Figure 16,

Φ_{vT} = 1.2.

The following values are then substituted into Equation C-3:

Φ = 1.2

$\bar{x}$ = 0.905

ΔL = 18 inch

X_1 = 1.0

X_2 = 0.809

R_{f_1} = 0

R_{f_2} = 0.009

As a result, the pressure drop is

$$\Delta P = 2.02 \text{ (Friction)} - 0.86 \text{ (Momentum)} = 1.16 \text{ psi} = 60.1 \text{ millimeters mercury.}$$

The chart below summarizes the remainder of the step by step calculations. The resulting pressure profile is shown in Figure 36.

CALCULATION OF PRESSURE DROP

Incremental Length, Inches	Mean Quality	$\overline{Re}_f$	$\overline{Re}_v$	X	Flow Mechanism	Φ	$\bar{R}_f$	ΔP, mm$_{Hg}$
0 - 18	0.905	286	35,100	0.00664	VT	1.20	0.0045	60.1
18 - 36	0.719	846	27,800	0.0138	VT	1.24	0.0116	42.8
36 - 54	0.531	1410	20,600	0.0231	VT	1.29	0.0179	21.7
54 - 72	0.344	1970	13,300	0.0453	TT	1.58	0.0310	-0.3
72 - 91	0.151	2540	6,050	0.116	TT	1.93	0.0757	-6.9

Average R_f for 100 to 5% quality = 0.1448

Quality from 5 to 5%

Assume slug flow in the last 0.4 foot of tube. Pressure drop can be calculated according to Equation 27.

$$\Delta P_{TP} = \frac{4 f_o \Psi \frac{L}{D_e} \left(\frac{w_f + w_g}{A_r}\right)^2}{\left[\left(\frac{V_f}{V_f + V_g}\right)\rho_f + \left(\frac{V_g}{V_f + V_g}\right)\rho_g\right]}$$

This pressure drop can usually be expected to be negligible (i.e. less than 1 mm of Hg) as it was in this case.

To calculate liquid inventory from Equation 29,

$$R_v = 0.83\left(\frac{V_v}{V_v+V_f}\right) = 0.83\left[\frac{1}{1+\left(\frac{1-x}{x}\right)\frac{v_f}{v_v}}\right]$$

$$\simeq 0.83\left[\frac{1}{1+\frac{v_f}{x v_v}}\right]$$

Taking $\bar{x} \simeq 0.025$, $R_v \simeq 0.82$ and $R_f \simeq 0.18$.

Pressure fluctuations can be estimated by using Figures 20, 21 and 22. Taking $\bar{x} \simeq 0.025$ gives $\beta = 0.975$.

To obtain the maximum amplitude, assume $\beta = 0.9$ for which $\bar{x} = 0.0036$. From Figure 20,

$$\frac{a}{\sqrt{\left(\frac{u_m}{u'_m}\right)^2 - 1}} = 5.2 \text{ gm/cm}^2 = 0.0738 \text{ lb/in}^2$$

but

$$u_m = u_o\left[\bar{x} + \frac{\rho_v}{\rho_f}(1-x)\right]_{\bar{x}=0.025} = 5.58 \text{ FT/SEC}$$

From Figure 22 for $D = 0.319$ inch (8.10 millimeters), $u'_m = (0.56 + 0.03)$ meter per second $\equiv 1.94$ feet per second.

Therefore, for water,

$$a = 0.0738\sqrt{\left(\frac{5.58}{1.94}\right)^2 - 1} = 0.20 \text{ pound per square inch}$$

For mercury, then,

$$a = \pm 0.20\ \frac{1}{1.25 \cdot 10^{-3} \cdot 62.4} = \pm 2.56 \text{ psi}$$

The frequency of this fluctuation, determined from Figure 21, for $\beta = 0.9$,

$$N = \frac{D}{u_m - u'_m} n = 0.4$$

$$n = \frac{0.4 \cdot 12 \text{ inch per foot}}{0.319 \text{ inch}} (5.58 - 1.94) = 55 \text{ cycles per second}$$

For the tube as a whole, the profile is given in Figure 36 . The liquid volume fraction is

$$R_{f_{TOT}} = 0.95\ (0.145) + 0.05\ (0.18) = 0.150.$$

NOMENCLATURE

A	Area or constant
b	Displacement of the interface
B	Amplitude of interface displacement
B^*	Wave amplitude where entrainment, or plugging (B_3^*), occurs
$\dot{B}$	$dB/d\theta$
$\ddot{B}$	$d^2B/d\theta^2$
C	Constant, complex wave velocity (wave celerity)
C_d	Drag coefficient
C_R	Propagation celerity (Figure 5)
d	Differential operator
D	Tube diameter
e	Base for natural logarithms
E	Constant
f	Friction factor, function to be determined
f_o	Moody friction factor
F	Force
F_{max}	Maximum growth rate factor (see Figure 8)
F_R	Froude number
G	Mass velocity
g	Gravitational constant, 32.2 ft/sec^2
h_{vf}	Latent heat of vaporization
K	Constant of integration

L	Length
L^*	Breakup length
L_s^*	Length for slugging
$\ln$	Natural logarithm
M	Mass
n	Pressure oscillation frequency
N	Drop distribution function (see Section 4.2, Reduced Frequency (see Figure 21)
P	Pressure
Q	Heat transfer rate
r	Radius
R	Volume fraction
Re	Reynold's number, $\frac{\rho_f u_2 \delta}{\mu_f} = Re_f$
Re_{fn}	Film Reynold's number for neutral stability
ss	Stainless steel
S	Growth rate factor (see Figure 2)
T/S	Condensing test section
u	Velocity
u_2	Interface velocity of liquid film
u_∞	Velocity outside of boundary layer
v	Specific volume
V	Volume
V	Volume flow rate
Ve	Vertical velocity component of interface
w	Flow rate

W_f Film Weber number, $W_f = \rho_f \delta u_2^2/\sigma$

x Quality, w_v/w_T or flowing quality

y Distance normal to film surface

Greek Symbols

α Wave number, $2\pi/\lambda$

α' $2\pi\delta/\lambda$

β $\ddot{B}/B$

Γ Condensate loading, lb/sec-in of tube periphery

δ Drop size, film thickness

Δ Finite differential

ϵ Slip u_f/u_v

θ Time

λ Wave length

μ Viscosity

ρ Density

σ Surface tension

τ Shear stress

Φ $\sqrt{\frac{(\Delta P/\Delta L)_{TPF}}{(\Delta P/\Delta L)_{one\ phase}}}$

X $\sqrt{\frac{(\Delta P/\Delta L)_f}{(\Delta P/\Delta L)_g}}$

ψ Stream function (Equation 1), slug flow friction factor multiplier in Equation 27

Subscripts

c Critical, gravitational constant

d Drag

g	Gas or vapor
f	Liquid, film
F	Fraction, friction
Htr	Heater
i	Imaginary
l	Liquid
m	Mixture
max	Maximum
n	Normal
o	Initial, zero gravity
p	Pipe
r	Real
re	Relative
s	Static, slug flow
sat	Saturation
sd	Single drop
T	Total
t	Turbulent
TP	Two phase
T/S	Condensing test section
V	Volume
v	Vapor
w	Wall

z	Interface
∞	Great distance outside of boundary layer
δ	Drop
v	Viscous
σ	Surface tension

REFERENCES

1. "The SNAP II Power Conversion System Topical Report No. 7, Mercury Materials Evaluation," TRW Report No. ER-4103, 1961.

2. "The SNAP II Power Conversion System Topical Report No. 14, Mercury Materials Evaluation and Selection," TRW Report No. ER-4461, 1961.

3. "The SNAP II Power Conversion System Topical Report No. 8, Mercury Condensing Research Studies," TRW Report No. ER-4442, 1961.

4. "The SNAP II Power Conversion System Topical Report No. 13, Orbital Force Field Boiling and Condensing Experiment (OFFBACE)," TRW Report No. ER-4670, October, 1962.

5. "Government-Industry Conference on Mercury Condensing," NASA TND-1188, April 18, 1961, Pasadena, California.

6. Collier, J.G. and G.F. Hewitt. "Data on the Vertical Flow of Air-Water Mixtures in the Annular and Dispersed Flow Regimes, Part II. Film Thickness and Entrainment Data and Analysis of Pressure Drop Measurements," Transactions of the Institute of of Chemical Engineers, Vol. 39, 1961.

7. Nusselt, W. "The Surface Condensation of Steam," ZVDI, 1916.

8. Calvert, S. and B. Williams. "Upward Co-Current Annular Flow of Air and Water in Smooth Tubes," American Institute of Chemical Engineers Journal, 1955.

9. Collins, D.E. "Co-Current Gas Absorption," Ph.D. Thesis, Purdue University.

10. Dunkler, A.E. "An Investigation of Pressure Drop for Isothermal Two-Phase Film Flow in a Vertical Tube," M.S. Thesis, University of Delaware, 1949.

11. Dunkler, A.E. "Hydrodynamics of Liquid Films in Single and Two-Phase Flows," Ph.D. Thesis, University of Delaware, 1951.

12. Kinney, G.L., A.E. Abramson, and J.L. Sloop. "Internal-Liquid-Film-Cooling Experiments with Air-Stream Temperatures to 2000°F in 2- and 4-Inch Diameter Horizontal Tubes," NACA Report 1087, 1952.

13. Brauer, H. "Strömung und Wärmeubergang bei Rieselfilmen," VDT Forach., 457, 1956.

14. Knuth, E.L. "The Mechanics of Film Cooling," Memo No. 20-85, Jet Propulsion Laboratory, California Institute of Technology, 1953.

15. Laird, A.D.K. "Stability Considerations in Vertical Annular Two-Phase Flow," Ph.D. Thesis, University of California, 1951.

16. Lin, C.C. The Theory of Hydrodynamic Stability, Cambridge University Press, 1955.

17. Feldman, S. "On the Hydrodynamic Stability of Two Viscous Incompressible Fluids in Parallel Uniform Shearing Motion," Journal of Fluid Mechanics, Vol. 2, Part 4, 343-370, 1957.

18. Charvonia, D.A. "A Review of the Published Literature Pertaining to the Annular, Two-Phase Flow of Liquid and Gaseous Media in a Pipe," Project Squid, Technical Report PUR-32-R, December 1958.

19. Chandraseknar, S. Hydrodynamic and Hydromagnetic Stability, Clarenden Press, Oxford, 1961.

20. York, J.L., H.E. Stubbs, and M.R. Tek. "The Mechanism of Disintegration of Liquid Sheets," ASME Transactions, Vol. 75, 1953, p. 1279.

21. Ostrach, S. "Convection Phenomena in Fluids Heated from Below," ASME Transactions, Vol. 79, No. 2, 1957, pp 299-307.

22. Lilleleht, L.U. and T.J. Hanratty. "Measurement of Interfacial Structure for Co-Current Air-Water Flow," Journal of Fluid Mechanics, August 1961.

23. Koestel, A. and J.J. Reinmann. "Mercury Condenser Research and Development," in NASA Technical Note D-1188, Government-Industry Conference on Mercury Condensing, Pasadena,California, April 18, 1961.

24. Ostrach, S. and P.R. Thornton. "Stability of Compressible Boundary Layers Induced by a Moving Wave," Journal of Aero-Space Science, Vol. 29, No. 3, 1962.

25. Charvonia, D.A. "An Experimental Investigation of the Mean Liquid Film Thickness and the Characteristics of the Interfacial Surface in Annular, Two-Phase Flow," ASME Paper No. 61-WA-253, 1961.

26. Warner, C.F. and J.M. Murphy. "Investigation of Annular Two-Phase Flow and Heat Transfer to and from Gases with Large Temperature Differences," Report No. F-G1-1, Jet Propulsion Center, Purdue University, Lafayette, Indiana, March 1961.

27. Eisenklam, P., N. Dombrowski, and D. Hasson. "Drop Formation from Rapidly Moving Liquid Sheets," Imperial College Report JRL No. 44, Ministry of Aviation, May 1959.

28. Weber, C. "Zum Zerfall eines Flüssyhertsstrahles," ZAMM, Vol. 11, p. 136, 1931.

29. Lamb, H. Hydrodynamics, Sixth Edition, Dover Publications, 1952, p. 457.

30. Knuth, E.L. "The Mechanics of Film Cooling," Parts 1 and 2," Jet Propulsion Laboratory, November-December, 1954, January 1955.

31. Emmens, H., C. Chang, and B. Watson. "Taylor Instability of Finite Surface Waves," Journal of Fluid Mechanics, Vol. 7, Part 2, February 1960.

32. Schlichting, H. Boundary Layer Theory, Fourth Edition, McGraw-Hill, 1955, p. 401.

33. Altman, M., F.W. Slauto, and R.H. Norris. "Local Heat Transfer and Pressure Drop for Refrigerant-22 Condensing in Horizontal Tubes," American Institute of Chemical Engineers, Chemical Engineering Symposium Series, Vol. 50, No. 30, 1960.

34. Seminov, N.I. "Pressure Pulsations During the Flow of Gas-Liquid Mixtures in Pipes," AEC-tr-4496.

35. Kozlov, B.K. "Types of Gas-Liquid Mixtures and Stability Boundaries in Vertical Tubes," Zhur Tech Fiz, Vol. 24, No. 4, p. 656, 1952.

36. Kraziahova, L.I. "Some Characteristics of the Flow of a Two-Phase Mixture in a Horizontal Pipe," Zhur Tech Fiz, Vol. 24, No. 4, pp. 654-669, AERE Lib Translation 695, Harwell, January, 1957.

37. Baher, O. "Simultaneous Flow of Oil and Gas," Oil & Gas Journal, p. 185, July 26, 1954.

38. Bergelin, O.P. and C. Gazley. "Co-Current Gas-Liquid Flow in Horizontal Tubes," Heat Transfer and Fluid Mechanics Institute, 1949.

39. Chato, J.C. "Laminar Condensation," ASHRAE Journal, February 1962.

40. Lockhart, R.W. and R.C. Martinelli. "Proposed Correlation of Data for Isothermal Two-Phase Two-Component Flow in Pipes," Chemical Engineering Progress, Vol. 45, No. 1, p. 39, January 1949.

41. Martinelli, R.C., L.M.K. Boelter, T.H.M. Taylor, E.G. Thomsen, E.H. Morrin. "Isothermal Pressure Drop for Two-Phase Two-Component Flow in a Horizontal Pipe," Transactions of the ASME, Vol. 66, p. 139, 1944.

42. Martinelli, R.C. and D.B. Nelson. "Prediction of Pressure Drop During Forced Circulation Boiling of Water," Transactions of the ASME, Vol. 70, p. 695, 1948.

43. Martinelli, R.C., J.A. Putnam, and R.W. Lockhart. "Two-Phase, Two-Component Flow in the Viscous Region," Transactions of the American Institute of Chemical Engineers, Vol. 42, p. 681, 1946.

44. Armand, A.A. "Resistance to Motion of a Binary System in Horizontal Tubes," Izvestiya V.T.I. No. 1, 1946.

45. Welch, J.F. and J.W. Westwater. "Microscopic Study of Dropwise Condensation," ASME

46. Proceedings of the General Discussion on Heat Transfer, The Institute of Mechanical Engineers, The American Society of Mechanical Engineers, September 11-13, 1951.

47. Schlichting, H. "Experimental Investigations of the Problem of Surface Roughness," NASA Technical Memo No. 823.

48. Rouse, H. and J.W. Howe. Basic Mechanics of Fluids, New York: John Wiley & Sons, 1953.

49. Misra, B. and C.F. Bonilla. "Heat Transfer in the Condensation of Metal Vapors; Mercury and Sodium up to Atmospheric Pressure," Chemical Engineering Symposium Series, Vol. 52, No. 18, 1956.

50. "Thermodynamic Properties of Mercury," Thompson Ramo Wooldridge Inc., TM-777, March 20, 1956.

51. Gazley, C. "Co-Current Gas-Liquid Flow, III, Interfacial Shear and Stability," Heat Transfer and Fluid Mechanics Institute, 1949.

52. Bikerman, J. Surface Chemistry, New York: Academic Press, 1960.

53. Briggs, L.J. "The Limiting Negative Pressure of Mercury in Pyrex Glass," Journal of Applied Physics, Vol. 24, No. 4, April, 1953.

54. Smith, A.R. and E.S. Thompson. "Mercury for the Generation of Light, Heat, and Power" Transations of ATME, Vol. 64, p. 647, 1942.

55. Liquid Metals Handbook, United States Atomic Energy Commission and Department of the Navy, 1953.

56. Owens, J.J. and J.F. Nejedlik. "Materials Compatability with Mercury at Temperatures Below 1000°F," Presented at the Corrosion by Heat Transfer Symposium, AIME Annual Meeting, New York, February 22, 1962.

57. Eckert, E.R.G. Introduction to the Transfer Heat and Mass, New York: McGraw-Hill Book Co. Inc, 1950.

DISTRIBUTION LIST

National Aeronautics and Space Administration — 1
Washington 25, D.C.
Attention: William H. Woodward (RN)

National Aeronautics and Space Administration — 1
Washington 25, D.C.
Attention: Fred Schulman (RN)

National Aeronautics and Space Administration — 1
Washington 25, D.C.
Attention: James J. Lynch (RN)

National Aeronautics and Space Administration — 1
Washington 25, D.C.
Attention: Herbert Rochen (RN)

National Aeronautics and Space Administration — 1
Ames Research Center
Moffet Field, California
Attention: Librarian

National Aeronautics and Space Administration — 1
Goddard Space Flight Center
Greenbelt, Maryland
Attention: Librarian

National Aeronautics and Space Administration — 1
Langley Research Center
Hampton, Virginia
Attention: Librarian

National Aeronautics and Space Administration — 3
Lewis Research Center
21000 Brookpark Road
Cleveland 35, Ohio
Attention: Librarian

National Aeronautics and Space Administration — 1
Lewis Research Center
21000 Brookpark Road
Cleveland 35, Ohio
Attention: Bernard Lubarsky (SPD)

National Aeronautics and Space Administration Lewis Research Center 21000 Brookpark Road Cleveland 35, Ohio Attention Henry O. Slone (SPD-SEPO)	1
National Aeronautics and Space Administration Lewis Research Center 21000 Brookpark Road Cleveland 35, Ohio Attention Robert Denington (SPD-SEPO)	
National Aeronautics and Space Administration Scientific and Technical Information Facility Box 5700 Bethesda 14, Maryland Attention: NASA Representative	2 and reproducible
National Aeronautics and Space Administration Lewis Research Center 21000 Brookpark Road Cleveland 35, Ohio Attention: John J. Fackler (SEPPO)	1
National Aeronautics and Space Administration Lewis Research Center 21000 Brookpark Road Cleveland 35, Ohio Attention Norman T. Musial Patent Counsel	1
National Aeronautics and Space Administration Lewis Research Center 21000 Brookpark Road Cleveland 35, Ohio Office of Reliability and Quality Assurance	1
National Aeronautics and Space Administration Lewis Research Center 21000 Brookpark Road Cleveland 35, Ohio Attention: Harold J. Christenson (FSCD)	1

National Aeronautics and Space Administration
Lewis Research Center
21000 Brookpark Road
Attention: Robert G. Dorsch (FSCD) — 1

National Aeronautics and Space Administration
Lewis Research Center
21000 Brookpark Road
Cleveland 35, Ohio
Attention: Robert E. English (ADED) — 2

National Aeronautics and Space Administration
Lewis Research Center
21000 Brookpark Road
Cleveland 35, Ohio
Attention: Seymour Lieblein (FSCD) — 1

National Aeronautics and Space Administration
Manned Spacecraft Center
Houston 1, Texas
Attention: Librarian — 1

National Aeronautics and Space Administration
George C. Marshall Space Flight Center
Huntsville, Alabama
Attention: Librarian — 1

National Aeronautics and Space Administration
George C. Marshall Space Flight Center
Huntsville, Alabama
Attention: Ernst Stuhlinger — 1

National Aeronautics and Space Administration
George C. Marshall Space Flight Center
Huntsville, Alabama
Attention: Russell H. Shelton — 1

National Aeronautics and Space Administration
Jet Propulsion Laboratory
2800 Oak Grove Drive
Pasadena 3, California
Attention: Librarian — 1

National Aeronautics and Space Administration — 2
Jet Propulsion Laboratory
2800 Oak Grove Drive
Pasadena 3, California
Attention: John Paulson

National Aeronautics and Space Administration — 1
Western Operations Office
150 Pico Boulevard
Santa Monica, California
Attention: John Keeler

Aeronautical Systems Division — 1
Wright-Patterson Air Force Base, Ohio
Attention: R. J. Benzing (ASRCNL)

Aeronautical Systems Division — 1
Wright-Patterson Air Force Base, Ohio
Attention: Bernard Chasman (ASRCEA)

Aeronautical Systems Division — 3
Wright-Patterson Air Force Base, Ohio
Attention: George E. Thompson (ASRMFP-1)

U. S. Atomic Energy Commission — 2
Technical Reports Library
Washington 25, D. C.
Attention: J. M. O'Leary

U. S. Atomic Emergy Commission — 3
Technical Information Service Extension
P. O. Box 62
Oak Ridge, Tennessee

U. S. Atomic Energy Commission — 2
Washington 25, D. C.
Attention: R. M. Scroggins

Argonne National Laboratory — 1
9700 South Cross Avenue
Argonne, Illinois
Attention: Librarian

Argonne National Laboratory — 1
9700 South Cross Avenue
Argonne, Illinois
Attention: John F. Marchaterre

Brookhaven National Laboratory 1
Upton, Long Island, New York
Attention: Librarian

Brookhaven National Laboratory 1
Upton, Long Island, New York
Attention: O. A. Dwyer

Oak Ridge National Laboratory 1
Oak Ridge, Tennessee
Attention: Herbert W. Hoffman

Oak Ridge National Laboratory 1
Oak Ridge, Tennessee
Attention: W. D. Manly

Oak Ridge National Laboratory 1
Oak Ridge, Tennessee
Attention: Arthur Fraas

Columbia University 1
Department of Chemical Engineering
New York 27, New York
Attention: Charles F. Bonilla

Stanford University 1
Palo Alto, California
Attention: W. C. Reynolds,
Mechanical Engineering Department

University of Connecticut 1
Storrs, Connecticut
Attention: W. Hilding,
Mechanical Engineering Department

The RAND Corporation 1
1700 Main Street
Santa Monica, California

Advanced Technology Laboratories 1
Division of American Standard
369 Whisman Road
Mountain View, California
Attention: Library

Aerojet-General Corporation
P. O. Box 296
Azusa, California
Attention: Librarian

2

Aerojet-General Nucleonics
P. O. Box 77
San Ramon, California
Attention: Librarian

2

Aerojet-General Nucleonics
P.O. Box 77
San Ramon,California
Attention: John R. Payne

1

AiResearch Manufacturing Company
Sky Harbor Airport
402 South 36th Street
Phoenix, Arizona
Attention: Librarian

2

AiResearch Manufacturing Company
Sky Harbor Airport
402 South 36th Street
Phoenix, Arizona
Attention: E.A . Kovacevich

1

AiResearch Manufacturing Company
9851-9951 Sepulveda Blvd.
Los Angeles 45, California
Attention: Librarian

1

AiResearch Manufacturing Company
9851-9951 Sepulveda Blvd.
Los Angeles 45, California
Attention: James J. Killackey

1

Atomics International
8900 DeSoto Avenue
Canoga Park, California
Attention: Louis Bernath

1

Avco
Research and Advanced Development Department
201 Lowell Street.
Wilmington, Massachusetts
Attention: Librarian

1

Babcock and Wilcox Company — 1
Research Center
Alliance, Ohio
Attention: W. Markert, Jr.

Electro-Optical Systems, Inc. — 2
Advanced Power Systems Division
Pasadena, California
Attention: Joseph Neustein

Euratom — 1
Common Research Center of Ispra
Casella postale no. 1
Ispra (Varese)
Italy
Attention: Bernard P. Millot
Heat Transfer Division

General Atomic — 1
John Jay Hopkins Laboratory
P. O. Box 608
San Diego 12, California
Attention: Librarian

General Motors Corporation — 1
Allison Division
Indianapolis 6, Indiana
Attention: Librarian

Geoscience Ltd. — 1
8686 Dunaway Drive
La Jolla, California
Attention: H. F. Poppeniek

Hughes Aircraft Company — 1
Engineering Division
Culver City, California
Attention: Tom B. Carvey, Jr.

Jacobs Engineering Company — 1
774 East Green Street
Pasadena, California
Attention: Wayne Cochran

Marquardt Aircraft Company P. O. Box 2013 Van Nuys, California Attention: Librarian	1
The Martin Company Nuclear Division P. O. Box 5042 Baltimore 20, Maryland Attention: Librarian	1
MSA Research Corporation Callery, Pennsylvania Attention: Fredrick Tepper	1
Plasmadyne Corporation 3839 South Main Street Santa Anna, California Attention: Librarian	1
Pratt & Whitney Aircraft CANEL P. O. Box 611 Middletown, Connecticut Attention: Librarian	3
Rocketdyne Canoga Park, California Attention: Librarian	1
Southwest Research Institute 8500 Culebra Road San Antonio 6, Texas Attention: W. D. Weatherford, Jr.	1
Sundstrand Denver 2480 West 70th Avenue Denver 21, Colorado Attention: Librarian	1
Pratt & Whitney Aircraft 400 Main Street East Hartford 8, Connecticut Attention: Librarian	2

Pratt & Whitney Aircraft
400 Main Street
East Hartford 8, Connecticut
Attention: Richard Curry

1

Pratt & Whitney Aircraft
400 Main Street
East Hartford 8, Connecticut
Attention: Eugene Szetela

1

Union Carbide Nuclear Company
P. O. Box X
Oak Ridge, Tennessee
Attention: X-10 Laboratory Records Department

2

United Nuclear Corporation
Development Division
5 New Street
White Plains, New York
Attention: Librarian

1

Westinghouse Electric Corporation
Astronuclear Laboratory
P. O. Box 10864
Pittsburgh 36, Pennsylvania
Attention: Librarian

1

Westinghouse Electric Corporation
Aero-Space Department
Lima, Ohio
Attention: Librarian

1

Advanced Research Projects Agency
Pentagon
Washington 25, D. C.
Attention: John Huth

1

U. S. Atomic Energy Commission
Germantown, Maryland
Attention: Col. William A. Tesch

1

U. S. Atomic Emergy Commission
Germantown, Maryland
Attention: G. M. Anderson

1

Atomic Energy Commission Chicago Operations Office 9800 South Cass Avenue Argonne, Illinois Attention: Librarian	1
Atomic Energy Commission New York Operations Office 376 Hudson Street New York 14, New York Attention: Librarian	1
Atomic Energy Commission Canoga Park Area Office P. O. Box 591 Canoga Park, California Attention: Librarian	1
University of California Berkeley, California Attention: R. A. Seban	1
Institute For Defense Analysis Washington, D. C. Attention: Librarian	1
Flight Propulsion Laboratory Department General Electric Company Cincinnati 15, Ohio Attention: Morris A. Zipkin	2
General Electric Company Missile and Space Vehicle Department P. O. Box 8555 Philadelphia 1, Pennsylvania Attention: Librarian	1
General Electric Company Missile and Space Vehicle Department P. O. Box 8555 Philadelphia 1, Pennsylvania Attention: Edward Ray	1

Aerospace Corporation El Segundo, California Attention: R. Champetier	1
Massachusetts Institute of Technology Cambridge 39, Massachusetts Attention: Warren M. Rohsenow	1
University of Michigan Department of Chemical and Metallurgical Engineering Ann Arbor, Michigan Attention: Richard E. Balzhiser	1
Southern Methodist University Engineering School Dallas 22, Texas Attention: Harold A. Blum	1
University of Wisconsin Madison 6, Wisconsin Attention: Max W. Carbon	1
Los Alamos Scientific Laboratory Los Alamos, New Mexico Attention: R. G. Gido	1